THE UNIVERSITY OF CHICAGO

THE PHYSICAL AND EVOLUTIONARY ORIGINS OF ALLOSTERY

A DISSERTATION SUBMITTED TO
THE FACULTY OF THE DIVISION OF THE PHYSICAL SCIENCES
AND
THE FACULTY OF THE DIVISION OF THE BIOLOGICAL SCIENCES AND THE
PRITZKER SCHOOL OF MEDICINE
IN CANDIDACY FOR THE DEGREE OF
DOCTOR OF PHILOSOPHY

GRADUATE PROGRAM IN BIOPHYSICAL SCIENCES

BY
ERIC ROUVIERE

CHICAGO, ILLINOIS
AUGUST 2025

TABLE OF CONTENTS

LIST OF FIGURES

LIST OF TABLES

ACKNOWLEDGMENTS

I express my gratitude to all those who have helped me along the way during the past six years.

Foremost, I thank Prof. Ranganathan, my primary advisor, for shaping all aspects of my scientific education. In particular, I have greatly benefited from his relentless commitment to the merit of a scientific question and his guidance in developing a *research program* aimed at addressing the most fundamental problems in basic biology. I thank Prof. Murugan for his mentorship and his willingness to support and guide projects based on my own ideas. I thank Prof. Rivoire at ESPCI Paris, who began as a collaborator and quickly became a close advisor, dedicating significant time to our discussions. Everything I know about conducting theoretical research—from posing a problem to communicating the findings—is a result of his mentorship. I thank Prof. Tom Witten and Prof. Tobin Sosnick, members of my thesis committee, who have provided both scientifically valuable and personally encouraging feedback on this work over the years. I thank the members of the Ranganathan, Murugan, and Rivoire groups, as well as others at Chicago, who have helped advance this work through many useful discussions—particularly Kabir Husain, Bryan Andrews, Riccardo Ravasio, Nachi Stern, Yaakov Kleeorin, Marion Chauveau, Vedant Sachdeva, Diane Schnitkey, Steven Wasserman, Federica Ferretti, Maryn Carlson, Nikša Praljak, Ayanna Matthews, and Samar Alqatari. Lastly, I thank my parents, Pierre and Charlotte, my sister Madeleine, and my partner Fatimah for their continued support.

ABSTRACT

Allostery is a fundamental property of proteins, describing the functional coupling between distantly separated sites within the molecule. In different manifestations, this property enables signal transduction, gene expression, and regulation. Although decades of research have advanced our understanding of allosteric proteins, fundamental questions persist. In this thesis, I present my work on two of these questions: What physical principles enable allostery? And how can allosteric function emerge in proteins through evolution?

I begin by presenting a reduced theoretical framework that physically represents generic proteins. By making minimal assumptions, I derive the essential physical conditions necessary for allostery. What emerges is a basic classification of allostery into two forms: mechanisms that couple distant sites through soft normal modes within a single state, and mechanisms that rely on multiple states, with effective interactions emerging only upon switching between them. This framework unifies all previously proposed models of allostery.

Building on this work, I investigate what determines the form of allostery that emerges through evolution. I analyze an elastic network model of a protein across a range of physical and evolutionary constraints and find that a continuum of mechanisms exists, operating on a combination of the soft mode and multi-state principles. I find that when the system has the capacity for frustration, the multi-state mechanism produces stronger allosteric effects and is selectively favored.

Finally, I consider how allosteric function can emerge in proteins even without direct selection. This question is motivated by the finding that many proteins have latent allosteric function—properties that exist in the protein but are not part of its native role. Previous computational and experimental data suggest that allosteric architectures enhance a protein's adaptability by wiring distant sites to functional regions. I hypothesize that fluctuating environments select for evolvable designs and, as a byproduct, allosteric architectures. Using a minimal binding model, I show that periodically switching selective pressures promote the

emergence of evolvable, allosteric sequences. These results show how a protein's design reflects not only its present function but also the statistical structure of its evolutionary past.

CHAPTER 1

INTRODUCTION: THE PROBLEM OF ALLOSTERY

1.1 Introducing allostery

Proteins provide the machinery for the cell to maintain proper function, adaptation, and growth. As a group, they perform many specialized tasks, with nearly every protein playing a distinct role. However, these tasks can be broadly classified into a few elementary categories. Perhaps their most basic function is to bind other molecules. Proteins bind ions, small molecules, lipids, DNA, RNA, and other proteins. Beyond binding, many proteins (enzymes) catalyze chemical reactions and are responsible for processing matter into energy and accumulating biomass. Furthermore, binding and catalysis are often coupled to other binding or catalytic events. For example, in metabolism, enzyme activity is often modulated by the binding of an effector molecule at a site distinct from the active site, where catalysis occurs [16]. In cell signaling, ligand binding to a G-protein-coupled receptor on the extracellular surface ultimately facilitates the dissociation of the G-protein on the intracellular surface [39]. In gene regulation, binding of an inducer molecule to the ligand-binding domain of a transcription factor promotes the DNA-binding domain's interaction with a specific DNA sequence [50]. This coupling of spatially separated molecular events within a protein (or other macromolecule) is called allostery. In its many forms, allosteric behavior enables nearly all cellular processes [53, 24, 30, 6, 20].

Before continuing, it is important to understand the length scales relevant for allostery. A small protein domain is roughly 25 Å across (e.g., PDZ domain [9]), while a large protein can be greater than 100 Å across (e.g,. Glutamate synthase [8]). The interactions between atoms occur on the scale of 1–5 Å. A carbon-carbon covalent bond is 1.54 Å, a hydrogen bond is 3 Å, and a salt bridge between two charged residues is 2.8–4.0 Å [4]. Thus, the length scale of a protein is roughly an order of magnitude larger than the length scale of the interactions. The distances associated with allostery range from just beyond a protein contact (5.5 Å in a PDZ domain[38]) to over 100 Å, as in the case of the aspartate receptor [36], but can

generally be thought of as spanning the same scale as the protein itself.

The long-range communication of allostery presents a question: how can two distant sites be coupled in a protein when atomic interactions are short-ranged? Despite decades of research, a complete mechanistic understanding remains unclear.

In this thesis, I take a theoretical approach to the problem, which has historically been much less popular than the experimental approach, for which there is already a substantial body of work. In the remainder of this chapter, I first define allosteric coupling between sites in quantitative terms. I then present a simple calculation to build intuition for how non-allosteric material should behave. Finally, I discuss previous theoretical models proposed to explain allostery.

1.2 A quantitative definition of allosteric coupling

A protein in solution is a thermal system, meaning that it exchanges energy with the solvent, leading it to sample different structural conformations. Such systems are quantitatively defined by their *energy landscape* $U_p(\mathbf{r})$, a function that relates a protein's configuration of atomic coordinates $\mathbf{r}$ to its potential energy. At thermal equilibrium, the stability of a system is determined by its free energy,

$$F[U] = -\beta^{-1} \log \int e^{-\beta U(\mathbf{r})}\, d\mathbf{r}, \tag{1.1}$$

where $\beta = (k_B T)^{-1}$ is the inverse temperature and the integral is over Cartesian coordinates of the atomic positions.

When a ligand binds, it interacts with the protein by applying forces, breaking bonds, etc.—generally altering its energy landscape. (I use the case of ligand binding to describe allostery, but the concepts equally apply to other chemical modifications such as phosphorylation and mutation.) The ligand-induced change in the landscape can be represented as a

function $V(\mathbf{r})$, so the ligand-bound energy landscape becomes $U_p(\mathbf{r}) + V(\mathbf{r})$. The tightness with which the ligand binds is measured by its binding free energy, defined as the difference in free energy between the unbound and bound states, $\Delta F = F[U_p + V] - F[U_p]$.

Allostery is fundamentally about communication between multiple sites. For simplicity, consider a protein with two binding sites, a and b. Ligand binding at site a is described by the landscape $U_p(\mathbf{r}) + V_a(\mathbf{r})$, and similarly for binding at site b: $U_p(\mathbf{r}) + V_b(\mathbf{r})$. When both ligands are bound, the energy landscape is $U_p(\mathbf{r}) + V_a(\mathbf{r}) + V_b(\mathbf{r})$. We take the energies to be additive precisely because allostery requires separated sites such that the two bound ligands do not directly interact. The corresponding binding free energies are

$$\begin{aligned} \Delta F_a &= F[U_p + V_a] - F[U_p] \\ \Delta F_b &= F[U_p + V_a] - F[U_p] \\ \Delta F_{ab} &= F[U_p + V_a + V_b] - F[U_p] \end{aligned} \tag{1.2}$$

Although the energies are assumed to be additive, the binding free energies need not be. The allosteric coupling is defined as the non-additivity in the binding free energies:

$$\Delta\Delta F = \Delta F_a + \Delta F_b - \Delta F_{ab}. \tag{1.3}$$

When binding at one site increases the affinity for the ligand at the other site (also known as positive cooperativity), $\Delta\Delta F > 0$.

1.3 A calculation of interacting perturbations in a non-allosteric material

The concept of allostery—the energy of interaction ($\Delta\Delta F$) between two spatially separated perturbations—extends beyond proteins. This type of phenomenon has been studied extensively in physics. For example, defects in a crystal interact over distances greater than

the lattice spacing [15], and inclusions in membranes can influence each other by straining the surrounding membrane [35]. The key difference between these physical systems and allosteric proteins is that proteins can have evolutionarily optimized architectures that enable long-range interactions, unlike in homogeneous, isotropic materials where interaction energies decay rapidly with distance [35]. In fact, the framework of continuum elasticity, commonly used to describe such materials, can be used to calculate a null expectation for how perturbations should interact in non-allosteric soft elastic matter.

Here I present such a calculation. For simplicity, consider a linear, isotropic, elastic medium subject to perturbations in the form of applied forces. The analog of the protein's energy landscape for continuous systems—the elastic energy functional.

$$U[\mathbf{u}] = \frac{\mu}{2} \int d\mathbf{x} \, (\nabla \mathbf{u})^2. \tag{1.4}$$

The field $\mathbf{u}(\mathbf{x})$ describes the displacement of each point $\mathbf{x}$ of the system and its gradient $\nabla \mathbf{u}$ gives (a simplified version of) the strain tensor and $(\nabla \mathbf{u})^2 = \sum_{i,j} (\partial_i u_j)^2$. μ describes the stiffness of the medium. To model the effect of an external force field $\mathbf{F}(\mathbf{x})$, we include the work done by the force in the functional,

$$U[\mathbf{u}] = \int d\mathbf{x} \, \left\{ \frac{\mu}{2} (\nabla \mathbf{u})^2 - \mathbf{F}(\mathbf{x}) \cdot \mathbf{u}(\mathbf{x}) \right\}. \tag{1.5}$$

Minimizing U with respect to $\mathbf{u}(\mathbf{x})$, gives the equilibrium equation

$$\mu \nabla^2 \mathbf{u}(\mathbf{x}) = -\mathbf{F}(\mathbf{x}). \tag{1.6}$$

This is a linear equation. In general, linear equations have a solution that can be written in

terms of the Green's function $G(\mathbf{x}, \mathbf{y})$ of the operator:

$$\mathbf{u}(\mathbf{x}) = \int d\mathbf{y}\, G(\mathbf{x}, \mathbf{y}) \cdot \mathbf{F}(\mathbf{y}). \tag{1.7}$$

In this case, the operator is the Laplacian $\mu\nabla^2$ whose Green's function in 3d is $G(\mathbf{x}, \mathbf{y}) = -\frac{\mathbf{I}}{4\pi\mu\,\|\mathbf{x}-\mathbf{y}\|}$, where $\mathbf{I}$ is the identity matrix. Substituting (1.7) into (1.5) gives the minimum energy,

$$E = -\frac{1}{2}\iint d\mathbf{x}\, d\mathbf{y}\, \mathbf{F}(\mathbf{x}) \cdot G(\mathbf{x}, \mathbf{y}) \cdot \mathbf{F}(\mathbf{y}). \tag{1.8}$$

To model ligand binding at each site, assume two distinct force distributions $\mathbf{F}(\mathbf{x}) = \mathbf{F}_a(\mathbf{x}) + \mathbf{F}_b(\mathbf{x})$. The elastic energy becomes

$$E = -\frac{1}{2}\iint d\mathbf{x}\, d\mathbf{y}\, \Big[\mathbf{F}_a(\mathbf{x}) + \mathbf{F}_b(\mathbf{x})\Big] \cdot G(\mathbf{x}, \mathbf{y}) \cdot \Big[\mathbf{F}_a(\mathbf{y}) + \mathbf{F}_b(\mathbf{y})\Big], \tag{1.9}$$

and the elastic interaction energy (allosteric coupling) is given by the cross-term

$$\Delta\Delta E = -\iint d\mathbf{x}\, d\mathbf{y}\, \mathbf{F}_a(\mathbf{x}) \cdot G(\mathbf{x}, \mathbf{y}) \cdot \mathbf{F}_b(\mathbf{y}). \tag{1.10}$$

If we assume the perturbations are point forces $\mathbf{F}_a(\mathbf{x}) = \mathbf{F}_a\,\delta(\mathbf{x} - \mathbf{x}_a), \mathbf{F}_b(\mathbf{x}) = \mathbf{F}_b\,\delta(\mathbf{x} - \mathbf{x}_b)$ separated by $d = \|\mathbf{x}_a - \mathbf{x}_b\|$, the interaction energy reduces to

$$\Delta\Delta E = \frac{\mathbf{F}_a \cdot \mathbf{F}_b}{4\pi\mu d}. \tag{1.11}$$

This shows that in the simplest elastic materials with no explicit allosteric design, we expect the coupling energy to decrease with distance as a power law. In fact, for more natural types of perturbations, such as force dipoles, the energy of interaction decays with a higher power [57].

1.4 Review of previous theoretical models of allostery.

Allostery has long stood as a central puzzle in protein biochemistry, emerging from early efforts to explain cooperative binding in hemoglobin (Hb), the oxygen-transport protein in red blood cells. Long before Hb structures were resolved, experiments revealed that Hb binds oxygen in an all-or-none manner, producing a sigmoidal binding curve [3, 1]. The sigmoidal shape deviates from the hyperbolic shape expected for independent binding sites with constant affinity. In the 1920s, Adair measured this behavior and proposed that oxygen binds sequentially and that affinity increases as more oxygen molecules bind. Without structural data, Adair deduced that Hb is a tetramer and argued that the binding sites likely do not interact directly. What was left unexplained was how binding at one site alters the affinity at others.

To explain allostery in Hb and later other proteins, numerous theoretical models have been proposed, serving various purposes: fitting experimental data [33, 27], identifying minimal physical requirements for allosteric phenomena [19, 31, 45], exploring evolutionary conditions favoring its emergence [42], and guiding its engineering into synthetic materials [43, 57, 37]. This diversity of perspectives and objectives has led to a proliferation of models whose common principles are difficult to discern.

The first theoretical models of allostery coarse-grained the high-dimensional conformational space that proteins sample into a few discrete states (Fig. 1.1AB) and defined rules for transitioning between these states. These models are often referred to as thermodynamic or phenomenological models. Monod, Wyman, and Changeux (MWC) introduced such a model to describe the cooperative binding of oxygen to hemoglobin [33]. Their original model makes assumptions that limit its applicability, but its core principle is general. The MWC principle relies on the presence of two or more states that the protein samples in the absence of ligands, and ligands bind to each state with different affinities (Fig. 1.1A). The

two states were originally interpreted as two structurally distinct conformations, and we call the mechanism described by the model a “conformational switch”. However, the principle applies irrespective of the physical nature of the states and is also often described in terms of “population shift” [52, 2, 40].

Another early model proposed by Koshland, Nemethy, and Filmer (KNF) [27] assumes the protein consists multiple parts (subunits) whose state changes upon binding ligand. As with the MWC model, the KNF model is thermodynamic and applies irrespective of the physical nature of the states, but these states are, again, most often interpreted as representing different conformations of the subunits. A key difference from the MWC model is that each ligation condition, whether unbound, single-bound, or double-bound, is associated with a single state of the subunits. Since states are defined by the presence or absence of ligands, this mechanism is said to operate by “induced fit” [26, 5]. Another notable distinction is that cooperativity is explicitly introduced through a parameter representing the interaction between subunits, which is not required in the MWC model (Fig. 1.1B).

Different variations of these models have been proposed [13], including models that represent the MWC and KNF models as particular cases of a more general model with more states [14, 22].

From a general thermodynamic standpoint, a “state" is any ensemble of configurations associated with a minimum of free energy. Accordingly, some models interpret one of the states to represent the ensemble of unfolded configurations of a protein, as in the ensemble model of Hilser and Thompson [23]. In this model, each domain of a protein can exist in either a folded or unfolded state, with only the folded state being capable of binding ligand. In this model, interaction energies between domains are also introduced explicitly and depend on the state of the domains.

A change of state does not necessarily imply a structural difference: distinct states of thermodynamic models may share the same mean structural conformation. This point is

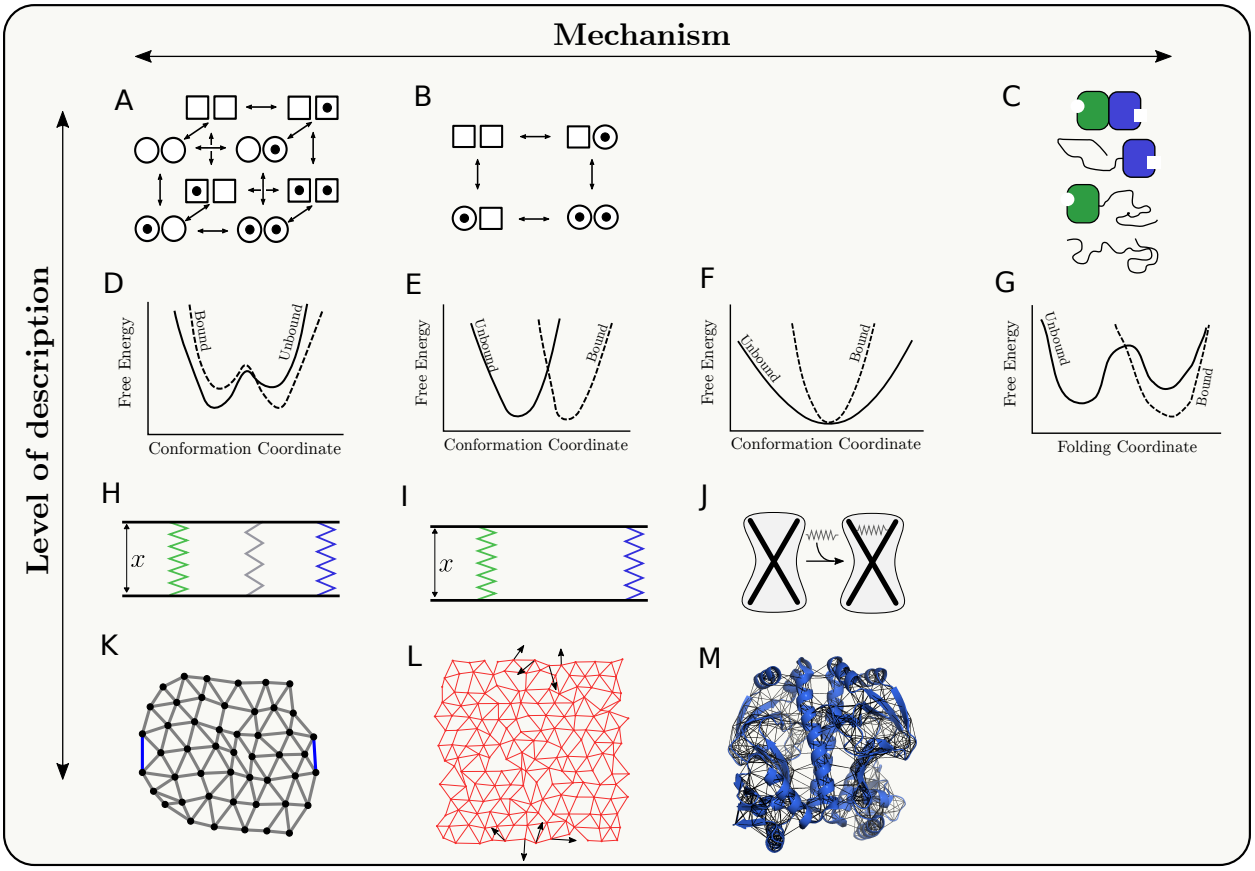

Figure 1.1: Variety of theoretical models of cooperativity. Each row organizes models by level of description: top row (A–C); thermodynamic models; second row (D–G); free energy landscapes; third row (H–J); minimal physical models; bottom row (K–M); microscopic physical models. Each column organizes models by mechanism: first column (A, D, H, K); conformational switch mechanism with pre-existing conformational states; second column (B, E, I, L); induced fit mechanism with one pre-existing conformational state where conformational changes are induced by ligand binding; third column (F, J, M); dynamic mechanism with one pre-existing conformational state where ligand binding stiffens the system without changing its mean conformation; fourth column (C, G); folding mechanism, where folded and unfolded states are in equilibrium and ligands can bind and stabilize the folded state. (A) MWC model [33]; (B) KNF model [27]; (C) ensemble model [23]; (D–G) commonly drawn free energy landscapes [2, 18, 52]; (H–I) minimal elastic models [45]; (J) scissor model [31]; (K) frustrated elastic network model [45]; (L) linear elastic network models [12, 57]; (M) elastic network derived from an experimentally determined structure [44].

illustrated through a calculation by Cooper and Dryden [7] where ligand binding only alters the fluctuations around a mean conformation that remains unchanged. This behavior is instantiated by a flexible protein that stiffens upon binding: the first ligand incurs an entropic penalty when binding, but not the second ligand that binds an already stiffened protein. This mechanism is often termed “entropic", “dynamic" or “dynamics-driven" allostery [7, 19, 25].

To illustrate thermodynamic models, free energy landscapes are often depicted along a coordinate with local minima representing the different states. The KNF model, where the protein exists in a single conformation for each ligation condition is, for instance, depicted by a free energy landscape with a single minimum. In this representation, ligand binding changes the location of the minimum (Fig. 1.1E), and cooperativity requires the minimum of the single-bound landscape (not shown) to be greater than the minimum of the unbound or doubly bound landscapes [2, 18, 55]. On the other hand, the MWC model is represented by a free energy landscape with two local minima that ligand binding tilts to change the height of the minima (Fig. 1.1D) [52, 5]. In this representation, cooperativity requires both minima of the single-bound landscape to be above the stable minima of the unbound and doubly-bound landscapes. The ensemble model can similarly be represented with two minima in the unbound state, for the folded and unfolded states, and a single minimum in the bound state (Fig. 1.1G). Finally, the dynamic mechanism is often depicted as a broad free energy basin that narrows upon ligand binding (Fig. 1.1F) [2, 18, 55].

Thermodynamic models and their corresponding free energy landscape representations describe different mechanisms of allostery but do not reveal the physical process by which allosteric transitions occur. A variety of other models have been proposed to fill this gap. Some models provide a conceptual description by using analogies, for instance, allostery has been compared to a domino-like chain reaction of side chains [25]. Such informal analogies to inertial macroscopic objects have, however, obvious limitations. Other models, based on evolutionary analyses of coevolution across homologous proteins, provide insights into

the structural organization of networks of amino acids involved in allostery [49, 41]. These analyses indicate that allostery is widespread beyond proteins known to be allosterically regulated, but they do not reveal the underlying physical processes. These limitations are overcome by physical models, defined by an energy landscape rather than a free energy landscape. Models of this sort fall into two classes: minimal models, which involve a minimal number of degrees of freedom, and microscopic models, which integrate a large number of degrees of freedom.

Minimal models provide the simplest physical instantiation of the different mechanisms of cooperativity. For instance, in previous work with Olivier Rivoire and Rama Ranganathan, I introduced a minimal model to compare the physical constraints behind the conformational switch and induced fit mechanisms [45]. The model consists of two rigid bars, connected by springs and constrained to a single degree of freedom (Fig. 1.1HI). Ligand binding is modeled as changing the rest length of a spring, which induces a conformational change. The difference between the conformational switch and induced fit mechanisms lies in the stiffness of a third spring that can cause bistability. This model reveals that the conformational switch mechanism is more effective than induced fit when accounting for the limited extent to which a ligand can perturb a protein. Similarly, McLeish and colleagues proposed a scissor model to study dynamic allostery [31]. Their model consists of two rigid bars connected at a hinge, allowing only rotation between them (Fig. 1.1J). Ligand binding is modeled by the addition of a harmonic spring that stiffens motions about the hinge, and the binding of a second ligand introduces another spring.

Microscopic models address how long-range cooperativity can emerge from the collective action of particles with short-range interactions. One common type of model in this class is disordered elastic networks, either derived from structural data or designed *in silico* to have an allosteric function. Their motivation extends beyond proteins, encompassing applications for designing allosteric materials [37] and for understanding generic properties of

genotype-to-phenotype maps [12]. In a study by Yan et al., such networks were optimized for long-range cooperativity by varying the location of springs within the network [57]. The resulting networks are characterized by a soft normal mode connecting the two distant binding sites and operate on an induced fit mechanism. Ligand binding, simulated through applied displacements at the binding sites, induces strain along this soft mode. Additionally, elastic networks have been employed to investigate the dynamic mechanism of cooperativity (Fig. 1.1M) [44, 51, 10]. These works, along with several others [43, 56, 17, 47, 48, 54], provide physical and geometrical insights into the mechanisms by which the effect of a perturbation propagates from one location to another in heterogeneous elastic materials.

Most studies of elastic network models are limited to the linear regime that excludes conformational switches, even though elastic networks are fundamentally nonlinear and have rugged landscapes that enable conformational switches. We previously took advantage of this possibility to examine the conditions that lead to the evolution of an induced fit or a conformational switch mechanism. Nonlinearity has also been introduced explicitly into elastic networks to account for conformational switches [40]. Alternatively, microscopic models have also been devised whose constituent elements are themselves switch-like, such as spin models, where the elementary degrees of freedom are in one of two discrete states [42]. These models can be seen as reflecting the different rotameric states of side chains, a feature shown to play a role in allostery [11].

Microscopic models differ not only by the nature of the interactions between constituents of the "proteins", but also by the nature of the interaction between proteins and ligands. In elastic networks, ligand binding has been modeled by imposed displacement [43, 57], imposed force [17, 12, 46], or a change in the rest length [45] or spring constant [19, 31, 46] of a bond, while in spin glass models, it is natural to treat ligand binding as an applied field [21, 42]. The implications of each modeling choice have, however, not been examined.

Finally, another class of computational models investigates allostery by means of molec-

ular dynamics simulations using interaction potentials tailored to quantitatively capture the properties of real proteins [28, 32, 29, 34]. These models aim to describe allostery in particular proteins, rather than to provide general principles. As such, they fall outside the scope of the models that we intend to unify, but we will discuss how the data they provide can be used to recognize the principle at play in specific proteins.

References

[1] G_ S_ Adair, AV Bock, and H Field Jr. The hemoglobin system: Vi. the oxygen dissociation curve of hemoglobin. *Journal of Biological Chemistry*, 63(2):529–545, 1925.

[2] Lalima G Ahuja, Susan S Taylor, and Alexandr P Kornev. Tuning the "violin" of protein kinases: The role of dynamics-based allostery. *IUBMB life*, 71(6):685–696, 2019.

[3] Christian Bohr, Karl Hasselbalch, and August Krogh. Über einen in biologischer beziehung wichtigen einfluss, den die kohlensäurespannung des blutes auf dessen sauerstoffbindung übt. *Skandinavisches Archiv für Physiologie*, 16:401–412, 1904. English translation by Ulf Marquardt for CHEM-342, January 1997.

[4] Charles R. Cantor and Paul R. Schimmel. *Biophysical Chemistry: Part I: The Conformation of Biological Macromolecules*. W. H. Freeman, San Francisco, 1980. ISBN 9780716711888.

[5] Jean-Pierre Changeux and Stuart Edelstein. Conformational selection or induced fit? 50 years of debate resolved. *F1000 biology reports*, 3, 2011.

[6] Jean-Pierre Changeux and Stuart J Edelstein. Allosteric mechanisms of signal transduction. *Science*, 308(5727):1424–1428, 2005.

[7] A Cooper and DTF Dryden. Allostery without conformational change: a plausible model. *European Biophysics Journal*, 11:103–109, 1984.

[8] Magali Cottevieille, Eric Larquet, Slavica Jonic, Maxim V Petoukhov, Gianluca Caprini, Stefano Paravisi, Dmitri I Svergun, Maria A Vanoni, and Nicolas Boisset. The subnanometer resolution structure of the glutamate synthase 1.2-mda hexamer by cryoelectron microscopy and its oligomerization behavior in solution: functional implications. *Journal of Biological Chemistry*, 283(13):8237–8249, 2008.

[9] Declan A Doyle, Alice Lee, John Lewis, Eunjoon Kim, Morgan Sheng, and Roderick MacKinnon. Crystal structures of a complexed and peptide-free membrane protein–binding domain: molecular basis of peptide recognition by pdz. *Cell*, 85(7):1067–1076, 1996.

[10] Igors Dubanevics and Tom CB McLeish. Computational analysis of dynamic allostery and control in the sars-cov-2 main protease. *Journal of the Royal Society Interface*, 18 (174):20200591, 2021.

[11] Kateri H DuBay, Jacques P Bothma, and Phillip L Geissler. Long-range intra-protein communication can be transmitted by correlated side-chain fluctuations alone. *PLoS computational biology*, 7(9):e1002168, 2011.

[12] Sandipan Dutta, Jean-Pierre Eckmann, Albert Libchaber, and Tsvi Tlusty. Green function of correlated genes in a minimal mechanical model of protein evolution. *Proceedings of the National Academy of Sciences*, 115(20):E4559–E4568, 2018.

[13] William A Eaton, Eric R Henry, James Hofrichter, Stefano Bettati, Cristiano Viappiani, and Andrea Mozzarelli. Evolution of allosteric models for hemoglobin. *IUBMB life*, 59 (8-9):586–599, 2007.

[14] Manfred Eigen. New looks and outlooks on physical enzymology. *Quarterly reviews of biophysics*, 1(1):3–33, 1968.

[15] J.D. Eshelby. The elastic interaction of point defects. *Acta Metallurgica*, 3(5):487–490, 1955. doi:10.1016/0001-6160(55)90140-1.

[16] Philip Richard Evans, GWt Farrants, and Peter John Hudson. Phosphofructokinase: structure and control. *Philosophical Transactions of the Royal Society of London. B, Biological Sciences*, 293(1063):53–62, 1981.

[17] Holger Flechsig. Design of elastic networks with evolutionary optimized long-range communication as mechanical models of allosteric proteins. *Biophysical journal*, 113(3): 558–571, 2017.

[18] Jingjing Guo and Huan-Xiang Zhou. Protein allostery and conformational dynamics. *Chemical reviews*, 116(11):6503–6515, 2016.

[19] Rhoda J Hawkins and Tom CB McLeish. Coarse-grained model of entropic allostery. *Physical review letters*, 93(9):098104, 2004.

[20] Kerstin Helmstaedt, Sven Krappmann, and Gerhard H Braus. Allosteric regulation of catalytic activity: Escherichia coli aspartate transcarbamoylase versus yeast chorismate mutase. *Microbiology and molecular biology reviews*, 65(3):404–421, 2001.

[21] Mathieu Hemery and Olivier Rivoire. Evolution of sparsity and modularity in a model of protein allostery. *Physical review E*, 91(4):042704, 2015.

[22] JUDITH HERzFELD and H Eugene Stanley. A general approach to co-operativity and its application to the oxygen equilibrium of hemoglobin and its effectors. *Journal of molecular biology*, 82(2):231–265, 1974.

[23] Vincent J Hilser and E Brad Thompson. Intrinsic disorder as a mechanism to optimize allosteric coupling in proteins. *Proceedings of the National Academy of Sciences*, 104 (20):8311–8315, 2007.

[24] Kenji Kamata, Morihiro Mitsuya, Teruyuki Nishimura, Jun-ichi Eiki, and Yasufumi Nagata. Structural basis for allosteric regulation of the monomeric allosteric enzyme human glucokinase. *Structure*, 12(3):429–438, 2004.

[25] Alexandr P Kornev and Susan S Taylor. Dynamics-driven allostery in protein kinases. *Trends in biochemical sciences*, 40(11):628–647, 2015.

[26] Daniel E Koshland Jr. The key–lock theory and the induced fit theory. *Angewandte Chemie International Edition in English*, 33(23-24):2375–2378, 1995.

[27] DE Koshland Jr, G Nemethy, and D Filmer. Comparison of experimental binding data and theoretical models in proteins containing subunits. *Biochemistry*, 5(1):365–385, 1966.

[28] Jue Li, Dong-Qing Wei, Jing-Fang Wang, and Yi-Xue Li. A negative cooperativity mechanism of human cyp2e1 inferred from molecular dynamics simulations and free energy calculations. *Journal of chemical information and modeling*, 51(12):3217–3225, 2011.

[29] Fengjiao Liu, John ZH Zhang, and Ye Mei. The origin of the cooperativity in the streptavidin-biotin system: A computational investigation through molecular dynamics simulations. *Scientific reports*, 6(1):27190, 2016.

[30] Lauren T May, Katie Leach, Patrick M Sexton, and Arthur Christopoulos. Allosteric modulation of g protein–coupled receptors. *Annu. Rev. Pharmacol. Toxicol.*, 47(1):1–51, 2007.

[31] Thomas CB McLeish, TL Rodgers, and Mark R Wilson. Allostery without conformation change: modelling protein dynamics at multiple scales. *Physical biology*, 10(5):056004, 2013.

[32] Hongqing Meng, Chaoqun Li, Yan Wang, and Guangju Chen. Molecular dynamics simulation of the allosteric regulation of eif4a protein from the open to closed state, induced by atp and rna substrates. *PloS one*, 9(1):e86104, 2014.

[33] Jacque Monod, Jeffries Wyman, and Jean-Pierre Changeux. On the nature of allosteric transitions: a plausible model. *J Mol Biol*, 12(1):88–118, 1965.

[34] Prithviraj Nandigrami and John J Portman. Coarse-grained molecular simulations of allosteric cooperativity. *The Journal of chemical physics*, 144(10), 2016.

[35] Roland R Netz. Inclusions in fluctuating membranes: Exact results. *Journal de Physique I*, 7(7):833–852, 1997.

[36] Karen M Ottemann, Wenzhong Xiao, Yeon-Kyun Shin, and Daniel E Koshland Jr. A piston model for transmembrane signaling of the aspartate receptor. *Science*, 285(5434): 1751–1754, 1999.

[37] Nidhi Pashine. Local rules for fabricating allosteric networks. *Physical Review Materials*, 5(6):065607, 2021.

[38] Chad M Petit, Jun Zhang, Paul J Sapienza, Ernesto J Fuentes, and Andrew L Lee. Hidden dynamic allostery in a pdz domain. *Proceedings of the National Academy of Sciences*, 106(43):18249–18254, 2009.

[39] Kristen L Pierce, Richard T Premont, and Robert J Lefkowitz. Seven-transmembrane receptors. *Nature reviews Molecular cell biology*, 3(9):639–650, 2002.

[40] Riccardo Ravasio, Solange Marie Flatt, Le Yan, Stefano Zamuner, Carolina Brito, and Matthieu Wyart. Mechanics of allostery: contrasting the induced fit and population shift scenarios. *Biophysical journal*, 117(10):1954–1962, 2019.

[41] Kimberly A Reynolds, Richard N McLaughlin, and Rama Ranganathan. Hot spots for allosteric regulation on protein surfaces. *Cell*, 147(7):1564–1575, 2011.

[42] Olivier Rivoire. Parsimonious evolutionary scenario for the origin of allostery and co-evolution patterns in proteins. *Physical Review E*, 100(3):032411, 2019.

[43] Jason W Rocks, Nidhi Pashine, Irmgard Bischofberger, Carl P Goodrich, Andrea J Liu, and Sidney R Nagel. Designing allostery-inspired response in mechanical networks. *Proceedings of the National Academy of Sciences*, 114(10):2520–2525, 2017.

[44] Thomas L Rodgers, Philip D Townsend, David Burnell, Matthew L Jones, Shane A Richards, Tom CB McLeish, Ehmke Pohl, Mark R Wilson, and Martin J Cann. Modulation of global low-frequency motions underlies allosteric regulation: demonstration in crp/fnr family transcription factors. *PLoS biology*, 11(9):e1001651, 2013.

[45] Eric Rouviere, Rama Ranganathan, and Olivier Rivoire. Emergence of single-versus multi-state allostery. *PRX Life*, 1(2):023004, 2023.

[46] Midas Segers, Aderik Voorspoels, Takahiro Sakaue, and Enrico Carlon. Mechanisms of dna-mediated allostery. *arXiv preprint arXiv:2305.03962*, 2023.

[47] Menachem Stern, Daniel Hexner, Jason W Rocks, and Andrea J Liu. Supervised learning in physical networks: From machine learning to learning machines. *Physical Review X*, 11(2):021045, 2021.

[48] Menachem Stern, Andrea J Liu, and Vijay Balasubramanian. Physical effects of learning. *Physical Review E*, 109(2):024311, 2024.

[49] Gürol M Süel, Steve W Lockless, Mark A Wall, and Rama Ranganathan. Evolutionarily conserved networks of residues mediate allosteric communication in proteins. *Nature structural biology*, 10(1):59–69, 2003.

[50] Marc Taraban, Hongli Zhan, Andrew E Whitten, David B Langley, Kathleen S Matthews, Liskin Swint-Kruse, and Jill Trewhella. Ligand-induced conformational changes and conformational dynamics in the solution structure of the lactose repressor protein. *Journal of molecular biology*, 376(2):466–481, 2008.

[51] Philip D Townsend, Thomas L Rodgers, Ehmke Pohl, Mark R Wilson, Tom CB McLeish, and Martin J Cann. Global low-frequency motions in protein allostery: Cap as a model system. *Biophysical reviews*, 7:175–182, 2015.

[52] Chung-Jung Tsai and Ruth Nussinov. A unified view of "how allostery works". *PLoS computational biology*, 10(2):e1003394, 2014.

[53] Brian F Volkman, Doron Lipson, David E Wemmer, and Dorothee Kern. Two-state allosteric behavior in a single-domain signaling protein. *Science*, 291(5512):2429–2433, 2001.

[54] Maximilian Vossel, Bert L de Groot, and Aljaž Godec. The allosteric lever: towards a principle of specific allosteric response. *arXiv preprint arXiv:2311.12025*, 2023.

[55] Nan Wu, Mauricio Barahona, and Sophia N Yaliraki. Allosteric communication and signal transduction in proteins. *Current Opinion in Structural Biology*, 84:102737, 2024.

[56] Le Yan, Riccardo Ravasio, Carolina Brito, and Matthieu Wyart. Architecture and coevolution of allosteric materials. *Proceedings of the National Academy of Sciences*, 114(10):2526–2531, 2017.

[57] Le Yan, Riccardo Ravasio, Carolina Brito, and Matthieu Wyart. Principles for optimal cooperativity in allosteric materials. *Biophysical journal*, 114(12):2787–2798, 2018.

CHAPTER 2

GENERAL THEORY OF COOPERATIVE ALLOSTERY

ABSTRACT

Allostery is a basic property of proteins that represents the functional coupling of distantly positioned amino acids. In different manifestations, this property underlies signal transmission, cooperative binding, regulation, and evolvability—the elementary features of molecular processes in living cells. While thermodynamic models have provided excellent abstract phenomenological descriptions and classifications of allostery, we lack comparable descriptions and classifications of the underlying physical principles. Here we use simple models amenable to analytical calculations to elucidate these principles and show that they provide a unifying link between phenomenological models and the atomistic details of intramolecular communication in specific systems. All forms of allostery are thus recast as special combinations of two core principles. The organization of allostery by these principles may provide a simpler and more universal language to describe the physics of allostery in proteins.

This project was conceived by me with guidance from Olivier Rivoire and Rama Ranganathan. I performed all of the calculations and analyses. This work will soon be submitted and is currently available at arXiv:2411.06519

2.1 Introduction

While allostery is most often associated with biomolecules, it is a purely physical phenomenon. However, a physical theory that describes how many short-range interactions in a material collectively give rise to specific long-range couplings in a system remains missing. Because of this, several fundamental questions remain unanswered. What are the different types of allosteric mechanisms? Are some types better suited for specific tasks, for example, what is the best mechanism for very long-range tasks, or those where the perturbation of ligand binding is quite subtle? In the context of proteins where data are available, it is not clear what features are the essential ones versus those that are a specific detail only relevant to the particular system.

At its essence, allostery describes the thermodynamic coupling of two sites of a protein when they do not directly interact. This coupling, often termed cooperativity, is a thermodynamic phenomenon, and thus its existence is agnostic to the physical mechanism through which it is implemented.

Various theoretical models have been proposed to explain allostery, each differing in their level of physical detail. At the most abstract level, thermodynamic (or phenomenological) models reduce the high-dimensional conformational space that proteins sample into a few discrete states and define rules for the free energy of each state [35, 25, 20, 13, 12, 21, 60]. While these models have successfully explained and fit data [35, 25, 20, 59, 29], they lack the detail needed to describe the physics of allosteric mechanisms.

On the other hand, molecular dynamics models define the chemical interactions between all atoms, enabling granular descriptions of the sequence of motions in allosteric transitions [30, 2, 27]. However, this level of detail makes it challenging to separate general principles from features unique to individual proteins.

Between these two extremes exist reduced physical models that assume simplified interactions between coarse-grained amino acid groups. A common example is elastic network models, where amino acid groups interact through ideal springs, and structural motions are approximated within linear response [53, 23, 3]. These simplifications allow for exact calculation of the allosteric cooperativity between binding sites [34, 11, 58]. However, a drawback of these models is that they often rely on assumptions that limit the range of possible allosteric behaviors. For instance, the linear response approximation in elastic networks prevents the existence of multiple metastable conformational states.

The wide variety of models has led to numerous proposed forms of allostery, each emphasizing different key physical behaviors, such as multiple conformational states [35, 54, 40, 42, 44], changes in protein dynamics upon binding [8, 18, 34], and folding and intrinsic disorder [21]. What remains unclear is how these different models of allostery relate to one

another. Are they simply alternative implementations of the same underlying principle, or do they rely on fundamentally distinct principles? If the latter, how many unique principles can enable allostery?

To address these questions, we present a physical framework in which a protein has two non-overlapping binding sites and investigate the conditions in which ligand binding is allosterically coupled. We assume a generic form of an energy landscape that can approximate any protein, and show that only two physical principles can enable allostery. The first principle is to have soft normal modes (low-energy correlated motions around a structure) that couple the two sites with ligand binding, engaging the same modes from both sites. This is the only solution when a protein's energy landscape is described by a single energy basin. The second principle requires two or more states that bind ligands with different affinities—the same principle described by the well-known MWC model [35]. We show that different physical implementations of each principle correspond to previously proposed forms of allostery.

Previous works have unified allosteric models at the thermodynamic level [13, 20, 22, 60], however, this level of description lacks the notion of normal modes. Consequently, the soft mode principle is missed and forms of allostery that depend on this principle [8, 18, 34, 61, 56, 43, 57, 58, 11] are not described by these unifications. By considering generic energy landscapes, we overcome this limitation and make inroads toward a general physical theory of allostery.

2.2 Formulation of allosteric cooperativity at the energy landscape level

Several proposals have been made to quantitatively define allostery, including structural [57], catalytic (V systems) [35], and information-theoretic [32] definitions. However, the most widely used and most biologically relevant quantity is a thermodynamic one, termed

cooperativity (a.k.a. thermodynamic coupling [9] or allosteric efficiency [19]), which quantifies how the energetic impact of one perturbation depends on the application of another perturbation.

We deliberately consider one of the simplest microscopic models of allosteric cooperativity. The model consists of N beads that take the role of amino acids in a protein (Fig. 2.1A). Beads interact with each other through a potential $U_p(\mathbf{r})$ that is a function of the bead coordinates $\mathbf{r} = (\mathbf{r}_1, \mathbf{r}_2, \ldots, \mathbf{r}_N)$, where $\mathbf{r}_i = (x_i, y_i, z_i)$.

Ligand binding is treated as a perturbation of U_p and acts only on the few beads that define each binding site. The first binding site, labeled site a, is defined by a set of beads $\mathcal{B}_a$, and the ligand binding perturbation at this site is given by a function $V_a(\mathbf{r}_a)$ where $\mathbf{r}_a = \{\mathbf{r}_i\}$ for $i \in \mathcal{B}_a$. Similarly, the second binding site, b, is comprised of beads in $\mathcal{B}_b$, and the perturbation on this site is given by $V_b(\mathbf{r}_b)$ where $\mathbf{r}_b = \{\mathbf{r}_i\}$ for $i \in \mathcal{B}_b$. To describe allosteric cooperativity the sites are taken to have no overlap, $\mathcal{B}_a \cap \mathcal{B}_b = \emptyset$. To simplify notation in the main text, we write V_a and V_b as functions of all the degrees of freedom $\mathbf{r}$, with it implied that only the binding site degrees of freedom are acted upon.

With indicator variables σ_a, σ_b that take value 1 if the ligand is bound to the site and 0 if unbound, we can write the energy landscapes of the four binding conditions (unbound: $\sigma_a = \sigma_b = 0$, bound at a: $\sigma_a = 1, \sigma_b = 0$, bound at b: $\sigma_a = 0, \sigma_b = 1$ and doubly bound: $\sigma_a = \sigma_b = 1$) as

$$U_{\sigma_a\sigma_b}(\mathbf{r}) = U_p(\mathbf{r}) + \sigma_a V_a(\mathbf{r}_a) + \sigma_b V_b(\mathbf{r}_b). \tag{2.1}$$

The partition function for each energy is $Z_{\sigma_a\sigma_b} = h_0^{-dN} \int d\mathbf{r} \exp(-\beta U_{\sigma_a\sigma_b})$ and the corresponding free energy is $F_{\sigma_a\sigma_b} = -\beta^{-1} \log Z_{\sigma_a\sigma_b}$. We choose units where $h_0 = 1$, and it is omitted going forward. Binding cooperativity measures the extent to which binding at one site changes the binding free energy at the other site and is defined as

$$\Delta\Delta F = F_{10} + F_{01} - F_{11} - F_{00} = -\frac{1}{\beta} \log \left[\frac{Z_{10} Z_{01}}{Z_{00} Z_{11}} \right]. \tag{2.2}$$

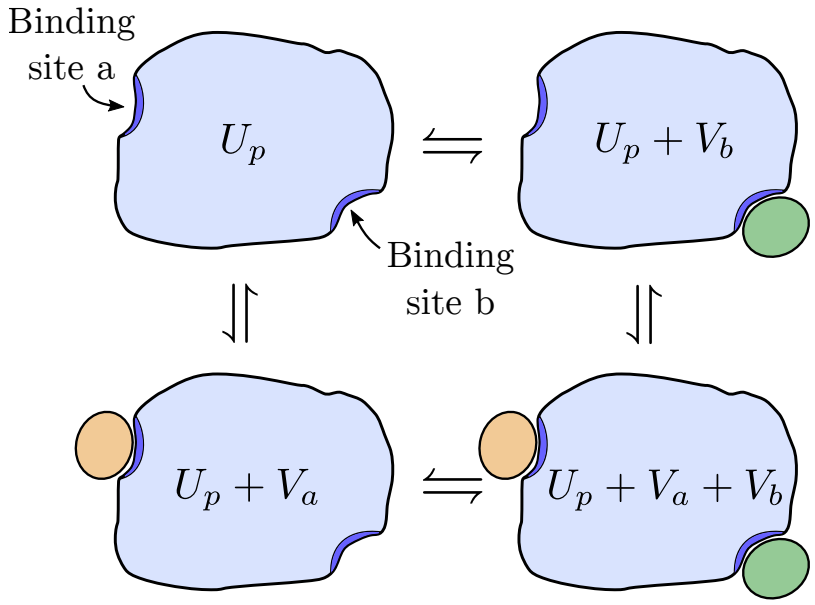

Figure 2.1: The model considers a protein with two binding sites, a and b, resulting in four distinct ligation states: apo, bound at a, bound at b, and doubly bound. Ligand binding at sites a and b perturbs the protein's energy landscape, U_p, by V_a and V_b, respectively.

This definition establishes positive cooperativity when $\Delta\Delta F > 0$ and negative cooperativity when $\Delta\Delta F < 0$. Since the free energy is the sum of energetic and entropic contributions $F = E - TS$, the cooperativity also decomposes into energetic and entropic contributions $\Delta\Delta F = \Delta\Delta E - T\Delta\Delta S$. In this model, the different mechanisms previously studied are associated with different choices of the protein potential U_p and ligand potentials V_a, V_b.

2.3 Condition for nonzero cooperativity

Before considering more specific cases, we show here that a general condition must be satisfied for cooperativity to be possible, regardless of the type of ligand perturbation. At each binding site, we defined a linear collective variable (CV),

$$X_a(\mathbf{r}) = \mathbf{u}_a^\top \mathbf{r}, \quad X_b(\mathbf{r}) = \mathbf{u}_b^\top \mathbf{r}. \tag{2.3}$$

Here $\mathbf{u}_a$ and $\mathbf{u}_b$ are dimensionless unit vectors that have nonzero entries only on beads in $\mathcal{B}_a$ and $\mathcal{B}_b$, respectively, and describe a single mode of each binding site. We assume that ligands interact with the protein only along the collective variables,

$$V_a(\mathbf{r}) = g_a(X_a(\mathbf{r})), \quad V_b(\mathbf{r}) = g_b(X_b(\mathbf{r})) \tag{2.4}$$

The results of this calculation hold for the more general case of arbitrary V_a, V_b (Appendix). The partition functions can now be expressed as

$$Z_{\sigma_a\sigma_b} = \int dx_a e^{-\sigma_a\beta g_a(x_a)} \int dx_b e^{-\sigma_b\beta g_b(x_b)} \tilde{Z}(x_a, x_b), \tag{2.5}$$

$$\tilde{Z}(x_a, x_b) = \int d\mathbf{r}\delta(\mathbf{u}_a^\top \mathbf{r} - x_a)\delta(\mathbf{u}_b^\top \mathbf{r} - x_b)e^{-\beta U_p(\mathbf{r})}. \tag{2.6}$$

Taking the log of $\tilde{Z}$ gives a so-called free energy surface of the unperturbed system as a function of the binding site collective variables,

$$\tilde{F}(x_a, x_b) = -\beta^{-1} \log \tilde{Z}(x_a, x_b). \tag{2.7}$$

If $\tilde{F}$ is separable, $\tilde{F}(x_a, x_b) = \tilde{F}_a(x_a) + \tilde{F}_b(x_b)$, both $\tilde{Z}(x_a, x_b)$ and $Z_{\sigma_a\sigma_b}$ factor, leading to no cooperativity: $\Delta\Delta F = 0$. Cooperativity therefore requires $\tilde{F}$ to be non-separable. This implies that the potential for allostery lies in the "protein" landscape U_p even before the details of the ligand perturbations are specified.

2.3.1 A General Multi-State Model

We assume the energy landscape of a protein may be complex with an arbitrary number of minima. The shape of the energy landscape around each energy minimum $\mathbf{R}_i$ can be approximated by expanding to second order, $U_p(\mathbf{r}) \approx \epsilon_i + \frac{1}{2}(\mathbf{r} - \mathbf{R}_i)^\top H_i(\mathbf{r} - \mathbf{R}_i)$, with $\epsilon_i = U_p(\mathbf{R}_i)$ where $H_i = \nabla\nabla^\top U_p|_{\mathbf{r}=\mathbf{R}_i}$ is the Hessian of U_p at $\mathbf{R}_i$. By treating each local

basin as a state, the full energy landscape can be approximated by summing over the basins,

$$U_p(\mathbf{r}) \approx F_p(\mathbf{r}) = -\frac{1}{\beta} \log \left(\sum_{i=1}^{n} e^{-\beta \frac{1}{2} (\mathbf{r}-\mathbf{R}_i)^\top H_i (\mathbf{r}-\mathbf{R}_i) + \epsilon_i} \right). \tag{2.8}$$

This form accurately approximates the regions of an energy landscape that contribute most to the free energy—around the energy minima. The corresponding free energy surface (derived in the Appendix) is,

$$\tilde{F}(x_a, x_b) = -\frac{1}{\beta} \log \left(\sum_{i=1}^{n} C_i e^{-\beta (\frac{1}{2} \mathbf{x}_i^\top A_i^{-1} \mathbf{x}_i + \epsilon_i)} \right), \tag{2.9}$$

where

$$\mathbf{x}_i = \begin{pmatrix} x_a - \mathbf{u}_a^\top \mathbf{R}_i \\ x_b - \mathbf{u}_b^\top \mathbf{R}_i \end{pmatrix}, \text{ and } A_i = \begin{pmatrix} \mathbf{u}_a^\top H_i^+ \mathbf{u}_a & \mathbf{u}_a^\top H_i^+ \mathbf{u}_b \\ \mathbf{u}_a^\top H_i^+ \mathbf{u}_b & \mathbf{u}_b^\top H_i^+ \mathbf{u}_b \end{pmatrix}, \tag{2.10}$$

and

$$C_i = \sqrt{\frac{(2\pi)^{dN-2}}{h_0^{2(dN-2)} \beta^{dN-2} \det(A_i) \det(H_i)}} \tag{2.11}$$

is a constant for each state i. Here H_i^+ is the pseudo-inverse of H_i. Cooperativity can only occur when (2.9) is not separable, which can occur in two independent ways.

The first way is a property of the curvature of each basin and is most easily seen when only one basin exists, $n = 1$ (for notation we omit the subscripts). In this case, the free energy surface, up to an additive constant, simplifies to $\tilde{F}(x_a, x_b) = \frac{1}{2} \mathbf{x}^\top A^{-1} \mathbf{x}$, and is non-separable only when $|\mathbf{u}_a^\top H^+ \mathbf{u}_b| > 0$. Physically, $\mathbf{u}_a^\top H^+ \mathbf{u}_b$ represents the correlation between the collective variables of the two binding sites. Diagonalizing H^+ expresses this term in normal modes, $\mathbf{u}_a^\top H^+ \mathbf{u}_b = \mathbf{u}_a^\top Q \Lambda^+ Q^\top \mathbf{u}_b$. The columns of Q are the normal modes of H and thus $Q^\top \mathbf{u}_a$ and $Q^\top \mathbf{u}_b$ describe the overlap of the ligand binding motion with each normal mode. Λ is a diagonal matrix whose entries give the stiffnesses of each normal mode.

When $\mathbf{u}_a^\top H^+ \mathbf{u}_b$ is small, the cooperativity scales as $\Delta\Delta F \sim \mathbf{u}_a^\top H^+ \mathbf{u}_b$ (Appendix). This

result implies that when a protein's energy landscape is well described by a single quadratic potential, allostery can only occur when the binding sites are coupled through the normal modes. Furthermore, the contribution of a mode is inversely proportional to its stiffness, making the softest modes the main contributors of cooperativity. We refer to this as the soft mode principle.

The second way cooperativity can occur is when there are multiple, distinct states ($n > 1$). In this case, there are many conditions when $\tilde{F}$ is non-separable even when the binding sites are uncoupled within each state $\mathbf{u}_a^\top H_i^+ \mathbf{u}_b = 0$. For example, in a two-state landscape, cooperativity is possible when the minima are separated in both x_a and x_b (i.e. $\mathbf{u}_a^\top \mathbf{R}_1 \neq \mathbf{u}_a^\top \mathbf{R}_2$ and $\mathbf{u}_b^\top \mathbf{R}_1 \neq \mathbf{u}_b^\top \mathbf{R}_2$), or when the conformational fluctuations at the binding sites differ in the two states, (i.e. $\mathbf{u}_a^\top H_1^+ \mathbf{u}_a \neq \mathbf{u}_a^\top H_2^+ \mathbf{u}_a$ and $\mathbf{u}_b^\top H_1^+ \mathbf{u}_b \neq \mathbf{u}_b^\top H_2^+ \mathbf{u}_b$).

This case, where multiple states exist and within each state the binding sites are uncoupled ($\mathbf{u}_a^\top H_i^+ \mathbf{u}_b = 0$), corresponds to the key features of the MWC model. We refer to these features as the MWC principle.

This calculation shows that even without describing the physical nature of the ligand perturbations g_a, g_b, one of two physical principles must hold for cooperativity to arise—through soft modes that couple binding sites within a single state (soft mode principle) or by having multiple distinct states (MWC principle).

In the following sections of this chapter, we consider specific cases for U_p and V_a, V_b and solve for cooperativity.

2.4 Quadratic landscape with first and second order perturbations.

What cooperative mechanisms can arise solely from local changes around the minimum of a single basin? To investigate this, we consider the $n = 1$ case of (2.8) with $\mathbf{R}_1 = \mathbf{0}$ and

$\epsilon_1 = 0$ for convenience,

$$U_p = U_{\text{quad}} = \frac{1}{2}\mathbf{r}^\top H \mathbf{r}. \tag{2.12}$$

For the ligand potentials (2.4), we consider polynomials up to second order, $g_a(x) = \frac{1}{2}k_a x^2 - f_a x + c_a$ and $g_b(x) = \frac{1}{2}k_b x^2 - f_b x + c_b$. The constant terms do not affect the cooperativity and are set to zero going forward. The full partition function becomes,

$$Z_{\sigma_a \sigma_b} = C \int dx_a e^{-\sigma_a \beta g_a(x_a)} \int dx_b \; e^{-\sigma_b \beta g_b(x_b)} e^{-\frac{1}{2}\beta \mathbf{x}^\top A^{-1} \mathbf{x}} \tag{2.13}$$

Here, C is a constant that has the constant term of (2.9) folded into it. With the partition functions, the cooperativity (2.2) can be solved but takes a lengthy analytical form and is left in the Appendix. Of interest, are the limits that correspond to different ligand perturbation conditions.

2.4.1 Applied Force

When ligand binding is modeled as a constant force, ($k_a = k_b = 0$ giving $V_a(\mathbf{r}) = -f_a \mathbf{u}_a^\top \mathbf{R}$, $V_b(\mathbf{r}) = -f_b \mathbf{u}_b^\top \mathbf{R}$), the cooperativity reduces to (2.14).

Applied Force Limit

When $k_a = k_b = 0$,

$$\Delta\Delta F = f_a f_b \mathbf{u}_a^\top H^+ \mathbf{u}_b. \tag{2.14}$$

(2.14) indicates that cooperativity occurs when there are normal modes that couple the binding sites and when the ligand applies forces that push on the same modes in the same direction. Within the context of a particular physical system, structural rigidity imposes constraints on the normal mode structure. In particular, as a folded protein must maintain some stiffness, cooperativity is optimized by making only some modes softer. Negative cooperativity $\Delta\Delta F < 0$ is optimized under the same conditions as positive cooperativity,

except that ligand forces must push the soft modes in opposite directions. In both cases, the cooperativity is purely energetic with no change in entropy upon ligand binding $\Delta\Delta F = \Delta\Delta E$. This form of cooperativity, previously calculated in different quadratic allosteric models [19, 11, 48, 4] follows the induced fit (IF) mechanism: ligands induce a conformational change through applying a force, each of the energy landscapes has a single minimum, ligand binding results in the translation of the minimum and there is a notion of a direct physical coupling between sites, here mediated through the soft modes.

Recent work has shown that linear elastic networks can be optimized for long-range allosteric tasks by varying the stiffness of the bonds [43, 57, 58, 14, 11, 44]. These models operate on the induced fit mechanism: an applied force or displacement of a few beads induces strain along one or several soft modes spanning the network, connecting a distant site.

2.4.2 Applied Stiffness

Next, we consider second order ligand perturbations ($f_a = f_b = 0$, giving $V_a(\mathbf{r}) = \frac{1}{2}k_a(\mathbf{u}_a^\top \mathbf{r})^2$ and $V_b(\mathbf{r}) = \frac{1}{2}k_b(\mathbf{u}_b^\top \mathbf{r})^2$), thereby purely stiffening binding sites. In terms of proteins, this may correspond to binding a ligand that perfectly fits the geometry of the binding sites, thereby not causing a change in conformation. In this case, the cooperativity is given by:

Applied Stiffness Limit

When $f_a = f_b = 0$,

$$\Delta\Delta F = -\frac{1}{2\beta}\log\left(1 - \frac{k_a k_b \left(\mathbf{u}_a^\top H^+ \mathbf{u}_b\right)^2}{(1 + k_a \mathbf{u}_a^\top H^+ \mathbf{u}_a)(1 + k_b \mathbf{u}_b^\top H^+ \mathbf{u}_b)}\right). \tag{2.15}$$

When both ligands stiffen (or soften) $k_a k_b > 0$, cooperativity can only be positive and requires the term $\mathbf{u}_a^\top H^+ \mathbf{u}_b$ to be non-zero. This indicates that soft modes must couple binding

sites and that ligand binding must stiffen the same soft modes. This corresponds to the dynamic (or entropic) mechanism proposed by Cooper and Dryden [8] and studied extensively in minimal models and elastic networks by McLeish and colleagues[18, 34]. Additionally, this dynamic mechanism has been considered in a 1D model of allostery in DNA [48]. Negative cooperativity can occur when ligand binding stiffens one site but softens the other, $k_a k_b < 0$. Regardless of sign, this cooperativity is purely entropic, $\Delta\Delta F = -T\Delta\Delta S$.

2.4.3 Imposed Displacement

Another limit of interest is when both the stiffnesses and forces diverge, $|k_i| \to \infty$, $|f_i| \to \infty$, such that the ratio $f_i/k_i = d_i$ remains finite, $0 < |d_i| < \infty$. In fact, this case corresponds to adding a rigid spring that causes displacement d_i along the binding site CV x_i. In these quantities $i \in \{a, b\}$. Since the x_i degree of freedom cannot vary after ligand binding, the entropy (and thus the entropic contribution to the cooperativity) diverges; however, the energetic contribution to the cooperativity, $\Delta\Delta E$ remains finite.

Imposed Displacement Limit

When $|k_i| \to \infty$, $|f_i| \to \infty$ such that $d_i = f_i/k_i$ remains finite, $0 < |d_i| < \infty$, for $i \in \{a, b\}$,

$$\begin{aligned}\Delta\Delta E = &\frac{(\mathbf{u}_a^\top H^+ \mathbf{u}_b)^2 \left((\mathbf{u}_b^\top H^+ \mathbf{u}_b) d_a^2 + (\mathbf{u}_a^\top H^+ \mathbf{u}_a) d_b^2\right)}{2(\mathbf{u}_a^\top H^+ \mathbf{u}_a)(\mathbf{u}_b^\top H^+ \mathbf{u}_b)\left((\mathbf{u}_a^\top H^+ \mathbf{u}_b)^2 - (\mathbf{u}_a^\top H^+ \mathbf{u}_a)(\mathbf{u}_b^\top H^+ \mathbf{u}_b)\right)} \\ &- \frac{2(\mathbf{u}_a^\top H^+ \mathbf{u}_b)(\mathbf{u}_a^\top H^+ \mathbf{u}_a)(\mathbf{u}_b^\top H^+ \mathbf{u}_b) d_a d_b}{2(\mathbf{u}_a^\top H^+ \mathbf{u}_a)(\mathbf{u}_b^\top H^+ \mathbf{u}_b)\left((\mathbf{u}_a^\top H^+ \mathbf{u}_b)^2 - (\mathbf{u}_a^\top H^+ \mathbf{u}_a)(\mathbf{u}_b^\top H^+ \mathbf{u}_b)\right)}\end{aligned} \tag{2.16}$$

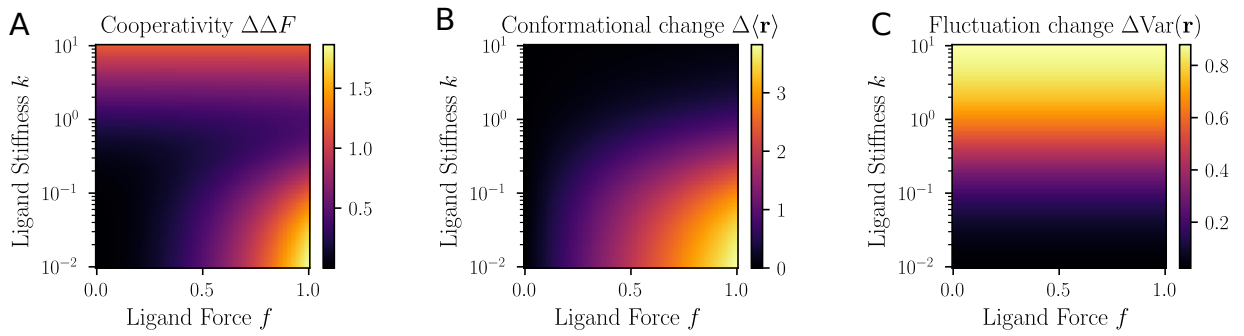

Figure 2.2: Cooperativity with quadratic landscapes. (a) Cooperativity $\Delta\Delta F$, (b) the mean conformational change upon ligand binding $\Delta\langle\mathbf{r}\rangle$, and (c) the change in the magnitude of fluctuations upon ligand binding $\Delta\mathrm{Var}(\mathbf{r})$, of a quadratic model with a soft mode where ligand binding can apply a force of magnitude f, stiffen with magnitude k or both. The two types of perturbation at each site (force and stiffness) act on the same soft mode that couples the sites. With quadratic landscapes, different types of ligand perturbations can drive cooperativity; applying a force results in a conformational change, while stiffening changes the magnitude of fluctuations. Parameter values for the figure are given in the Appendix.

2.4.4 Discussion of different soft mode mechanisms.

Both the induced fit (force) and dynamic (stiffness) mechanisms operate on the soft mode principle—binding sites coupled through soft normal modes—the difference lies in the details of the ligand binding interaction. In the general case, the ligand perturbations can be composed of both force and stiffness, however, the cooperativity does not take a simple analytical form (Appendix). We graphically represent $\Delta\Delta F$ for the model under a range of ligand stiffnesses $k = k_a = k_b$ and forces $f = f_a = f_b$. Fig. 2.2A shows two regions of cooperativity, one where force dominates, corresponding to the induced fit mechanism, and the other where stiffness dominates, corresponding to the dynamic mechanism.

While these two mechanisms operate on the same soft mode principle, physical features differ. This is apparent when representing the change in the mean conformation between the apo (00) and doubly bound (11) conditions, $\Delta\langle\mathbf{r}\rangle = \|\langle\mathbf{r}\rangle_{11} - \langle\mathbf{r}\rangle_{00}\|$ (here the subscript of the angle brackets denotes the ligation condition in which the average is taken). A conformational change occurs in the induced fit regime (Fig. 2.2B). The other

regime recapitulates the “allostery without a conformational change" feature of dynamic allostery. However, this regime shows large changes in root mean squared fluctuations $\Delta\mathrm{Var}(\mathbf{r}) = \left|\sqrt{\langle\mathbf{r}^2\rangle_{11} - \langle\mathbf{r}\rangle_{11}^2} - \sqrt{\langle\mathbf{r}^2\rangle_{00} - \langle\mathbf{r}\rangle_{00}^2}\right|$ upon binding of both ligands (Fig. 2.2C).

2.5 Allostery beyond linear response

Bistable Models

What new mechanisms of cooperativity are possible when the landscape has multiple states? The calculation above (ending with (2.9)) showed that when minima are separated in conformational space ($\mathbf{u}_a^\top\mathbf{R}_i \neq \mathbf{u}_a^\top\mathbf{R}_j$ and $\mathbf{u}_b^\top\mathbf{R}_i \neq \mathbf{u}_b^\top\mathbf{R}_j$, for at least one pair of states i, j), the free energy surface $\tilde{F}$ is non-separable, allowing for cooperativity. To explore this, we minimally extend the quadratic energy landscape ((2.12)) to introduce two basins in a manner that retains analytical tractability,

$$U_{\mathrm{bi}}(\mathbf{r}) = \frac{1}{2}\mathbf{r}^\top H\mathbf{r} - |\mathbf{g}^\top\mathbf{r}| - \mathbf{h}^\top\mathbf{r}. \tag{2.17}$$

Here, bistability is introduced through the absolute value term with minima at $\mathbf{R}_1 = H^+(\mathbf{h}+\mathbf{g})$ and $\mathbf{R}_2 = H^+(\mathbf{h}-\mathbf{g})$. Each minimum retains a quadratic basin with curvature H, and an additional linear term $\mathbf{h}^\top\mathbf{r}$ tilts the landscape, enabling one minimum to be lower energy than the other.

When a ligand applies a force ($V_a(\mathbf{r}) = -f_a\mathbf{u}_a^\top\mathbf{r}$, $V_b(\mathbf{r}) = -f_b\mathbf{u}_b^\top\mathbf{r}$), the cooperativity takes a lengthy analytical form. However, the essential principles can be illustrated in the zero temperature limit where the free energy converges to the ground state energy ($F \to E$

as $\beta \to \infty$) . In this case, the ground state cooperativity is,

$$\begin{aligned}\Delta\Delta E = & f_a f_b \mathbf{u}_a^\top H^+ \mathbf{u}_b \\ & + \left|(f_a \mathbf{u}_a + f_b \mathbf{u}_b + \mathbf{h})^\top H^+ \mathbf{g}\right| + \left|\mathbf{h}^\top H^+ \mathbf{g}\right| \\ & - \left|(f_a \mathbf{u}_a + \mathbf{h})^\top H^+ \mathbf{g}\right| - \left|(f_b \mathbf{u}_b + \mathbf{h})^\top H^+ \mathbf{g}\right|.\end{aligned} \tag{2.18}$$

The most important feature is that cooperativity has two components: an induced fit term identical to (2.14) for the single state case and new terms that depend on the bistability parameter $\mathbf{g}$. These extra terms describe a mechanism in which the forces $f_a \mathbf{u}_a$ and $f_b \mathbf{u}_b$ communicate by coupling to the bistable switch, induced when $\|\mathbf{g}\| > 0$. Since the cooperativity scales with the bistable parameter, $\Delta\Delta E$ can be arbitrarily large, irrespective of the strength of the perturbations, f_a, f_b. The contribution from the bistability is maximized when one minimum has initially lower energy, and the ligand forces push the system to stabilize the other minimum, an implementation of the MWC principle. This mechanism of allostery has been called population shift [54, 40]. However, we refer to it as the conformational switch mechanism as it makes clear that there is a physical switch (a transition between two or more states) and that these states differ by their conformation. Negative cooperativity emerges when the minima initially have equal energy and the ligand forces push the system in opposite directions.

In Fig. 2.3B, we show the cooperativity at nonzero temperature ($\beta = 1$) of a system with an internal mode that couples ligand binding sites with stiffness λ. The conformational switch has magnitude $\|\mathbf{g}\|$ under conditions where ligands apply a force. The data show that as in the zero temperature case, cooperativity can be achieved exclusively through the soft mode principle (2.3B bottom left), the MWC principle by influencing the conformational switch (2.3B top right), or a combination of the two (2.3B bottom right). When cooperativity emerges solely from the conformational switch (no soft mode contribution), the system can be analytically written exactly as an MWC model (SI).

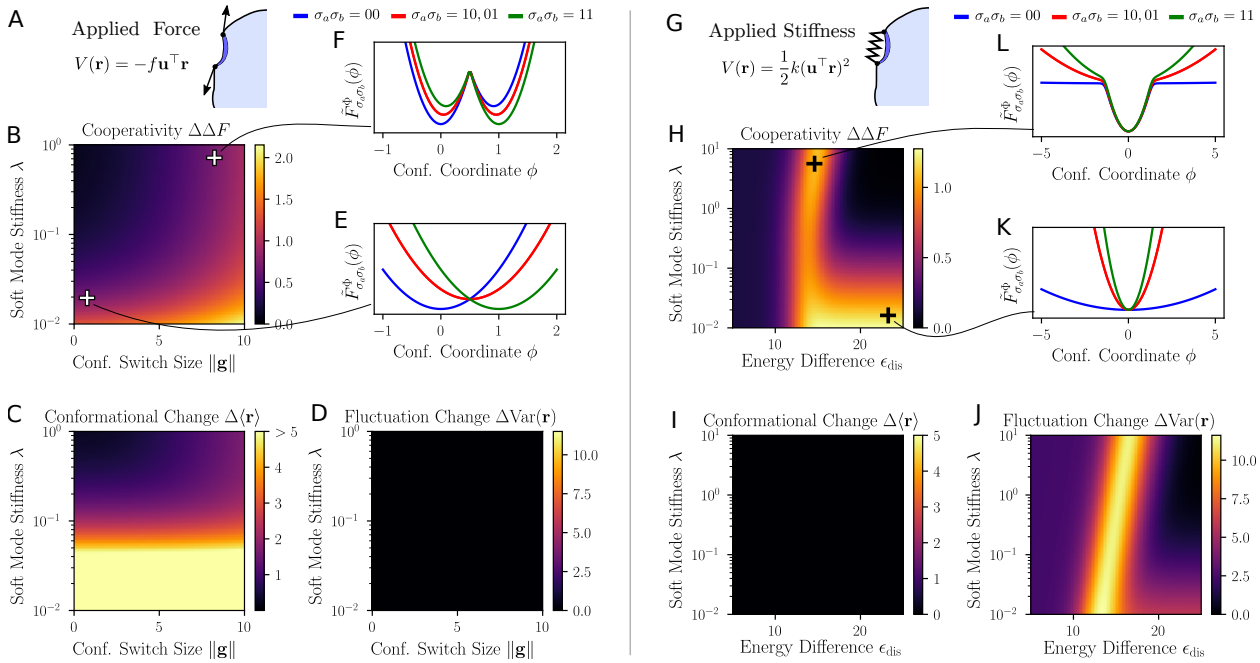

Figure 2.3: .
Different physical implementations of allosteric principles. The plots on the left half (A–F) describe allosteric mechanisms of a bistable landscape with bistability of strength $\|\mathbf{g}\|$ and a mode that couples binding sites with stiffness λ. Ligand binding is modeled as an applied force (A). (B) The cooperativity $\Delta\Delta F$, (C) the mean conformational change upon ligand binding $\Delta\langle\mathbf{r}\rangle$, and (D) the change in the magnitude of fluctuations upon ligand binding $\Delta\text{Var}(\mathbf{r})$ are plotted over a range of $\|\mathbf{g}\|$ and λ. (E) The free energy along the conformational change coordinate, $\tilde{F}^{\Phi}_{\sigma_a\sigma_b}(\phi)$, for the system located at the lower-left + mark in (B), for the four ligation conditions. In this regime, the induced fit mechanism is observed. (F) $\tilde{F}^{\Phi}_{\sigma_a\sigma_b}(\phi)$ for the system at the top-right + mark of (B), for the four ligation conditions. In this regime, the conformational switch mechanism is observed. The plots on the right half (G–L) describe the allosteric mechanisms of a landscape with an ordered state and a disordered state. In the ordered state, a mode couples binding sites with stiffness λ. The two states are separated in energy by ϵ_{dis}, and ligand binding is modeled as an applied stiffness (G). (H) The cooperativity $\Delta\Delta F$, (I) the mean conformational change upon ligand binding $\Delta\langle\mathbf{r}\rangle$, and (J) the change in the magnitude of fluctuations upon ligand binding $\Delta\text{Var}(\mathbf{r})$ are shown over a range of λ and ϵ_{dis}. (K) The free energy along a conformational coordinate, $\tilde{F}^{\Phi}_{\sigma_a\sigma_b}(\phi)$, for the system located at the lower-right + mark in (H), for the four ligation conditions. In this regime, the dynamic mechanism is observed. (L) $\tilde{F}^{\Phi}_{\sigma_a\sigma_b}(\phi)$ for the system at the top-center + mark of (H), for the four ligation conditions. In this regime, the order-disorder mechanism is observed. For these landscapes, $U_{\sigma_a\sigma_b} = F_{\text{q,d}} - \sigma_a k_a(\mathbf{u}_a^\top\mathbf{r})^2 - \sigma_b k_b(\mathbf{u}_b^\top\mathbf{r})^2$ in (2.20), and we set $\Delta\mathbf{R}$ of (2.19) to be the soft mode, since there is no conformational change upon binding. Numerical values for the plots are listed in the SI.

Plots of free energy surfaces help to intuitively differentiate various mechanisms. We define a collective variable Φ in which the conformational change $\Delta\mathbf{R} = \langle\mathbf{r}\rangle_{11} - \langle\mathbf{r}\rangle_{00}$ takes place,

$$\Phi(\mathbf{r}) = \frac{\Delta\mathbf{R}}{\|\Delta\mathbf{R}\|} \cdot (\mathbf{r} - \langle\mathbf{r}\rangle_{00}). \tag{2.19}$$

and compute free energy surfaces

$$\tilde{F}^{\Phi}_{\sigma_a\sigma_b}(\phi) = -\frac{1}{\beta}\log\left[\int d\mathbf{r}\ \delta(\Phi(\mathbf{r}) - \phi)e^{-\beta U_{\sigma_a\sigma_b}(\mathbf{r})}\right] \tag{2.20}$$

for systems using the induced fit (Fig. 2.3E) and conformational switch (Fig. 2.3F) mechanisms. Here, $U_{\sigma_a\sigma_b} = U_{\text{bi}} - \sigma_a f_a \mathbf{u}_a^\top \mathbf{r} - \sigma_b f_b \mathbf{u}_b^\top \mathbf{r}$. These computed 1D landscapes recapitulate the landscapes often drawn to illustrate the induced fit and conformational switch mechanisms [1, 15, 55, 54, 5]. Note that both mechanisms in Fig. 2.3E-F are underpinned by a conformational change and have no contribution from changes in conformational fluctuations (compare Figs. 2.3C-D). An interesting distinction between these two mechanisms is how they scale with the magnitude of the ligand forces. By taking $f_a = f_b = f$, $g = \|\mathbf{g}\|$, and $\mathbf{h} = -f(\mathbf{u}_a + \mathbf{u}_b)/2$, we find that the induced fit component scales as $\kappa^{-1}f^2$ while the conformational switch component scales as $\kappa^{-1}gf$, where κ is an effective spring constant. These results suggest that the conformational switch mechanism is preferred when ligand binding imposes a subtle effect (e.g. when the ligand closely fits the geometry of the binding site).

Many previous physical models used to explain allosteric cooperativity make use of the conformational switch mechanism. For example, elastic networks where the conformational switch is explicitly added [40], elastic networks where the conformational switch emerges through an evolutionary selection for cooperativity [44], or spin-glass models [42]. In addition, many coarse-grained models involve a double (or multi) basin energy landscape imposed by design [37, 36, 28, 10, 31, 7] and display conformational switch-like behavior.

Order-disorder Models

Bistable landscapes achieve cooperativity through spatially distinct minima that make the free energy surface $\tilde{F}$ non-separable. However, non-separability can be achieved even when minima overlap ($\mathbf{R}_i = \mathbf{R}_j$ for all pairs of states i, j) if the magnitude of fluctuations at the binding sites differs between states: $\mathbf{u}_a^\top H_i^+ \mathbf{u}_a \neq \mathbf{u}_a^\top H_j^+ \mathbf{u}_a$ and $\mathbf{u}_b^\top H_i^+ \mathbf{u}_b \neq \mathbf{u}_b^\top H_j^+ \mathbf{u}_b$ for at least one pair of states i, j. This condition occurs in systems with an order-disorder transition where the ordered state is low energy and low entropy, and the disordered state is high energy and high entropy. In proteins, the most obvious implementation of this condition is the global folding transition: the native state is enthalpically stable and lower entropy than the unfolded state [62]. However, more subtle transitions exist, including partial or local folding [46, 47] as well as transitions between a compact, yet disordered, molten globule and a well-packed native state [38].

To study allostery through order-disorder transitions, we again consider the simplest model that captures this property without loss of generality. Thus, we take a protein energy landscape that comprises a sum of two potentials—an ordered state with a quadratic potential (U_{quad}) and another potential to describe the disordered state (ϵ_{dis}),

$$U_{\text{dis}}(\mathbf{r}) = \frac{1}{2}\mathbf{r}^\top H_{\text{dis}}\mathbf{r} + \epsilon_{\text{dis}}. \tag{2.21}$$

Here $\epsilon_{\text{dis}} > 0$ represents the change in energy from breaking interactions between residues in the ordered state. To describe the high conformational entropy of the disordered state in an analytically tractable manner, we consider $\det H_{\text{dis}} \ll \det H$, where det denotes the pseudo-determinant. The two states can then be integrated to produce a free energy landscape,

$$F_{\text{q,d}}(\mathbf{r}) = -\beta^{-1} \log \left[e^{-\beta U_{\text{quad}}(\mathbf{r})} + e^{-\beta U_{\text{dis}}(\mathbf{r})} \right]. \tag{2.22}$$

Since the ordered and disordered states have different entropies, ligand interactions that modulate the entropy have the greatest effect. Thus, we consider the limit where ligand binding just changes the stiffness of the system, $V_a(\mathbf{r}) = \frac{1}{2}k_a(\mathbf{u}_a^\top \mathbf{r})^2$, $V_b(\mathbf{r}) = \frac{1}{2}k_b(\mathbf{u}_b^\top \mathbf{r})^2$. To examine cooperativity, we consider a landscape where the native state curvature H has one internal mode that couples binding sites with stiffness λ and an energy difference between ordered and disordered states of ϵ_{dis}. We take the curvature of the disordered state to be isotropic, $H_{\text{dis}} \propto I$ such that the disordered state lacks coupling between binding sites ($\mathbf{u}_a^\top H_{\text{dis}}^+ \mathbf{u}_b = 0$).

Fig. 2.3H shows the cooperativity of this minimal system. At low values of ϵ_{dis} ($\beta\epsilon_{\text{dis}} \ll \log(\det H/\det H_{\text{dis}})$) the model is in the disordered state for all ligation conditions and no cooperativity occurs. At high values of ϵ_{dis} ($\beta\epsilon_{\text{dis}} \gg \log(\det H/\det H_{\text{dis}})$) the model occupies the ordered state for all ligation conditions and cooperativity occurs through the dynamic mechanism of the soft mode principle (Fig. 2.3H bottom right and the associated 1d free energy landscape in Fig. 2.3K). At intermediate values of ϵ_{dis}, the model is disordered in the absence of ligands and ordered in the presence of ligands. In this case, cooperativity occurs even without a soft mode in the ordered state, emerging purely through the switching from disordered to ordered states (Fig. 2.3H top center and the associated 1d free energy landscape in Fig. 2.3L). Thus, cooperativity emerges from the relative decrease in entropy of the disordered state upon ligand binding. When cooperativity emerges solely from this mechanism (no soft mode contribution), the system can again be written exactly as an MWC model (SI).

This analysis helps to mechanistically unify different forms of allostery described in previous works. In both limits (marked in Fig. 2.3H) we obtain the behavior of "allostery without conformational change". However, one case depends on the normal modes within the native state as described by Cooper and Dryden (Fig. 2.3K) [8], while the other depends on engaging a switch between two states with different entropies (Fig. 2.3L). The

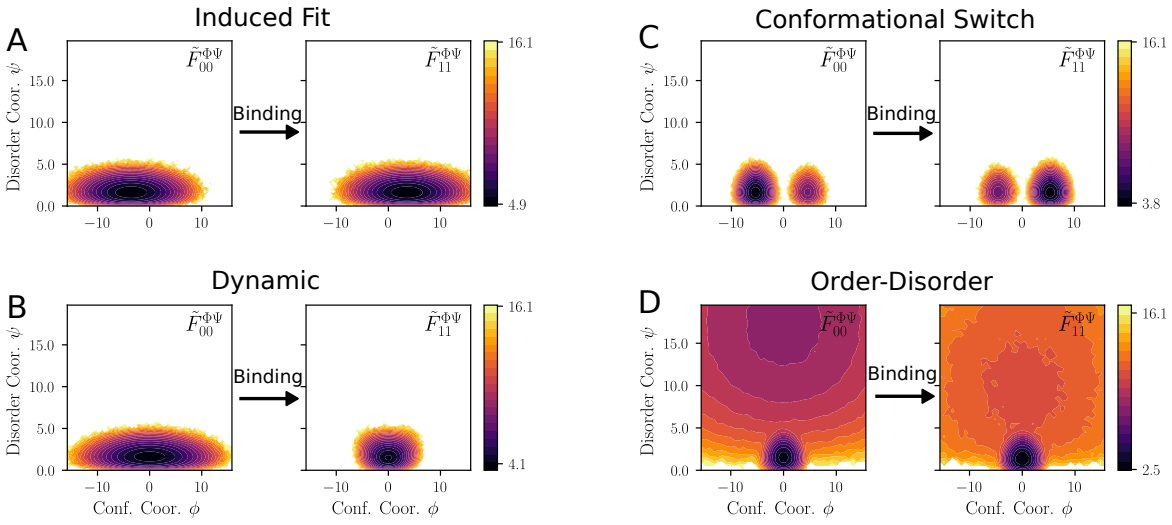

Figure 2.4: Free energy surfaces along simple collective variables can be used to distinguish different mechanisms of cooperativity. The variable ϕ measures progress along a single conformational direction, and the variable ψ measures structural disorder. Each panel shows the free energy surface for the apo and doubly bound conditions for the (A) induced fit, (B) dynamic, (C) conformational switch, and (D) order-disorder mechanisms. Surfaces are calculated using equilibrium Monte Carlo simulations.

case of folding-mediated allostery can be seen as a combination of both change in average conformation and overall entropy [21].

Distinguishing mechanisms in proteins

The work presented here suggests a different organizational structure for mechanisms of allostery than presently used. Current classifications focus on distinguishing whether allostery arises through ligand-induced changes in conformation (the “structure" view) or internal disorder (the “dynamics" view). The work presented here argues that the central distinguishing characteristic is whether cooperativity operates on the soft mode or multi-state principle, with changes in conformation and dynamics representing an important but orthogonal characteristic. The distinction is not trivial in terms of defining the operating mechanism. If single-state, allostery must arise through the coupling of ligand perturbations to (soft) normal modes of the protein. If multi-state, allostery may have nothing to do with normal modes,

arising instead through biasing the occupancy of different macroscopic states in the free energy landscape. The issue of dynamics is distinct, resolving whether the allosteric mechanism makes use of enthalpic or entropic changes in the system. Consistent with this, the simple models of multi-state allostery making use of either change in conformation (Fig. 2.3F) or dynamics (Fig. 2.3L) converge analytically (as expected) to the same thermodynamic model (MWC, SI). Similarly, the requirement for engagement of internal soft modes is true for all forms of single-state allostery, regardless of whether the mechanism involves conformational change or not.

This thinking clarifies the right collective variables (CVs) in which the physics of allostery should be classified. The CV Φ (2.19) distinguishes the induced fit (Fig. 2.3E) and conformational switch mechanisms (Fig. 2.3F). However, it fails to identify two minima for the two-state order-disorder mechanism because there is no change in the mean conformation (Fig. 2.3K and L). To address this, we need an orthogonal CV, Ψ, that measures root mean squared fluctuations around conformations.

$$\Psi(\mathbf{r}) = \left\| (\mathbf{r} - \langle \mathbf{r} \rangle_{00}) - \left((\mathbf{r} - \langle \mathbf{r} \rangle_{00}) \cdot \widehat{\Delta \mathbf{R}} \right) \widehat{\Delta \mathbf{R}} \right\|, \tag{2.23}$$

where $\widehat{\Delta \mathbf{R}} = \Delta \mathbf{R} / \|\Delta \mathbf{R}\|$. This CV measures the conformational deviations in directions other than $\Delta \mathbf{R}$. As allostery can arise through any combination of these CVs, measuring the free energy surface over both Φ and Ψ represents a complete basis to classify allosteric mechanisms.

$$\tilde{F}^{\Phi\Psi}_{\sigma_a \sigma_b}(\phi, \psi) = -\frac{1}{\beta} \log \left(\frac{1}{h_0^{dN-2}} \int d\mathbf{r} \; \delta(\Phi(\mathbf{r}) - \phi) \delta(\Psi(\mathbf{r}) - \psi) e^{-\beta U_{\sigma_a \sigma_b}(\mathbf{r})} \right). \tag{2.24}$$

For example, Fig. 2.4 shows Monte Carlo estimates of free energy surfaces over these two CVs for the four limiting cases explored analytically in this study. The induced fit (Fig. 2.4A) and dynamic (Fig. 2.4B) mechanism both operate on the soft mode principle (left panels),

and the conformational switch (Fig. 2.4C) and order-disorder (Fig. 2.4D) mechanisms both operate on the MWC principle (right panels). For real proteins, the classification could be achieved experimentally [24, 17] or through molecular dynamics simulations [45, 6] by plotting free energy landscapes along these collective variables.

Discussion

Previous work has stressed the importance of different physical features in allostery: conformational changes, dynamical changes, multiple preexisting conformational states, soft normal modes, intrinsic disorder, and folding. The diversity of these features and the varying levels of abstraction in the models that implement them make it challenging to distinguish fundamental physical principles of allostery from those details that are idiosyncratic to specific systems. In this work, we propose a physical framework in which the essential conditions for allosteric cooperativity can be identified.

The main result is that cooperativity only emerges when the system satisfies one (or a combination) of two physical principles. The first is a soft mode principle where, within a single state, binding sites are coupled through soft normal modes, and ligand binding at different sites perturbs the same modes. The second is the MWC principle, which occurs when the system has multiple states with different affinities for the ligands. Upon binding, the system undergoes a switch-like transition between the states. While the MWC principle can be fully defined at a thermodynamic level, namely the MWC model [35], the soft mode principle requires a physical description of the energy landscape around a minimum and, by nature, is not captured in thermodynamic models.

We show that each principle can have various specific implementations that recapitulate observed forms of allostery. Both the induced fit and dynamic mechanisms operate on the soft mode principle, with the difference between them arising from how ligand binding perturbs the soft mode—either by applying a force or by stiffening the modes. The conformational

switch (or population-shift [54]) mechanism, where the two states have different conformations, and the order-disorder mechanism, where the two states have different magnitudes of fluctuations, both operate on the MWC principle. The cases we have considered (Fig. 2.3) represent limiting forms of allostery in which we can analytically illustrate and therefore fully understand the mechanism. Specific implementations of allostery in a real protein need not conform strictly to these limiting conditions. However, these more complicated cases can be understood as nothing more than a combination of these archetypal mechanisms. In this sense, we suggest that the core physical principles that distinguish mechanisms of allostery are fully described in the cases explored in this work.

This work is formulated at the level of energy landscapes with no inherent notion of the internal geometry of proteins. As a result, we can say nothing about the patterns of amino acid interaction through which forces are transmitted within proteins to mediate coupling between ligand binding sites. Previous work has explored how cooperativity should scale with the distance between binding sites or with the size of the protein [58, 40, 48], and has probed how structural rigidity contributes to allostery [52, 58]. In addition, the sector hypothesis for proteins proposes that allostery is mediated through physically contiguous networks of collectively acting amino acids [51, 16, 26, 41]. More generally, sectors have been linked to the core constraints that enable native state folding [49], active site function [16, 33, 50], and the capacity of proteins to adapt to fluctuating conditions of selection [33, 50, 39]. In this regard, the simple physical models described here represent a foundation for understanding more general rules by which evolution builds allostery in biological macromolecules.

References

[1] Lalima G Ahuja, Susan S Taylor, and Alexandr P Kornev. Tuning the "violin" of protein kinases: The role of dynamics-based allostery. *IUBMB life*, 71(6):685–696, 2019.

[2] Karunesh Arora and Charles L Brooks III. Large-scale allosteric conformational transi-

tions of adenylate kinase appear to involve a population-shift mechanism. *Proceedings of the National Academy of Sciences*, 104(47):18496–18501, 2007.

[3] Ali Rana Atilgan, SR Durell, Robert L Jernigan, Melik C Demirel, O Keskin, and Ivet Bahar. Anisotropy of fluctuation dynamics of proteins with an elastic network model. *Biophysical journal*, 80(1):505–515, 2001.

[4] Ilya A Balabin, Weitao Yang, and David N Beratan. Coarse-grained modeling of allosteric regulation in protein receptors. *Proceedings of the National Academy of Sciences*, 106(34):14253–14258, 2009.

[5] Jean-Pierre Changeux and Stuart Edelstein. Conformational selection or induced fit? 50 years of debate resolved. *F1000 biology reports*, 3, 2011.

[6] Christophe Chipot and Andrew Pohorille. *Free energy calculations*, volume 86. Springer, 2007.

[7] Jhih-Wei Chu and Gregory A Voth. Coarse-grained free energy functions for studying protein conformational changes: a double-well network model. *Biophysical Journal*, 93 (11):3860–3871, 2007.

[8] A Cooper and DTF Dryden. Allostery without conformational change: a plausible model. *European Biophysics Journal*, 11:103–109, 1984.

[9] Michel A Cuendet, Harel Weinstein, and Michael V LeVine. The allostery landscape: Quantifying thermodynamic couplings in biomolecular systems. *Biophysical Journal*, 112(3):354a, 2017.

[10] Michael D Daily, George N Phillips Jr, and Qiang Cui. Many local motions cooperate to produce the adenylate kinase conformational transition. *Journal of molecular biology*, 400(3):618–631, 2010.

[11] Sandipan Dutta, Jean-Pierre Eckmann, Albert Libchaber, and Tsvi Tlusty. Green function of correlated genes in a minimal mechanical model of protein evolution. *Proceedings of the National Academy of Sciences*, 115(20):E4559–E4568, 2018.

[12] William A Eaton, Eric R Henry, James Hofrichter, Stefano Bettati, Cristiano Viappiani, and Andrea Mozzarelli. Evolution of allosteric models for hemoglobin. *IUBMB life*, 59 (8-9):586–599, 2007.

[13] Manfred Eigen. New looks and outlooks on physical enzymology. *Quarterly reviews of biophysics*, 1(1):3–33, 1968.

[14] Holger Flechsig. Design of elastic networks with evolutionary optimized long-range communication as mechanical models of allosteric proteins. *Biophysical journal*, 113(3): 558–571, 2017.

[15] Jingjing Guo and Huan-Xiang Zhou. Protein allostery and conformational dynamics. *Chemical reviews*, 116(11):6503–6515, 2016.

[16] Najeeb Halabi, Olivier Rivoire, Stanislas Leibler, and Rama Ranganathan. Protein sectors: evolutionary units of three-dimensional structure. *Cell*, 138(4):774–786, 2009.

[17] Nolan C Harris, Yang Song, and Ching-Hwa Kiang. Experimental free energy surface reconstruction from single-molecule force spectroscopy using jarzynski's equality. *Physical review letters*, 99(6):068101, 2007.

[18] Rhoda J Hawkins and Tom CB McLeish. Coarse-grained model of entropic allostery. *Physical review letters*, 93(9):098104, 2004.

[19] Mathieu Hemery and Olivier Rivoire. Evolution of sparsity and modularity in a model of protein allostery. *Physical review E*, 91(4):042704, 2015.

[20] JUDITH HERzFELD and H Eugene Stanley. A general approach to co-operativity and its application to the oxygen equilibrium of hemoglobin and its effectors. *Journal of molecular biology*, 82(2):231–265, 1974.

[21] Vincent J Hilser and E Brad Thompson. Intrinsic disorder as a mechanism to optimize allosteric coupling in proteins. *Proceedings of the National Academy of Sciences*, 104 (20):8311–8315, 2007.

[22] Vincent J Hilser, James O Wrabl, and Hesam N Motlagh. Structural and energetic basis of allostery. *Annual review of biophysics*, 41(1):585–609, 2012.

[23] Konrad Hinsen. Analysis of domain motions by approximate normal mode calculations. *Proteins: Structure, Function, and Bioinformatics*, 33(3):417–429, 1998.

[24] Gerhard Hummer and Attila Szabo. Free energy surfaces from single-molecule force spectroscopy. *Accounts of chemical research*, 38(7):504–513, 2005.

[25] DE Koshland Jr, G Nemethy, and D Filmer. Comparison of experimental binding data and theoretical models in proteins containing subunits. *Biochemistry*, 5(1):365–385, 1966.

[26] Jeeyeon Lee, Madhusudan Natarajan, Vishal C Nashine, Michael Socolich, Tina Vo, William P Russ, Stephen J Benkovic, and Rama Ranganathan. Surface sites for engineering allosteric control in proteins. *Science*, 322(5900):438–442, 2008.

[27] Liwei Li, Vladimir N Uversky, A Keith Dunker, and Samy O Meroueh. A computational investigation of allostery in the catabolite activator protein. *Journal of the American Chemical Society*, 129(50):15668–15676, 2007.

[28] Wenfei Li, Wei Wang, and Shoji Takada. Energy landscape views for interplays among folding, binding, and allostery of calmodulin domains. *Proceedings of the National Academy of Sciences*, 111(29):10550–10555, 2014.

[29] Zhuang Liu, Thomas G Gillis, Srivatsan Raman, and Qiang Cui. A parameterized two-domain thermodynamic model explains diverse mutational effects on protein allostery. *Elife*, 12:RP92262, 2024.

[30] Liang Ma and Qiang Cui. Activation mechanism of a signaling protein at atomic resolution from advanced computations. *Journal of the American Chemical Society*, 129 (33):10261–10268, 2007.

[31] Paul Maragakis and Martin Karplus. Large amplitude conformational change in proteins explored with a plastic network model: adenylate kinase. *Journal of Molecular Biology*, 352(4):807–822, 2005.

[32] Christopher L McClendon, Gregory Friedland, David L Mobley, Homeira Amirkhani, and Matthew P Jacobson. Quantifying correlations between allosteric sites in thermodynamic ensembles. *Journal of chemical theory and computation*, 5(9):2486–2502, 2009.

[33] Richard N McLaughlin Jr, Frank J Poelwijk, Arjun Raman, Walraj S Gosal, and Rama Ranganathan. The spatial architecture of protein function and adaptation. *Nature*, 491 (7422):138–142, 2012.

[34] Thomas CB McLeish, TL Rodgers, and Mark R Wilson. Allostery without conformation change: modelling protein dynamics at multiple scales. *Physical biology*, 10(5):056004, 2013.

[35] Jacque Monod, Jeffries Wyman, and Jean-Pierre Changeux. On the nature of allosteric transitions: a plausible model. *J Mol Biol*, 12(1):88–118, 1965.

[36] Kei-ichi Okazaki and Shoji Takada. Dynamic energy landscape view of coupled binding and protein conformational change: induced-fit versus population-shift mechanisms. *Proceedings of the National Academy of Sciences*, 105(32):11182–11187, 2008.

[37] Kei-ichi Okazaki, Nobuyasu Koga, Shoji Takada, Jose N Onuchic, and Peter G Wolynes. Multiple-basin energy landscapes for large-amplitude conformational motions of proteins: Structure-based molecular dynamics simulations. *Proceedings of the National Academy of Sciences*, 103(32):11844–11849, 2006.

[38] OB Ptitsyn. Molten globule and protein folding. *Advances in protein chemistry*, 47: 83–229, 1995.

[39] Arjun S Raman, K Ian White, and Rama Ranganathan. Origins of allostery and evolvability in proteins: a case study. *Cell*, 166(2):468–480, 2016.

[40] Riccardo Ravasio, Solange Marie Flatt, Le Yan, Stefano Zamuner, Carolina Brito, and Matthieu Wyart. Mechanics of allostery: contrasting the induced fit and population shift scenarios. *Biophysical journal*, 117(10):1954–1962, 2019.

[41] Kimberly A Reynolds, Richard N McLaughlin, and Rama Ranganathan. Hot spots for allosteric regulation on protein surfaces. *Cell*, 147(7):1564–1575, 2011.

[42] Olivier Rivoire. Parsimonious evolutionary scenario for the origin of allostery and coevolution patterns in proteins. *Physical Review E*, 100(3):032411, 2019.

[43] Jason W Rocks, Nidhi Pashine, Irmgard Bischofberger, Carl P Goodrich, Andrea J Liu, and Sidney R Nagel. Designing allostery-inspired response in mechanical networks. *Proceedings of the National Academy of Sciences*, 114(10):2520–2525, 2017.

[44] Eric Rouviere, Rama Ranganathan, and Olivier Rivoire. Emergence of single-versus multi-state allostery. *PRX Life*, 1(2):023004, 2023.

[45] Benoît Roux. The calculation of the potential of mean force using computer simulations. *Computer physics communications*, 91(1-3):275–282, 1995.

[46] Louise Rundqvist, Jörgen Å den, Tobias Sparrman, Marcus Wallgren, Ulrika Olsson, and Magnus Wolf-Watz. Noncooperative folding of subdomains in adenylate kinase. *Biochemistry*, 48(9):1911–1927, 2009.

[47] Travis P Schrank, D Wayne Bolen, and Vincent J Hilser. Rational modulation of conformational fluctuations in adenylate kinase reveals a local unfolding mechanism for allostery and functional adaptation in proteins. *Proceedings of the National Academy of Sciences*, 106(40):16984–16989, 2009.

[48] Midas Segers, Aderik Voorspoels, Takahiro Sakaue, and Enrico Carlon. Mechanisms of dna-mediated allostery. *arXiv preprint arXiv:2305.03962*, 2023.

[49] Michael Socolich, Steve W Lockless, William P Russ, Heather Lee, Kevin H Gardner, and Rama Ranganathan. Evolutionary information for specifying a protein fold. *Nature*, 437(7058):512–518, 2005.

[50] Michael A Stiffler, Doeke R Hekstra, and Rama Ranganathan. Evolvability as a function of purifying selection in tem-1 β-lactamase. *Cell*, 160(5):882–892, 2015.

[51] Gürol M Süel, Steve W Lockless, Mark A Wall, and Rama Ranganathan. Evolutionarily conserved networks of residues mediate allosteric communication in proteins. *Nature structural biology*, 10(1):59–69, 2003.

[52] D Thirumalai, Changbong Hyeon, Pavel I Zhuravlev, and George H Lorimer. Symmetry, rigidity, and allosteric signaling: from monomeric proteins to molecular machines. *Chemical reviews*, 119(12):6788–6821, 2019.

[53] Monique M Tirion. Large amplitude elastic motions in proteins from a single-parameter, atomic analysis. *Physical review letters*, 77(9):1905, 1996.

[54] Chung-Jung Tsai and Ruth Nussinov. A unified view of "how allostery works". *PLoS computational biology*, 10(2):e1003394, 2014.

[55] Nan Wu, Mauricio Barahona, and Sophia N Yaliraki. Allosteric communication and signal transduction in proteins. *Current Opinion in Structural Biology*, 84:102737, 2024.

[56] Chunyan Xu, Dror Tobi, and I Bahar. Allosteric changes in protein structure computed by a simple mechanical model: hemoglobin t-r2 transition. *Journal of molecular biology*, 333(1):153–168, 2003.

[57] Le Yan, Riccardo Ravasio, Carolina Brito, and Matthieu Wyart. Architecture and coevolution of allosteric materials. *Proceedings of the National Academy of Sciences*, 114(10):2526–2531, 2017.

[58] Le Yan, Riccardo Ravasio, Carolina Brito, and Matthieu Wyart. Principles for optimal cooperativity in allosteric materials. *Biophysical journal*, 114(12):2787–2798, 2018.

[59] Ofer Yifrach and Amnon Horovitz. Nested cooperativity in the atpase activity of the oligomeric chaperonin groel. *Biochemistry*, 34(16):5303–5308, 1995.

[60] Luhao Zhang, Maodong Li, and Zhirong Liu. A comprehensive ensemble model for comparing the allosteric effect of ordered and disordered proteins. *PLOS Computational Biology*, 14(12):e1006393, 2018.

[61] Wenjun Zheng, Bernard R Brooks, and D Thirumalai. Low-frequency normal modes that describe allosteric transitions in biological nanomachines are robust to sequence variations. *Proceedings of the National Academy of Sciences*, 103(20):7664–7669, 2006.

[62] Andrej Šali, Eugene Shakhnovich, and Martin Karplus. How does a protein fold? *nature*, 369(6477):248–251, 1994.

Appendix for Chapter 2

Multi-basin Free Energy Surface

Any energy landscape can be well approximated by the following free energy landscape,

$$F_p(\mathbf{r}) = -\frac{1}{\beta}\log\sum_{i=1}^{n} e^{-\beta\frac{1}{2}(\mathbf{r}-\mathbf{R}_i)^\top H_i(\mathbf{r}-\mathbf{R}_i)+\epsilon_i}. \tag{2.25}$$

Each state is quadratic with curvature H_i, ground state $\mathbf{R}_i$ and ground state energy ϵ_i. Substituting F_p for U_p in (2.6) and solving the integral, we find,

$$\begin{aligned}
\tilde{Z}(x_a,x_b) &= \frac{1}{h_0^{dN-2}}\int d\mathbf{r}\delta(\mathbf{u}_a^\top\mathbf{r}-x_a)\delta(\mathbf{u}_b^\top\mathbf{r}-x_b)e^{-\beta F_p(\mathbf{r})} \\
&= \frac{1}{h_0^{dN-2}}\sum_{i=1}^{n}\int d\mathbf{r}\delta(\mathbf{u}_a^\top\mathbf{r}-x_a)\delta(\mathbf{u}_b^\top\mathbf{r}-x_b)e^{-\beta\frac{1}{2}(\mathbf{r}-\mathbf{R}_i)^\top H_i(\mathbf{r}-\mathbf{R}_i)+\beta\epsilon_i} \\
&= \frac{1}{h_0^{dN-2}}\sum_{i=1}^{n} e^{-\beta\epsilon_i}\int ds_a e^{i2\pi s_a x_a}\int ds_b e^{i2\pi s_b x_b}\int d\mathbf{r}\; e^{-\frac{1}{2}\beta(\mathbf{r}-\mathbf{R}_i)^\top H_i(\mathbf{r}-\mathbf{R}_i)-i2\pi(s_a\mathbf{u}_a+s_b\mathbf{u}_b)^\top\mathbf{r}} \\
&= \frac{1}{h_0^{dN-2}}\sum_{i=1}^{n} e^{-\beta\epsilon_i}\int ds_a e^{i2\pi s_a(x_a-\mathbf{u}_a^\top\mathbf{R}_i)}\int ds_b e^{i2\pi s_b(x_b-\mathbf{u}_b^\top\mathbf{R}_i)} \\
&\qquad\qquad \times\int d\mathbf{y}_i\; e^{-\frac{1}{2}\beta\mathbf{y}_i^\top H_i\mathbf{y}_i-i2\pi(s_a\mathbf{u}_a+s_b\mathbf{u}_b)^\top\mathbf{y}_i} \\
&= h_0^2\sum_{i=1}^{n} e^{-\beta\epsilon_i}\sqrt{\frac{(2\pi)^{dN}}{h_0^{2dN}\beta^{dN}\det(H_i)}}\int ds_a e^{i2\pi s_a(x_a-\mathbf{u}_a^\top\mathbf{R}_i)}\int ds_b e^{i2\pi s_b(x_b-\mathbf{u}_b^\top\mathbf{R}_i)} \\
&\qquad\qquad \times\left(e^{-2\pi^2\beta^{-1}(s_a\mathbf{u}_a+s_b\mathbf{u}_b)^\top H_i^+(s_a\mathbf{u}_a+s_b\mathbf{u}_b)}\right) \\
&= h_0^2\sum_{i=1}^{n} e^{-\beta\epsilon_i}\sqrt{\frac{(2\pi)^{dN}}{h_0^{2dN}\beta^{N}\det(H_i)}}\int d\mathbf{s} e^{-2\pi\beta^{-1}\mathbf{s}^\top A_i\mathbf{s}+i2\pi\mathbf{x}_i^\top\mathbf{s}} \\
&= \sum_{i=1}^{n}\sqrt{\frac{(2\pi)^{dN-2}}{h_0^{2(dN-2)}\beta^{dN-2}\det(A_i)\det(H_i)}}e^{-\beta(\frac{1}{2}\mathbf{x}_i^\top A_i^{-1}\mathbf{x}_i+\epsilon_i)}
\end{aligned}$$

On the third line, we write the delta functions in terms of their Fourier transforms, $\delta(t) = \int_{-\infty}^{\infty} e^{-i2\pi st} ds$. On the fourth line we used the substitution $\mathbf{y}_i = \mathbf{r} - \mathbf{R}_i$ and on the sixth line we introduced $\mathbf{s} = (s_a, s_b)$, $\mathbf{x}_i = (x_a - \mathbf{u}_a^\top \mathbf{R}_i, x_b - \mathbf{u}_b^\top \mathbf{R}_i)$ and

$$A_i = \begin{pmatrix} \mathbf{u}_a^\top H_i^+ \mathbf{u}_a & \mathbf{u}_a^\top H_i^+ \mathbf{u}_b \\ \mathbf{u}_a^\top H_i^+ \mathbf{u}_b & \mathbf{u}_b^\top H_i^+ \mathbf{u}_b \end{pmatrix}. \tag{2.26}$$

d is the number of spatial dimensions. The free energy surface is,

$$\tilde{F}(x_a, x_b) = -\frac{1}{\beta} \log \left(\sum_{i=1}^{n} C_i e^{-\beta(\frac{1}{2}\mathbf{x}_i^\top A_i^{-1} \mathbf{x}_i + \epsilon_i)} \right), \tag{2.27}$$

where,

$$C_i = \sqrt{\frac{(2\pi)^{dN-2}}{h_0^{2(dN-2)} \beta^{dN-2} \det(A_i) \det(H_i)}}. \tag{2.28}$$

Conditions for cooperativity

Cooperativity can only exist when the free energy surface is non-separable, i.e. when $\tilde{F}(x_a, x_b)$ can not be written as $\tilde{F}_a(x_a) + \tilde{F}_b(x_b)$. Since (2.27) is generally non-separable, we solve the few cases where it is separable to identify which conditions must be broken to achieve non-separability and cooperativity.

Single-state case

When there is only one state $n = 1$, (2.27) reduces to

$$\tilde{F}(x_a, x_b) = \frac{1}{2} \mathbf{x}^\top A^{-1} \mathbf{x} + \epsilon - \frac{1}{\beta} \log(C) \tag{2.29}$$

which is separable only when the off-diagonal entry of A^{-1} is zero. The subscripts have been dropped to simplify notation. The inverse of a symmetric 2×2 matrix is,

$$\begin{pmatrix} a & c \\ c & b \end{pmatrix}^{-1} = \frac{1}{ab - c^2} \begin{pmatrix} b & -c \\ -c & a \end{pmatrix}, \tag{2.30}$$

and so the condition for separability is,

$$\frac{-\mathbf{u}_a^\top H^+ \mathbf{u}_b}{\mathbf{u}_a^\top H^+ \mathbf{u}_a \mathbf{u}_b^\top H^+ \mathbf{u}_b - (2\mathbf{u}_a^\top H^+ \mathbf{u}_b)^2} = 0. \tag{2.31}$$

Thus in a single state system, cooperativity requires $\mathbf{u}_a^\top H^+ \mathbf{u}_b \neq 0$.

Multi-state case

When there are multiple states $n > 1$, separability requires $\mathbf{u}_a^\top H_i^+ \mathbf{u}_b = 0 \ \forall \ i \in \{1, \ldots, n\}$ (assumed in the following) as well as additional conditions. Without loss of generality we assume $n = 2$ condition. The free energy surface (2.27) reduces to,

$$\begin{aligned} \tilde{F}(x_a, x_b) = -\frac{1}{\beta} \log \Bigg[& C_1 e^{-\beta\left(\frac{1}{2}G_{11}^{(1)}(x_a - \mathbf{u}_a^\top \mathbf{R}_1)^2 + \frac{1}{2}G_{22}^{(1)}(x_b - \mathbf{u}_b^\top \mathbf{R}_1)^2 + \epsilon_1\right)} \\ & + C_2 e^{-\beta\left(\frac{1}{2}G_{11}^{(2)}(x_a - \mathbf{u}_a^\top \mathbf{R}_2)^2 + \frac{1}{2}G_{22}^{(2)}(x_b - \mathbf{u}_b^\top \mathbf{R}_2)^2 + \epsilon_2\right)} \Bigg] \end{aligned} \tag{2.32}$$

Here $G^{(i)} = A_i^{-1}$ and $G_{11}^{(i)}$ and $G_{22}^{(i)}$ are the diagonal entries of $G^{(i)}$. $\tilde{F}$ is only separable when the argument of the log takes the form: (Function of x_a)×(Function of x_b)×Constant. This is the case when either:

$$G_{11}^{(1)} = G_{11}^{(2)} \text{ and } \mathbf{u}_a^\top \mathbf{R}_1 = \mathbf{u}_a^\top \mathbf{R}_2 \quad \text{or} \quad G_{22}^{(1)} = G_{22}^{(2)} \text{ and } \mathbf{u}_b^\top \mathbf{R}_1 = \mathbf{u}_b^\top \mathbf{R}_2 \tag{2.33}$$

or both. This implies that non-separability arises when neither coordinate can be factored out of the log-sum. In particular, both of the following must hold:

$$\left(\mathbf{u}_a^\top H_1^+ \mathbf{u}_a \neq \mathbf{u}_a^\top H_2^+ \mathbf{u}_a \text{ or } \mathbf{u}_a^\top \mathbf{R}_1 \neq \mathbf{u}_a^\top \mathbf{R}_2\right) \quad \text{and} \quad \left(\mathbf{u}_b^\top H_1^+ \mathbf{u}_b \neq \mathbf{u}_b^\top H_2^+ \mathbf{u}_b \text{ or } \mathbf{u}_b^\top \mathbf{R}_1 \neq \mathbf{u}_b^\top \mathbf{R}_2\right). \tag{2.34}$$

In words this means that the two states need to be physically distinct.

When there are any number of states $n > 1$.

$$\left(\mathbf{u}_a^\top H_i^+ \mathbf{u}_a \neq \mathbf{u}_a^\top H_j^+ \mathbf{u}_a \text{ or } \mathbf{u}_a^\top \mathbf{R}_i \neq \mathbf{u}_a^\top \mathbf{R}_j\right) \quad \text{and} \quad \left(\mathbf{u}_b^\top H_i^+ \mathbf{u}_b \neq \mathbf{u}_b^\top H_j^+ \mathbf{u}_b \text{ or } \mathbf{u}_b^\top \mathbf{R}_i \neq \mathbf{u}_b^\top \mathbf{R}_j\right) \tag{2.35}$$

for at least one pair of states i, j.

Scaling of cooperativity within a single basin

Here we show that $\Delta\Delta F \sim \mathbf{u}_a^\top H^+ \mathbf{u}_b$ when $\mathbf{u}_a^\top H^+ \mathbf{u}_b$ is small when there is a single basin ($n = 1$). The free energy surface when $n = 1$ simplifies to,

$$\tilde{F}(x_a, x_b) = \frac{1}{2}\mathbf{x}_1^\top A_1^{-1} \mathbf{x}_1 + \epsilon - \frac{1}{\beta}\log(C) \tag{2.36}$$

Going forward, we omit the subscripts on the Hessian and other parameters in this section, and we drop the constant terms as they do not contribute to the cooperativity. Let $G = A^{-1}$. The quadratic terms can be written as,

$$\frac{1}{2}\mathbf{x}^\top A^{-1}\mathbf{x} = \frac{1}{2}G_{11}(x_a - \mathbf{u}_a^\top \mathbf{R})^2 + \frac{1}{2}G_{22}(x_b - \mathbf{u}_b^\top \mathbf{R})^2 + G_{12}(x_a - \mathbf{u}_a^\top \mathbf{R})(x_b - \mathbf{u}_b^\top \mathbf{R}). \tag{2.37}$$

The partition function (for which we omit the factor h_0^{-2} because it does not contribute to the cooperativity) becomes

$$Z_{\sigma_a\sigma_b} = \int dx_a e^{-\beta(\sigma_a g_a(x_a)+\frac{1}{2}G_{11}(x_a-\mathbf{u}_a^\top\mathbf{R})^2)} \int dx_b e^{-\beta(\sigma_b g_b(x_b)+\frac{1}{2}G_{22}(x_b-\mathbf{u}_b^\top\mathbf{R})^2)} \times e^{-\beta G_{12}(x_a-\mathbf{u}_a^\top\mathbf{R})(x_b-\mathbf{u}_b^\top\mathbf{R})}, \tag{2.38}$$

We are interested in the onset of cooperativity, so we consider the condition where $\mathbf{u}_a^\top H^+\mathbf{u}_b$ is small (relative to $\mathbf{u}_a^\top H^+\mathbf{u}_a$ and $\mathbf{u}_b^\top H^+\mathbf{u}_b$). Since $G_{12} = -\mathbf{u}_a^\top H^+\mathbf{u}_b/(\mathbf{u}_a^\top H^+\mathbf{u}_a\mathbf{u}_b^\top H^+\mathbf{u}_b - (\mathbf{u}_a^\top H^+\mathbf{u}_b)^2)$, when $\mathbf{u}_a^\top H^+\mathbf{u}_b$ is small, then G_{12} is small and $e^{-\beta G_{12}(x_a-\mathbf{u}_a^\top\mathbf{R})(x_b-\mathbf{u}_b^\top\mathbf{R})}$ can be approximated by a Taylor expansion of around $G_{12}=0$ is,

$$e^{-\beta G_{12}(x_a-\mathbf{u}_a^\top\mathbf{R})(x_b-\mathbf{u}_b^\top\mathbf{R})} \approx 1 - \beta(x_a-\mathbf{u}_a^\top\mathbf{R})(x_b-\mathbf{u}_b^\top\mathbf{R})G_{12} + \mathcal{O}(G_{12}^2) \tag{2.39}$$

Using this, we get,

$$Z_{\sigma_a\sigma_b} = \int dx_a e^{-\beta(\sigma_a g_a(x_a)+\frac{1}{2}G_{11}(x_a-\mathbf{u}_a^\top\mathbf{R})^2)} \int dx_b e^{-\beta(\sigma_b g_b(x_b)+\frac{1}{2}G_{22}(x_b-\mathbf{u}_b^\top\mathbf{R})^2)} \times (1-\beta(x_a-\mathbf{u}_a^\top\mathbf{R})(x_b-\mathbf{u}_b^\top\mathbf{R})G_{12}) \tag{2.40}$$

$$= Z^*_{\sigma_a\sigma_b} - \beta G_{ab}\Omega_{\sigma_a\sigma_b} \tag{2.41}$$

where

$$Z^*_{\sigma_a\sigma_b} = \int dx_a e^{-\beta(\sigma_a g_a(x_a)+\frac{1}{2}G_{11}(x_a-\mathbf{u}_a^\top\mathbf{R})^2)} \int dx_b e^{-\beta(\sigma_b g_b(x_b)+\frac{1}{2}G_{22}(x_b-\mathbf{u}_b^\top\mathbf{R})^2)} \tag{2.42}$$

and

$$\Omega_{\sigma_a\sigma_b} = \int dx_a e^{-\beta(\sigma_a g_a(x_a)+\frac{1}{2}G_{11}(x_a-\mathbf{u}_a^\top\mathbf{R})^2)} \int dx_b e^{-\beta(\sigma_b g_b(x_b)+\frac{1}{2}G_{22}(x_b-\mathbf{u}_b^\top\mathbf{R})^2)} \times (x_a-\mathbf{u}_a^\top\mathbf{R})(x_b-\mathbf{u}_b^\top\mathbf{R}) \tag{2.43}$$

Using these, the fraction in the log of the cooperativity (2.2) gives,

$$\frac{Z_{10}Z_{01}}{Z_{00}Z_{11}} = \frac{(Z^*_{10} - \beta A_{ab}\Omega_{10})(Z^*_{01} - \beta A_{ab}\Omega_{01})}{(Z^*_{00} - \beta A_{ab}\Omega_{00})(Z^*_{11} - \beta A_{ab}\Omega_{11})} \tag{2.44}$$

$$= \frac{Z^*_{10}Z^*_{01} - \beta A_{ab}\Omega_{10}Z^*_{01} - \beta A_{ab}\Omega_{01}Z^*_{10} + \beta^2 A^2_{ab}\Omega_{10}\Omega_{01}}{Z^*_{00}Z^*_{11} - \beta A_{ab}\Omega_{00}Z^*_{11} - \beta A_{ab}\Omega_{11}Z^*_{00} + \beta^2 A^2_{ab}\Omega_{00}\Omega_{11}} \tag{2.45}$$

$$= \frac{Z^*_{10}Z^*_{01} - \beta A_{ab}(\Omega_{10}Z^*_{01} + \Omega_{01}Z^*_{10})}{Z^*_{00}Z^*_{11} - \beta A_{ab}(\Omega_{00}Z^*_{11} + \Omega_{11}Z^*_{00})}. \tag{2.46}$$

On the last line, we neglected the order G^2_{12} terms. We also know that $Z^*_{10}Z^*_{01} = Z^*_{00}Z^*_{11}$. We use the relation,

$$\frac{a+b}{a+c} \approx 1 + \frac{b-c}{a} \tag{2.47}$$

which holds when $a \gg b$ and $a \gg c$.

$$\frac{Z_{10}Z_{01}}{Z_{00}Z_{11}} \approx 1 - \beta G_{12}\frac{\Omega_{10}Z^*_{01} + \Omega_{01}Z^*_{10} - \Omega_{00}Z^*_{11} - \Omega_{11}Z^*_{00}}{Z^*_{00}Z^*_{11}} \tag{2.48}$$

Now for the cooperativity when,

$$\Delta\Delta F = -\beta^{-1}\log\left(\frac{Z_{10}Z_{01}}{Z_{00}Z_{11}}\right) \approx G_{12}\frac{\Omega_{10}Z^*_{01} + \Omega_{01}Z^*_{10} - \Omega_{00}Z^*_{11} - \Omega_{11}Z^*_{00}}{Z^*_{00}Z^*_{11}} + \mathcal{O}(G^2_{12}) \tag{2.49}$$

Finally, this means that $\Delta\Delta F \sim \mathbf{u}_a^\top H^+ \mathbf{u}_b$ when small.

Derivation of Quadratic Cooperativities (2.14) and (2.15)

We assume ligand binding affects a single mode (2.4), and consider polynomial perturbations up to second order $g_a(x) = \frac{1}{2}k_a x^2 - f_a x$ and $g_b(x) = \frac{1}{2}k_b x^2 - f_b x$ (constant terms of the polynomials will not contribute to $\Delta\Delta F$ and have been omitted). Since we are considering the case where there is only one state ($n = 1$), the subscripts on the parameters are dropped

(e.g. $\mathbf{x}_1 \to \mathbf{x}$). We use the notation $A_{ab} = \mathbf{u}_a^\top H^+ \mathbf{u}_b$. The full partition function is,

$$Z_{\sigma_a\sigma_b} = \int dx_a e^{-\sigma_a \beta g_a(x_a)} \int dx_b \; e^{-\sigma_b \beta g_b(x_b)} e^{-\beta \tilde{F}(x_a, x_b)} \tag{2.50}$$

with,

$$\tilde{F}(x_a, x_b) = \frac{1}{2}\mathbf{x}^\top A^{-1}\mathbf{x} + \epsilon - \frac{1}{\beta}\log(C). \tag{2.51}$$

Recall, $\mathbf{x} = (x_a - \mathbf{u}_a^\top \mathbf{R}, x_b - \mathbf{u}_b^\top \mathbf{R})$. To compute the cooperativity (2.2) we need to compute the partition function for each binding condition.

$$Z_{\sigma_a\sigma_b} = Ce^{-\beta\epsilon} \int d\mathbf{x} \; e^{-\beta\left[\frac{1}{2}\mathbf{x}^\top A^{-1}\mathbf{x} + \sigma_a(\frac{1}{2}k_a x_a^2 - f_a x_a) + \sigma_b(\frac{1}{2}k_b x_b^2 - f_b x_b)\right]}. \tag{2.52}$$

Which can be rewritten as,

$$Z_{\sigma_a\sigma_b} = Ce^{-\beta\epsilon} \int d\mathbf{x} e^{-\beta\left(\frac{1}{2}\mathbf{x}^\top M_{\sigma_a\sigma_b}\mathbf{x} - \mathbf{h}_{\sigma_a\sigma_b}^\top \mathbf{x} + S_{\sigma_a\sigma_b}\right)}. \tag{2.53}$$

where,

$$M_{\sigma_a\sigma_b} = A^{-1} + \sigma_a k_a \mathbf{e}_1\mathbf{e}_1^\top + \sigma_b k_b \mathbf{e}_2\mathbf{e}_2^\top, \tag{2.54}$$

$$\mathbf{h}_{\sigma_a\sigma_b} = \sigma_a\left(f_a - k_a(\mathbf{u}_a^\top \mathbf{R})\right)\mathbf{e}_1 + \sigma_b\left(f_b - k_b(\mathbf{u}_b^\top \mathbf{R})\right)\mathbf{e}_2, \tag{2.55}$$

and

$$S_{\sigma_a\sigma_b} = \sigma_a\left[\frac{1}{2}k_a(\mathbf{u}_a^\top \mathbf{R})^2 - f_a\left(\mathbf{u}_a^\top \mathbf{R}\right)\right] + \sigma_b\left[\frac{1}{2}k_b(\mathbf{u}_b^\top \mathbf{R})^2 - f_b\left(\mathbf{u}_b^\top \mathbf{R}\right)\right]. \tag{2.56}$$

Here $\mathbf{e}_1 = (1,0),\ \mathbf{e}_2 = (0,1)$. This is a Gaussian integral and can computes to,

$$Z_{\sigma_a\sigma_b} = \frac{2\pi}{\beta}C\exp\left(-\beta\epsilon\right)\exp\left(-\beta S_{\sigma_a\sigma_b}\right)\exp\left(\frac{\beta}{2}\mathbf{h}_{\sigma_a\sigma_b}^\top M_{\sigma_a\sigma_b}^{-1}\mathbf{h}_{\sigma_a\sigma_b}\right)\left(\det M_{\sigma_a\sigma_b}\right)^{-\frac{1}{2}}. \tag{2.57}$$

In the ratio of the partition functions in the cooperativity (2.2), the terms $\frac{2\pi}{\beta}C\exp\left(-\beta\epsilon\right)\exp\left(-\beta S_{\sigma_a\sigma_b}\right)$ cancel. Using the Matrix determinant lemma,

$$\det(M_{00}) = \det(A^{-1}) \tag{2.58}$$

$$\det(M_{10}) = \det(A^{-1})\frac{1+k_aA_{aa}}{A_{aa}A_{bb}-A_{ab}^2} \tag{2.59}$$

$$\det(M_{01}) = \det(A^{-1})\frac{1+k_bA_{bb}}{A_{aa}A_{bb}-A_{ab}^2} \tag{2.60}$$

$$\det(M_{11}) = \det(A^{-1})\frac{1+k_aA_{aa}+k_bA_{bb}+k_ak_b(A_{aa}A_{bb}-A_{ab}^2)}{A_{aa}A_{bb}-A_{ab}^2} \tag{2.61}$$

We introduce the variables $h_a = f_a - k_a(\mathbf{u}_a^\top\mathbf{R})$ and $h_b = f_b - k_b(\mathbf{u}_b^\top\mathbf{R})$ to describe the effective forces that are combinations of the applied forces f_a, f_b and the forces that arise from the applied stiffness. Using the Sherman-Morrison formula,

$$\mathbf{h}_{00}^\top M_{00}^{-1}\mathbf{h}_{00} = 0 \tag{2.62}$$

$$\mathbf{h}_{10}^\top M_{10}^{-1}\mathbf{h}_{10} = \frac{h_aA_{aa}}{1+k_aA_{aa}} \tag{2.63}$$

$$\mathbf{h}_{01}^\top M_{01}^{-1}\mathbf{h}_{01} = \frac{h_bA_{bb}}{1+k_bA_{bb}} \tag{2.64}$$

$$\mathbf{h}_{11}^\top M_{11}^{-1}\mathbf{h}_{11} = \frac{2A_{ab}h_ah_b+A_{bb}h_b^2+A_{aa}A_{bb}h_b^2k_a+A_{aa}h_a^2(1+A_{bb}k_b)-A_{ab}^2(h_b^2k_a+h_a^2k_b)}{1+A_{bb}k_b-A_{ab}^2k_ak_b+A_{aa}(k_a+A_{bb}k_ak_b))} \tag{2.65}$$

Putting these together, the full cooperativity becomes

$$\Delta\Delta F = \frac{2h_ah_bA_{ab}\Big(1+k_aA_{aa}+k_bA_{bb}+k_ak_bA_{aa}A_{bb}\Big)-A_{ab}^2\Big(k_ah_b^2+k_bh_a^2+A_{aa}h_b^2k_a^2+A_{bb}h_a^2k_b^2\Big)}{2(1+k_aA_{aa})(1+k_bA_{bb})\Big(1+k_aA_{aa}+k_bA_{bb}+k_ak_b(A_{aa}A_{bb}-A_{ab}^2)\Big)}$$
$$-\frac{1}{2\beta}\log\left(1-\frac{k_ak_bA_{ab}^2}{(1+k_aA_{aa})(1+k_bA_{bb})}\right). \tag{2.66}$$

For the cases of (2.14) and (2.15), we took $\mathbf{R} = 0$, leading to $h_a, h_b = f_a, f_b$. When binding purely applies a force, the cooperativity reduces to (2.14).

$$\text{When} \quad k_a = k_b = 0 \quad \rightarrow \quad \Delta\Delta F = f_a f_b \mathbf{u}_a^\top H^+ \mathbf{u}_b, \tag{2.67}$$

and when binding purely stiffens, the cooperativity reduces to (2.15),

$$\text{When} \quad f_a = f_b = 0 \quad \rightarrow \quad \Delta\Delta F = -\frac{1}{2\beta} \log \left(1 - \frac{k_a k_b \left(\mathbf{u}_a^\top H^+ \mathbf{u}_b \right)^2}{(1 + k_a \mathbf{u}_a^\top H^+ \mathbf{u}_a)(1 + k_b \mathbf{u}_b^\top H^+ \mathbf{u}_b)} \right). \tag{2.68}$$

Another limit of interest is when both the stiffnesses and forces diverge, $|k_i| \to \infty$, $|f_i| \to \infty$, such that the ratio $f_i/k_i = d_i$ remains finite, $0 < |d_i| < \infty$. In fact, this case corresponds to adding a rigid spring that causes displacement d_i along the binding site CV x_i. In these quantities $i \in \{a, b\}$. Since the x_i degree of freedom cannot vary after ligand binding, the entropy (and thus the entropic contribution to the cooperativity) diverges; however, the energetic contribution to the cooperativity, $\Delta\Delta E$ remains finite.

When $|k_i| \to \infty$, $|f_i| \to \infty$ such that $d_i = f_i/k_i$ remains finite, $0 < |d_i| < \infty$, for $i \in \{a, b\}$,

$$\Delta\Delta E = \frac{\left((\mathbf{u}_a^\top H^+ \mathbf{u}_b) \left((\mathbf{u}_a^\top H^+ \mathbf{u}_b)(\mathbf{u}_b^\top H^+ \mathbf{u}_b) d_a^2 + (\mathbf{u}_a^\top H^+ \mathbf{u}_b)(\mathbf{u}_a^\top H^+ \mathbf{u}_a) d_b^2 - 2(\mathbf{u}_a^\top H^+ \mathbf{u}_a)(\mathbf{u}_b^\top H^+ \mathbf{u}_b) d_a d_b \right) \right)}{2(\mathbf{u}_a^\top H^+ \mathbf{u}_a)(\mathbf{u}_b^\top H^+ \mathbf{u}_b) \left((\mathbf{u}_a^\top H^+ \mathbf{u}_b)^2 - (\mathbf{u}_a^\top H^+ \mathbf{u}_a)(\mathbf{u}_b^\top H^+ \mathbf{u}_b) \right)} \tag{2.69}$$

Now let us try to simplify (2.66). First we will consider the symmetric case, where $k_a = k_b = k$, $f_a = f_b = f$, $d_a = d_b = f/k = d$ and $\mathbf{u}_a H^+ \mathbf{u}_a = \mathbf{u}_a H^+ \mathbf{u}_a = \kappa^{-1}$. Next, we nondimensionalize. In this problem, there are three different units: stiffness, force, and energy. The stiffness scale is set by the flexibility of the binding sites, κ. The relevant energy

scale is the thermal energy, β^{-1}. There is no clear force scale, so it is set by the energy and stiffness scales, $\sqrt{\kappa/\beta}$. Writing the symmetric version of (2.66).

$$\Delta\Delta F = \frac{2f^2 A_{ab}\Big(1 + 2k\kappa^{-1} + k^2\kappa^{-2}\Big) - A_{ab}^2\Big(2kf^2 + 2\kappa^{-1}f^2k^2\Big)}{2(1+k\kappa^{-1})^2\Big(1 + 2k\kappa^{-1} + k^2(\kappa^{-2} - A_{ab}^2)\Big)} - \frac{1}{2\beta}\log\left(1 - \frac{k^2A_{ab}^2}{(1+k\kappa^{-1})^2}\right). \tag{2.70}$$

The natural dimensionless variables are

$$\tilde{k} = k/\kappa, \quad \tilde{\eta} = A_{ab}\kappa, \quad \tilde{f} = f/\sqrt{\kappa/\beta}. \tag{2.71}$$

And,

$$\beta\Delta\Delta F = \frac{\tilde{f}^2\tilde{\eta}\Big(1 + (1-\tilde{\eta})\tilde{k}\Big)}{(1+\tilde{k})\Big(1 + 2\tilde{k} + (1-\tilde{\eta}^2)\tilde{k}^2\Big)} - \frac{1}{2}\log\left(1 - \tilde{\eta}^2\frac{\tilde{k}^2}{(1+\tilde{k})^2}\right). \tag{2.72}$$

In the pure force case $\tilde{k} = 0$, we find $\beta\Delta\Delta F = \tilde{\eta}\tilde{f}^2$ and in the pure stiffness case $\tilde{f} = 0$, we find $\beta\Delta\Delta F = -\frac{1}{2}\log\Big(1 - \tilde{\eta}^2\tilde{k}^2/(1+\tilde{k})^2\Big)$ and in the imposed displacement case, $|k| \to \infty$, $|f| \to \infty$ such that $d = f/k$ remains finite, we find $\beta\Delta\Delta E = \left(\frac{\tilde{f}}{\tilde{k}}\right)^2 \frac{\eta(1-\eta)}{1-\eta^2}$.

Derivation of Conformational Switch Cooperativity (2.18)

Starting with the bistable energy landscape $U_{\text{bi}}(\mathbf{r})$ defined in (2.17) and ligand perturbation that apply forces, $V_a(\mathbf{r}) = f_a\mathbf{u}_a^\top\mathbf{r}$, $V_b(\mathbf{r}) = f_b\mathbf{u}_b^\top\mathbf{r}$, the energy landscape of each binding condition is,

$$U_{\sigma_a\sigma_b}(\mathbf{r}) = U_{\text{bi}}(\mathbf{r}) - \sigma_a f_a\mathbf{u}_a^\top\mathbf{r} - f_b\mathbf{u}_b^\top\mathbf{r}. \tag{2.73}$$

Each of these energies will have two minima if the following condition is met,

$$\mathbf{g}^\top H^+\left(\mathbf{h} + \mathbf{f} - \mathbf{g}\right) < 0 < \mathbf{g}^\top H^+\left(\mathbf{h} + \mathbf{f} + \mathbf{g}\right), \tag{2.74}$$

where $\mathbf{f} = \sigma_a f_a \mathbf{u}_a + \sigma_b f_b \mathbf{u}_b$. For a generic quadratic potential with an applied force $U(\mathbf{r}) = \mathbf{r}^\top H \mathbf{r} - \mathbf{f}^\top \mathbf{r}$ there will be a minimum at $\mathbf{r}_{\min} = H^+ \mathbf{f}$ of energy $E = \min_{\mathbf{r}} U(\mathbf{r}) = -\frac{1}{2}\mathbf{f}^\top H^+ \mathbf{f}$. When there are two minima, they will have energies,

$$E_+ = -\frac{1}{2}(\mathbf{f}+\mathbf{h}+\mathbf{g})^\top H^+ (\mathbf{f}+\mathbf{h}+\mathbf{g}), \qquad E_- = -\frac{1}{2}(\mathbf{f}+\mathbf{h}-\mathbf{g})^\top H^+ (\mathbf{f}+\mathbf{h}-\mathbf{g}) \quad (2.75)$$

The ground state energy is,

$$E = \min(E_+, E_-) = \frac{1}{2}\left(E_+ + E_- - |E_+ - E_-|\right) \quad (2.76)$$

$$= -\frac{1}{2}\mathbf{f}^\top H^+ \mathbf{f} - \frac{1}{2}\mathbf{h}^\top H^+ \mathbf{h} - \frac{1}{2}\mathbf{g}^\top H^+ \mathbf{g} - \mathbf{f}^\top H^+ \mathbf{h} - |\mathbf{f}^\top H^+ \mathbf{g} + \mathbf{h}^\top H^+ \mathbf{g}| \quad (2.77)$$

The cooperativity of the bistable landscape becomes,

$$\begin{aligned}
\Delta\Delta E = &-\frac{1}{2}f_a^2 \mathbf{u}_a^\top H^+ \mathbf{u}_a - \frac{1}{2}\mathbf{h}^\top H^+ \mathbf{h} - \frac{1}{2}\mathbf{g}^\top H^+ \mathbf{g} - f_a \mathbf{u}_a^\top H^+ \mathbf{h} - \left| f_a \mathbf{u}_a^\top H^+ \mathbf{g} + \mathbf{h}^\top H^+ \mathbf{g} \right| \\
&-\frac{1}{2}f_b^2 \mathbf{u}_b^\top H^+ \mathbf{u}_b - \frac{1}{2}\mathbf{h}^\top H^+ \mathbf{h} - \frac{1}{2}\mathbf{g}^\top H^+ \mathbf{g} - f_b \mathbf{u}_b^\top H^+ \mathbf{h} - \left| f_b \mathbf{u}_b^\top H^+ \mathbf{g} + \mathbf{h}^\top H^+ \mathbf{g} \right| \\
&+\frac{1}{2}\mathbf{h}^\top H^+ \mathbf{h} + \frac{1}{2}\mathbf{g}^\top H^+ \mathbf{g} + \left| \mathbf{h}^\top H^+ \mathbf{g} \right| \\
&+\frac{1}{2}(f_a \mathbf{u}_a + f_b \mathbf{u}_b)^\top H^+ (f_a \mathbf{u}_a + f_b \mathbf{u}_b) + \frac{1}{2}\mathbf{h}^\top H^+ \mathbf{h} + \frac{1}{2}\mathbf{g}^\top H^+ \mathbf{g} + (f_a \mathbf{u}_a + f_b \mathbf{u}_b)^\top H^+ \mathbf{h} \\
&+\left| (f_a \mathbf{u}_a + f_b \mathbf{u}_b)^\top H^+ \mathbf{g} + \mathbf{h}^\top H^+ \mathbf{g} \right|
\end{aligned} \quad (2.78)$$

$$\begin{aligned}
\Delta\Delta E = f_a f_b \mathbf{u}_a^\top H^+ \mathbf{u}_b &+ \left| (f_a \mathbf{u}_a + f_b \mathbf{u}_b + \mathbf{h})^\top H^+ \mathbf{g} \right| + \left| \mathbf{h}^\top H^+ \mathbf{g} \right| \\
&- \left| (f_a \mathbf{u}_a + \mathbf{h})^\top H^+ \mathbf{g} \right| - \left| (f_b \mathbf{u}_b + \mathbf{h})^\top H^+ \mathbf{g} \right|.
\end{aligned} \quad (2.79)$$

2.6 Definitions of Quantities

Conformational Change: The conformational change is measured as the magnitude of the difference in the mean conformation with both ligand bound, $\langle \mathbf{r} \rangle_{11}$, and no ligand bound

$\langle \mathbf{r} \rangle_{00}$,

$$\Delta\langle \mathbf{r} \rangle = \|\langle \mathbf{r} \rangle_{11} - \langle \mathbf{r} \rangle_{00}\|. \tag{2.80}$$

Fluctuation Change: To measure the change in the magnitude of the fluctuations around the mean conformation we measure the change in the RMSF upon binding both ligands,

$$\Delta\mathrm{Var}(\mathbf{r}) = \left| \sqrt{\langle \mathbf{r}^2 \rangle_{11} - \langle \mathbf{r} \rangle_{11}^2} - \sqrt{\langle \mathbf{r}^2 \rangle_{00} - \langle \mathbf{r} \rangle_{00}^2} \right| \tag{2.81}$$

Here the subscripts on the angle brackets indicate the ligand binding condition for which the average is taken.

2.7 Connection to the MWC model.

Here we define an MWC model with two binding sites and show that the bistable and order-disorder cases reduce to the MWC model when there is no soft mode contribution to cooperativity.

MWC models make two assumptions: there exists an equilibrium of $k > 1$ states and, within each state, the binding free energies do not depend on whether a ligand is already bound (ie no cooperativity when locked in a single state). For simplicity, we assume the case of a symmetric protein so ligands bind to each site with the same binding energy for a given state. Denoting the free energy of the unbound condition of the kth state as $F_{00}^{(k)}$, the free energy of state k in the $i, j \in \{0, 1\}^2$ binding condition can be written as,

$$F_{ij}^{(k)} = F_{00}^{(k)} + (i + j)\Delta F^{(k)}. \tag{2.82}$$

The cooperativity, as before, is defined as $\Delta\Delta F = F_{10} + F_{01} - F_{00} - F_{11}$. The free energy

of each ligand binding condition is calculated by summing over states, which in this case we consider $k = 2$, $F_{ij} = -\beta^{-1} \log \left(e^{-\beta F_{ij}^{(1)}} + e^{-\beta F_{ij}^{(2)}} \right)$. The cooperativity can be written as,

$$\Delta\Delta F = -\beta^{-1} \log \left[\frac{\left(e^{-\beta F_{10}^{(1)}} + e^{-\beta F_{10}^{(2)}} \right) \left(e^{-\beta F_{01}^{(1)}} + e^{-\beta F_{01}^{(2)}} \right)}{\left(e^{-\beta F_{00}^{(1)}} + e^{-\beta F_{00}^{(2)}} \right) \left(e^{-\beta F_{11}^{(1)}} + e^{-\beta F_{11}^{(2)}} \right)} \right] \tag{2.83}$$

Defining the difference in free energies of the apo states $\Delta F_{00} = F_{00}^{(2)} - F_{00}^{(1)}$ and the difference of binding energies $\Delta F = \Delta F^{(2)} - \Delta F^{(1)}$ gives the two MWC parameters. With these parameters the cooperativity becomes,

$$\Delta\Delta F = -\beta^{-1} \log \left[\frac{\left(e^{-\beta (F_{00}^{(1)} + \Delta F^{(1)})} + e^{-\beta (F_{00}^{(2)} + \Delta F^{(2)})} \right)^2}{\left(e^{-\beta F_{00}^{(1)}} + e^{-\beta F_{00}^{(2)}} \right) \left(e^{-\beta (F_{00}^{(1)} + 2\Delta F^{(1)})} + e^{-\beta (F_{00}^{(2)} + 2\Delta F^{(2)})} \right)} \right] \tag{2.84}$$

The free energies of state 2 can be written in terms of the free energies of state 1 and the differences,

$$\Delta\Delta F = -\beta^{-1} \log \left[\frac{\left(e^{-\beta (F_{00}^{(1)} + \Delta F^{(1)})} + e^{-\beta (F_{00}^{(1)} + \Delta F_{00} + \Delta F^{(1)} + \Delta F)} \right)^2}{\left(e^{-\beta F_{00}^{(1)}} + e^{-\beta (F_{00}^{(1)} + \Delta F_{00})} \right) \left(e^{-\beta (F_{00}^{(1)} + 2\Delta F^{(1)})} + e^{-\beta (F_{00}^{(1)} + \Delta F_{00} + 2\Delta F^{(1)} + 2\Delta F)} \right)} \right] \tag{2.85}$$

$$= -\beta^{-1} \log \left[\frac{\left(1 + e^{-\beta (\Delta F_{00} + \Delta F)} \right)^2}{\left(1 + e^{-\beta \Delta F_{00}} \right) \left(1 + e^{-\beta (\Delta F_{00} + 2\Delta F)} \right)} \right]. \tag{2.86}$$

The cooperativity is often in terms of equilibrium constants $c = e^{-\beta \Delta F}$ and $L = e^{-\beta \Delta F_{00}}$,

$$\Delta\Delta F = -\beta^{-1} \log \left[\frac{(1 + cL)^2}{(1 + L)\left(1 + c^2 L\right)} \right] \tag{2.87}$$

Order-disorder Model: The order-disorder model ((2.22)) satisfies the two assumptions of the MWC model when $\mathbf{u}_a^\top H^+ \mathbf{u}_b = 0$. In this case, we can express ΔF and ΔF_{00} in terms of parameters of the order-disorder landscape (2.22). First we solve for ΔF_{00}. The free energy of the ordered and disordered apo states are,

$$F_{00}^{\text{ord}} = \frac{1}{2\beta} \log \left[\left(\frac{\beta h_0^2}{2\pi} \right)^{dN} \det H \right], \qquad F_{00}^{\text{dis}} = \epsilon + \frac{1}{2\beta} \log \left[\left(\frac{\beta h_0^2}{2\pi} \right)^{dN} \det H_0 \right]. \quad (2.88)$$

Here det is the pseudo-determinant since H is singular. The difference between these is,

$$\Delta F_{00} = F_{00}^{\text{dis}} - F_{00}^{\text{ord}} = \epsilon + \frac{1}{2\beta} \log \left[\frac{\det H_0}{\det H} \right]. \quad (2.89)$$

Next, we solve for ΔF. The binding free energies in the ordered and disordered states are,

$$\begin{aligned} \Delta F^{\text{ord}} &= \Delta F_{10}^{\text{ord}} - \Delta F_{00}^{\text{ord}} = \frac{1}{2\beta} \log \left[\left(\frac{\beta h_0^2}{2\pi} \right)^{N} \det H \right] - \frac{1}{2\beta} \log \left[\left(\frac{\beta h_0^2}{2\pi} \right)^{N} \det(H + k_a \mathbf{u}_a \mathbf{u}_a^\top) \right] \\ &= \frac{1}{2\beta} \log(1 + k_a \mathbf{u}_a^\top H^+ \mathbf{u}_a) \end{aligned} \quad (2.90)$$

and,

$$\begin{aligned} \Delta F^{\text{dis}} &= \Delta F_{10}^{\text{dis}} - \Delta F_{00}^{\text{dis}} = \frac{1}{2\beta} \log \left[\left(\frac{\beta h_0^2}{2\pi} \right)^{N} \det H_0 \right] - \frac{1}{2\beta} \log \left[\left(\frac{\beta h_0^2}{2\pi} \right)^{N} \det(H_0 + k_a \mathbf{u}_a \mathbf{u}_a^\top) \right] \\ &= \frac{1}{2\beta} \log(1 + k_a \mathbf{u}_a^\top H_0^+ \mathbf{u}_a). \end{aligned} \quad (2.91)$$

Quantities from binding site b do not appear because of symmetry $\mathbf{u}_a^\top H^+ \mathbf{u}_a = \mathbf{u}_b^\top H^+ \mathbf{u}_b$

and $\mathbf{u}_a^\top H_0^+ \mathbf{u}_a = \mathbf{u}_b^\top H_0^+ \mathbf{u}_b$. Finally,

$$\Delta F = \Delta F^{\text{dis}} - \Delta F^{\text{ord}} = \frac{1}{2\beta} \log \left(\frac{1 + k_a \mathbf{u}_a^\top H_0^+ \mathbf{u}_a}{1 + k_a \mathbf{u}_a^\top H^+ \mathbf{u}_a} \right). \tag{2.92}$$

Bistable Model: The bistable model ((2.17)) satisfies the two assumptions of the MWC model when there are two minima: $\mathbf{g}^\top H^+ (\mathbf{h} + \mathbf{f} - \mathbf{g}) < 0 < \mathbf{g}^\top H^+ (\mathbf{h} + \mathbf{f} + \mathbf{g})$ and no cooperativity exists in each state $\mathbf{u}_a^\top H^+ \mathbf{u}_b = 0$. Here we express ΔF and ΔF_{00} in terms of parameters of the bistable landscape. Let state 1 be the basin in $\mathbf{g}^\top \mathbf{r} > 0$ and state 2 be the basin $\mathbf{g}^\top \mathbf{r} \leq 0$. We consider conditions where the basins are distinct (i.e. the barrier is larger than the temperature). First we solve for ΔF_{00}.

$$\begin{aligned} F_{00}^{(1)} &= \frac{1}{2\beta} \log \left[\left(\frac{\beta h_0^2}{2\pi} \right)^N \det H \right] - \frac{1}{2} (\mathbf{h} + \mathbf{g})^\top H^+ (\mathbf{h} + \mathbf{g}), \\ F_{00}^{(2)} &= \frac{1}{2\beta} \log \left[\left(\frac{\beta h_0^2}{2\pi} \right)^N \det H \right] - \frac{1}{2} (\mathbf{h} - \mathbf{g})^\top H^+ (\mathbf{h} - \mathbf{g}) \end{aligned} \tag{2.93}$$

giving

$$\Delta F_{00} = F_{00}^{(2)} - F_{00}^{(1)} = 2\mathbf{h}^\top H^+ \mathbf{g} \tag{2.94}$$

Now we solve for ΔF_{00}. Since the ligand binding applies a force, the curvature does not change, and the binding free energies only depend on the change in the energy minimum. Because we assume a symmetric protein, we can write the free energies in terms of either binding site. Here we choose site a.

$$\Delta F^{(1)} = F_{10}^{(1)} - F_{00}^{(1)} = -\frac{1}{2} f_a^2 \mathbf{u}_a^\top H^+ \mathbf{u}_a - f_a \mathbf{u}_a^\top H^+ \mathbf{h} - f_a \mathbf{u}_a^\top H^+ \mathbf{g} \tag{2.95}$$

and instead

$$\Delta F^{(2)} = F_{10}^{(2)} - F_{00}^{(2)} = -\frac{1}{2} f_a^2 \mathbf{u}_a^\top H^+ \mathbf{u}_a - f_a \mathbf{u}_a^\top H^+ \mathbf{h} + f_a \mathbf{u}_a^\top H^+ \mathbf{g}. \tag{2.96}$$

Finally,

$$\Delta F = \Delta F^{(2)} - \Delta F^{(1)} = 2 f_a \mathbf{u}_a^\top H^+ \mathbf{g}. \tag{2.97}$$

2.8 Two physical principles enable allostery: Arbitrary ligand potentials

In the main text, we considered ligand potentials that act along one mode of the binding site. $V_a(\mathbf{r}_a) = g_a(\mathbf{u}_a^\top \mathbf{r}), \quad V_b(\mathbf{r}_b) = g_b(\mathbf{u}_b^\top \mathbf{r})$. Here we relax this assumption and find the same results.

We partition the degrees of freedom of the system, into degrees of freedom that describe binding site a, $\mathbf{r}_a$, binding site b, $\mathbf{r}_b$, and the rest of the degrees of freedom, $\mathbf{r}_r$ such that $\mathbf{r} = (\mathbf{r}_a, \mathbf{r}_r, \mathbf{r}_b)$. With this notation, we can write the four energy landscapes with ligand potentials as a function of either $\mathbf{r}_a$ or $\mathbf{r}_b$. we can write the four ligation conditions,

$$U_{\sigma_a \sigma_b}(\mathbf{r}) = U_p(\mathbf{r}) + \sigma_a V_a(\mathbf{r}_a) + \sigma_b V_b(\mathbf{r}_b) \tag{2.98}$$

and the partition functions as,

$$\begin{aligned} Z_{\sigma_a \sigma_b} &= \int d\mathbf{r} d\mathbf{x}_a d\mathbf{x}_b \; \delta(\mathbf{r}_a - \mathbf{x}_a)\delta(\mathbf{r}_b - \mathbf{x}_b) e^{-\beta U_p(\mathbf{r}) - \sigma_a \beta V(\mathbf{x}_a) - \sigma_b \beta V(\mathbf{x}_b)} && (2.99) \\ &= \int d\mathbf{x}_a e^{-\sigma_a \beta V(\mathbf{x}_a)} \int d\mathbf{x}_b e^{-\sigma_b \beta V(\mathbf{x}_b)} \int d\mathbf{r} \; \delta(\mathbf{r}_a - \mathbf{x}_a)\delta(\mathbf{r}_b - \mathbf{x}_b) e^{-\beta U_p(\mathbf{r})} && (2.100) \\ &= \int d\mathbf{x}_a e^{-\sigma_a \beta V(\mathbf{x}_a)} \int d\mathbf{x}_b e^{-\sigma_b \beta V(\mathbf{x}_b)} \; \tilde{Z}(\mathbf{x}_a, \mathbf{x}_b) && (2.101) \end{aligned}$$

with $\tilde{Z}(\mathbf{x}_a, \mathbf{x}_b) = \int d\mathbf{r} \; \delta(\mathbf{r}_a - \mathbf{x}_a)\delta(\mathbf{r}_b - \mathbf{x}_b) e^{-\beta U_p(\mathbf{r})}$. As before we have chosen units where the length scale h_0 of the partition function is one and is omitted. Using the Fourier transform definition of the multivariate delta function,

$$\delta(\mathbf{t}) = \int_{-\infty}^{\infty} d\mathbf{s} \; e^{-2\pi i \mathbf{s}^\top \mathbf{t}}, \tag{2.102}$$

we get,

$$\tilde{Z}(\mathbf{x}_a, \mathbf{x}_b) = \int d\mathbf{r} \int d\mathbf{s}_a e^{-2\pi i \mathbf{s}_a^\top (\mathbf{r}_a - \mathbf{x}_a)} \int d\mathbf{s}_b e^{-2\pi i \mathbf{s}_b^\top (\mathbf{r}_b - \mathbf{x}_b)} e^{-\beta U_p(\mathbf{r})} \tag{2.103}$$

$$= \int d\mathbf{s}_a e^{2\pi i \mathbf{s}_a^\top \mathbf{x}_a} \int d\mathbf{s}_b e^{2\pi i \mathbf{s}_b^\top \mathbf{x}_b} \int d\mathbf{r} e^{-\beta U_p(\mathbf{r}) - 2\pi i \mathbf{s}_a^\top \mathbf{r}_a - 2\pi i \mathbf{s}_b^\top \mathbf{r}_b}. \tag{2.104}$$

Now we use F_p of (2.8) to approximate any U_p. and define the vector $\mathbf{s} = (\mathbf{s}_a, \mathbf{0}, \mathbf{s}_b)$.

$$\tilde{Z} = \sum_{i=1}^{n} \int d\mathbf{s}_a e^{2\pi i \mathbf{s}_a^\top \mathbf{x}_a} \int d\mathbf{s}_b e^{2\pi i \mathbf{s}_b^\top \mathbf{x}_b} \int d\mathbf{r} e^{-\beta(\frac{1}{2}(\mathbf{r} - \mathbf{R}_i)^\top H_i (\mathbf{r} - \mathbf{R}_i) + \epsilon_i) - 2\pi i \mathbf{s}^\top \mathbf{r}} \tag{2.105}$$

$$= \sum_{i=1}^{n} e^{-\beta \epsilon_i} \int d\bar{\mathbf{s}} e^{2\pi i \bar{\mathbf{s}}^\top \bar{\mathbf{x}}} \int d\mathbf{y}_i e^{-\beta \frac{1}{2} \mathbf{y}_i^\top H_i \mathbf{y}_i - 2\pi i \mathbf{s}^\top (\mathbf{y}_i + \mathbf{R}_i)} \tag{2.106}$$

$$= \sum_{i=1}^{n} e^{-\beta \epsilon_i} \int d\bar{\mathbf{s}} e^{2\pi i \bar{\mathbf{s}}^\top (\bar{\mathbf{x}} - \bar{\mathbf{R}}_i)} \int d\mathbf{y}_i e^{-\beta \frac{1}{2} \mathbf{y}_i^\top H_i \mathbf{y}_i - 2\pi i \mathbf{s}^\top \mathbf{y}_i} \tag{2.107}$$

$$= \sum_{i=1}^{n} e^{-\beta \epsilon_i} \sqrt{\frac{(2\pi)^{dN}}{\beta \det(H_i)}} \int d\bar{\mathbf{s}} e^{2\pi i \bar{\mathbf{s}}^\top (\bar{\mathbf{x}} - \bar{\mathbf{R}}_i)} \; e^{-2\pi^2 \beta^{-1} \mathbf{s}^\top H^+ \mathbf{s}} \tag{2.108}$$

$$= \sum_{i=1}^{n} e^{-\beta \epsilon_i} \sqrt{\frac{(2\pi)^{dN}}{\beta \det(H_i)}} \int d\bar{\mathbf{s}} e^{2\pi i \bar{\mathbf{s}}^\top (\bar{\mathbf{x}} - \bar{\mathbf{R}}_i)} \; e^{-2\pi^2 \beta^{-1} \bar{\mathbf{s}}^\top \bar{G}_i \bar{\mathbf{s}}} \tag{2.109}$$

$$= \sum_{i=1}^{n} e^{-\beta \epsilon_i} \sqrt{\frac{(2\pi)^{dN}}{\beta \det(H_i)}} \int d\bar{\mathbf{s}} e^{-2\pi^2 \beta^{-1} \bar{\mathbf{s}}^\top \bar{G}_i \bar{\mathbf{s}} + 2\pi i (\bar{\mathbf{x}} - \bar{\mathbf{R}}_i)^\top \bar{\mathbf{s}}} \tag{2.110}$$

$$= \sum_{i=1}^{n} \sqrt{\frac{(2\pi)^{dN}}{\beta \det(H_i)}} \sqrt{\frac{(2\pi)^{l}}{\det(4\pi^2 \beta^{-1} \bar{G}_i)}} e^{-\frac{1}{2}\beta (\bar{\mathbf{x}} - \bar{\mathbf{R}}_i)^\top \bar{G}_i^{-1} (\bar{\mathbf{x}} - \bar{\mathbf{R}}_i) - \beta \epsilon_i} \tag{2.111}$$

$$\tag{2.112}$$

On the second line we introduced $\mathbf{y}_i = \mathbf{r} - \mathbf{R}_i$, $\bar{\mathbf{s}} = (\mathbf{s}_a, \mathbf{s}_b)$ and $\bar{\mathbf{x}} = (\mathbf{x}_a, \mathbf{x}_b)$. On the third line we introduce $\bar{\mathbf{R}}_i = (\mathbf{R}_i^a, \mathbf{R}_i^b)$ where $\mathbf{R}_i = (\mathbf{R}_i^a, \mathbf{R}_i^r, \mathbf{R}_i^b)$ describes the same way of partitioning the vector's entries into those associated with binding site a, binding site b and

the rest, as was done for $\mathbf{r} = (\mathbf{r}_a, \mathbf{r}_r, \mathbf{r}_b)$. One the fifth line we introduced,

$$\bar{G}_i = \begin{pmatrix} H^+_{i,aa} & (H^+_{i,ab})^\top \\ H^+_{i,ab} & H^+_{i,bb} \end{pmatrix} \tag{2.113}$$

where $H^+_{i,aa}, H^+_{i,ab}, H^+_{i,bb}$ are sub matrices of H^+_i that contain the entries that contribute to the product $\mathbf{s}^\top H^+_i \mathbf{s}$. On the last line, l is the number of dimensions of $\bar{\mathbf{s}}$. The resulting free energy surface is,

$$\tilde{F}(\mathbf{x}_a, \mathbf{x}_b) = -\frac{1}{\beta} \log \left(\sum_{i=1}^{n} \sqrt{\frac{(2\pi)^{dN}}{\beta \det(H_i)}} \sqrt{\frac{(2\pi)^l}{4\pi^2 \beta^{-1} \det(\bar{G}_i)}} e^{-\frac{1}{2}\beta(\bar{\mathbf{x}}-\bar{\mathbf{R}}_i)^\top \bar{G}_i^{-1}(\bar{\mathbf{x}}-\bar{\mathbf{R}}_i) - \beta\epsilon_i} \right). \tag{2.114}$$

When there is one state $n = 1$ (we drop the subscript), the free energy surface, up to a constant, is

$$\tilde{F}(\mathbf{x}_a, \mathbf{x}_b) = \frac{1}{2}(\bar{\mathbf{x}} - \bar{\mathbf{R}})^\top \bar{G}^{-1}(\bar{\mathbf{x}} - \bar{\mathbf{R}}). \tag{2.115}$$

G is a 2 by 2 block matrix. The inverse of a symmetric 2 by 2 block matrix is,

$$\begin{pmatrix} A & B^\top \\ B & C \end{pmatrix}^{-1} = \begin{pmatrix} A^{-1} + A^{-1}B^\top (C - BA^{-1}B^\top)^{-1} BA^{-1} & -A^{-1}B^\top (C - BA^{-1}B^\top)^{-1} \\ -(C - BA^{-1}B^\top)^{-1} BA^{-1} & (C - BA^{-1}B^\top)^{-1} \end{pmatrix} \tag{2.116}$$

The free energy surface is separable when the off-diagonal block of G^{-1} is zero. That is when

$$\left(H^+_{bb} - H^+_{ab}(H^+_{aa})^{-1}(H^+_{ab})^\top \right) H^+_{ab}(H^+_{aa})^{-1} = 0 \tag{2.117}$$

If we assume that H^+_{aa} and H^+_{bb} are invertible, non-zero, and have finite entries, then the solution occurs when $H^+_{ab} = 0$, that is there is no correlation between the degrees of freedom at binding site a and binding site b.

Numerical parameters for figures

Figures 2.2 - 2.4 use specific values for $H, H_{\text{dis}}, \mathbf{u}_a, \mathbf{u}_b, \mathbf{g}, \mathbf{h}$ and other parameters. For all figures, we use systems of 5 dimensions and choose diagonal Hessians so that the entries of $\mathbf{u}_a$ and $\mathbf{u}_b$ clearly describe the effect on the normal modes. For all figures $\beta = 1$. The function diag takes a vector and returns a diagonal matrix with the vector's entries on the diagonal, and normalize$(\mathbf{v}) = \mathbf{v}/\|\mathbf{v}\|$.

Parameters for Fig. 2.2

$H = \text{diag}((10, 0.5, 10, 10, 10))$, $\mathbf{u}_a = \text{normalize}((0.0, 0.9, 0.1, 0, 0))$, $\mathbf{u}_b = \text{normalize}((0.9, 0.1, 0.0, 0.1, 0))$.

Parameters for Fig. 2.3 Left Half

$H = \text{diag}((10, \lambda, 10, 10, 10))$, $\mathbf{u}_a = \text{normalize}((0.9, 0.1, 0.1, 0, 0))$, $\mathbf{u}_b = \text{normalize}((0.9, 0.1, 0.0, 0.1, 0))$, $\mathbf{g} = (g, 0, 0, 0, 0)$, $f_a = f_b = 1$, $\mathbf{h} = -(f_a\mathbf{u}_a + f_b\mathbf{u}_b)/2$.

Parameters for Fig. 2.3 Right Half

$H = \text{diag}((10, \lambda, 10, 10, 10))$, $H_{\text{dis}} = \text{diag}((0.01, 0.01, 0.01, 0.01, 0.01))$, $\mathbf{u}_a = \text{normalize}((0.0, 0.5, 0.5, 0, 0))$, $\mathbf{u}_b = \text{normalize}((0.0, 0.5, 0.0, 0.5, 0))$, $k_a = k_b = 1$.

Parameters for Fig. 2.4 A

$H = \text{diag}((1, 0.1, 1, 1, 1))$, $H_{\text{dis}} = \text{diag}((0.01, 0.01, 0.01, 0.01, 0.01))$, $\mathbf{u}_a = \text{normalize}((0.0, 0.5, 0.5, 0, 0))$, $\mathbf{u}_a = \text{normalize}((0.0, 0.5, 0.0, 0.5, 0))$, $f_a = f_b = 0.5$, $k_a = k_b = 0$, $\epsilon = 30$, $\mathbf{h} = -(f_a\mathbf{u}_a + f_b\mathbf{u}_b)/2$, $\mathbf{g} = (0, 0, 0, 0, 0)$.

Parameters for Fig. 2.4 B

$H = \text{diag}((1, 0.08, 1, 1, 1))$, $H_{\text{dis}} = \text{diag}((0.01, 0.01, 0.01, 0.01, 0.01))$, $\mathbf{u}_a = \text{normalize}((0.0, 0.5, 0.5, 0, 0))$,

$\mathbf{u}_a = \text{normalize}((0.0, 0.5, 0.0, 0.5, 0))$, $f_a = f_b = 0$, $k_a = k_b = 0.5$, $\epsilon = 30$, $\mathbf{h} = (0, 0, 0, 0, 0)$, $\mathbf{g} = (0, 0, 0, 0, 0)$.

Parameters for Fig. 2.4 C

$H = \text{diag}((1, 1, 1, 1, 1))$, $H_{\text{dis}} = \text{diag}((0.01, 0.01, 0.01, 0.01, 0.01))$, $\mathbf{u}_a = \text{normalize}((0.5, 0.0, 0.5, 0, 0))$, $\mathbf{u}_a = \text{normalize}((0.5, 0.0, 0.0, 0.5, 0))$, $f_a = f_b = 0.5$, $k_a = k_b = 0$, $\epsilon = 30$, $\mathbf{h} = -(f_a \mathbf{u}_a + f_b \mathbf{u}_b)/2$, $\mathbf{g} = (5, 0, 0, 0, 0)$.

Parameters for Fig. 2.4 D

$H = \text{diag}((1, 1, 1, 1, 1))$, $H_{\text{dis}} = \text{diag}((0.01, 0.01, 0.01, 0.01, 0.01))$, $\mathbf{u}_a = \text{normalize}((0, 0, 1, 0, 0))$, $\mathbf{u}_a = \text{normalize}((0, 0, 0, 1, 0))$, $f_a = f_b = 0$, $k_a = k_b = 0.5$, $\epsilon = 12$, $\mathbf{h} = (0, 0, 0, 0, 0)$, $\mathbf{g} = (0, 0, 0, 0, 0)$.

CHAPTER 3

OPTIMAL ALLOSTERY IN ELASTIC NETWORKS BEYOND LINEAR RESPONSE

ABSTRACT

Several physical mechanisms have been proposed to explain allostery in proteins. They differ by the number of internal states that they assume a protein to occupy, leaving open the question of what controls the emergence of these distinct physical forms of allostery. Here, we analyze a simplified model of protein allostery under a range of physical and evolutionary constraints. We find that a continuum of mechanisms between two archetypes emerges through evolution. In one limit, a single-state mechanism exists where ligand binding induces a displacement along a single normal mode, and in the other limit, a multi-state mechanism exists where ligand binding induces a switch across an energy barrier to a different stable state. Importantly, whenever the two mechanisms are possible, the multi-state mechanism confers a stronger allosteric effect and thus a selective advantage. This work defines the essential constraints that distinguish single- and multi-state allostery and sets the stage for a physical theory of its evolutionary origins.

The project was conceived by Olivier Rivoire, Rama Ranganathan, and me. I performed all the simulations, and Olivier Rivoire and I performed the mathematical analyses. This work is published in PRX Life 1, 023004 (2023).

3.1 Introduction

Allostery, the change of activity of a macromolecule in response to a perturbation at a distance from its active site, is thought to be a ubiquitous feature of proteins [15]. Initially described in the context of multimeric proteins [32, 31, 25], it is now understood to underlie the regulation of proteins with diverse structural architectures, from receptors to signaling proteins and metabolic enzymes [50, 24, 28, 5, 18].

Efforts to explain how allostery works date back decades with the phenomenological models of Monod, Wyman, Changeux (MWC model) and Koshland, Nemethy, Filmer (KNF model) [31, 25]. These models postulate that allosteric proteins occupy a small number

of internal states between which transitions occur either spontaneously or upon interaction with a ligand. The MWC model postulates a thermal equilibrium between two distinct states while the KNF model postulates that conformational changes are induced by binding events. These models have proved successful at fitting experimental data, and multiple extensions have been developed [25, 48, 20, 8]. They leave, however, a fundamental question unanswered: Under what physical and evolutionary conditions are one or several internal states expected in allosteric systems?

Strategically, questions of the origins of allosteric mechanisms are facilitated by reduced physical models. In such models, the emergence of one or several states can be rigorously analyzed as a function of applied physical and evolutionary constraints, permitting generalizable insights. Indeed, simplified models of proteins have been extensively studied in the context of protein folding, a problem that they helped to significantly advance [33]. More recently, several such models have been developed to study the physics and evolution of allostery [19, 53, 49, 40, 12, 54, 9, 37, 38, 41]. The idea is that by stripping down the complexities of real proteins to the essential physical features that control allostery, we can enable a foundation for better theory and experiment design. Here, we introduce a general model that encompasses previous work but extends to address the origin and properties of different forms of allostery.

Using this model, we show that two archetypal mechanisms of cooperative allostery can arise, depending on the physical and selective constraints under which evolution takes place. First, a single-state mechanism where ligand binding actuates a soft normal mode. Second, a multi-state mechanism where ligand binding stabilizes an alternate stable state, resulting in a switch-like conformational change. The former necessarily emerges when the energy landscape is constrained to be smooth. In contrast, when the energy landscape has the possibility to be rugged, we find that the second mechanism provides a statistically more likely and more cooperative mechanism. We elucidate the origin of this evolutionary outcome

with a simple analytical theory and provide a testable explanation for the pervasiveness of multiple states in allosteric proteins.

3.2 Model

Our model abstracts proteins into a two-dimensional elastic network of residues whose interactions depend on their types. Abstractly, the residues are shown as nodes in the network (Fig. 3.1A). The nodes can take Q values playing the role of the 20 amino acids constituting protein sequences (Fig. 3.1A). The energy of a network with sequence $\mathbf{s} = (s_1, \ldots, s_N)$ and conformation $\mathbf{r} = (\mathbf{r}_1, \ldots, \mathbf{r}_N)$ is of the form

$$\begin{aligned} U(\mathbf{r}, \mathbf{s}, \ell_{\text{act}}, \ell_{\text{allo}}) &= \frac{1}{2} \sum_{\langle i,j \rangle} k_{ij} \left(\delta r_{ij} - \ell_{ij} \right)^2 \\ &+ \frac{1}{2} k_{\text{act}} (\delta r_{\text{act}} - \ell_{\text{act}})^2 + \frac{1}{2} k_{\text{allo}} (\delta r_{\text{allo}} - \ell_{\text{allo}})^2 \end{aligned} \tag{3.1}$$

where the sum is over adjacent nodes in the network and where $\delta r_{ij} = ||\mathbf{r}_i - \mathbf{r}_j||$ is the distance between nodes i and j, k_{ij} is the stiffness of the spring that connects them and ℓ_{ij} is its rest length. Both the values of k_{ij} and ℓ_{ij} depend on the types s_i and s_j:

$$k_{ij} = K(s_i, s_j), \quad \ell_{ij} = L(s_i, s_j) + ||\mathbf{R}_i^{\text{dis}} - \mathbf{R}_j^{\text{dis}}||. \tag{3.2}$$

The values of $K(s_i, s_j)$ and $L(s_i, s_j)$ are given by $Q \times Q$ interaction tables (Fig. 3.1B-C), which are fixed during the evolution of networks. We set all entries of the spring stiffness table $K(s_i, s_j)$ to be stiff ($K = 1$) except for one soft interaction ($K = 0.01$). $\mathbf{R}_i^{\text{dis}}$ is a conformation generated from a disordered triangular lattice with mean spacing a (Methods). The entries of the rest length deviation table $L(s_i, s_j)$ are drawn uniformly in $[-\sigma a, \sigma a]$ where σ is a dimensionless parameter controlling the variation in the rest length deviations. When $\sigma = 0$, networks are spatially disordered yet have a zero energy ground state. As σ

increases, $L(s_i, s_j)$ becomes heterogeneous and the rest lengths deviate around the base rest lengths $||\mathbf{R}_i^{\text{dis}} - \mathbf{R}_j^{\text{dis}}||$.

To provide intuition about what σ represents, consider the absolute minimum energy of the network, known as the ground state energy,

$$E(\mathbf{s}, \ell_{\text{act}}, \ell_{\text{allo}}) = \min_{\mathbf{r}} U(\mathbf{r}, \mathbf{s}, \ell_{\text{act}}, \ell_{\text{allo}}). \tag{3.3}$$

The energy is substantially lower than other local minima associated with excited states when $\sigma = 0$. Increasing σ increases the heterogeneity of the rest lengths, which leads to networks where no single conformation can minimize the energy of all springs simultaneously. This phenomenon, known as frustration, increases the energy of the ground state and decreases the energy difference between the ground state and excited states. At large values ($\sigma = 0.3$) the energy is rugged with many nearly degenerate minima (Fig. 3.7).

We define two binding sites, an active and an allosteric site, on opposite sides of the network. The two sites correspond to springs of stiffnesses k_{act} and k_{allo} and rest lengths ℓ_{act} and ℓ_{allo} between nodes separated by distances δr_{act} and δr_{allo}. Binding at these sites is modeled by changing the rest length of one of these springs from one value representing the "solvent" ℓ_0 to another value representing a "ligand" ℓ_1 (colored bonds in Fig. 3.1D; their stiffness is, for simplicity, the same, $k_{\text{act}} = k_{\text{allo}} = 1$). Four ground-state energies are therefore defined, depending on whether the two sites are unbound, $E_{00} = E(\ell_0, \ell_0)$, one site is bound, $E_{01} = E(\ell_0, \ell_1)$ and $E_{10} = E(\ell_1, \ell_0)$, or both are bound, $E_{11} = E(\ell_1, \ell_1)$. These energies depend on the sequence $\mathbf{s}$ and are estimated using a variant of the Basin-Hopping algorithm [51] (Methods). Given the four energies, we quantify allostery by the binding cooperativity, the extent to which the binding energy at the active site depends on the presence of a ligand at the allosteric site, that is,

$$\Delta\Delta E(\mathbf{s}) = (E_{10}(\mathbf{s}) - E_{00}(\mathbf{s})) - (E_{11}(\mathbf{s}) - E_{01}(\mathbf{s})). \tag{3.4}$$

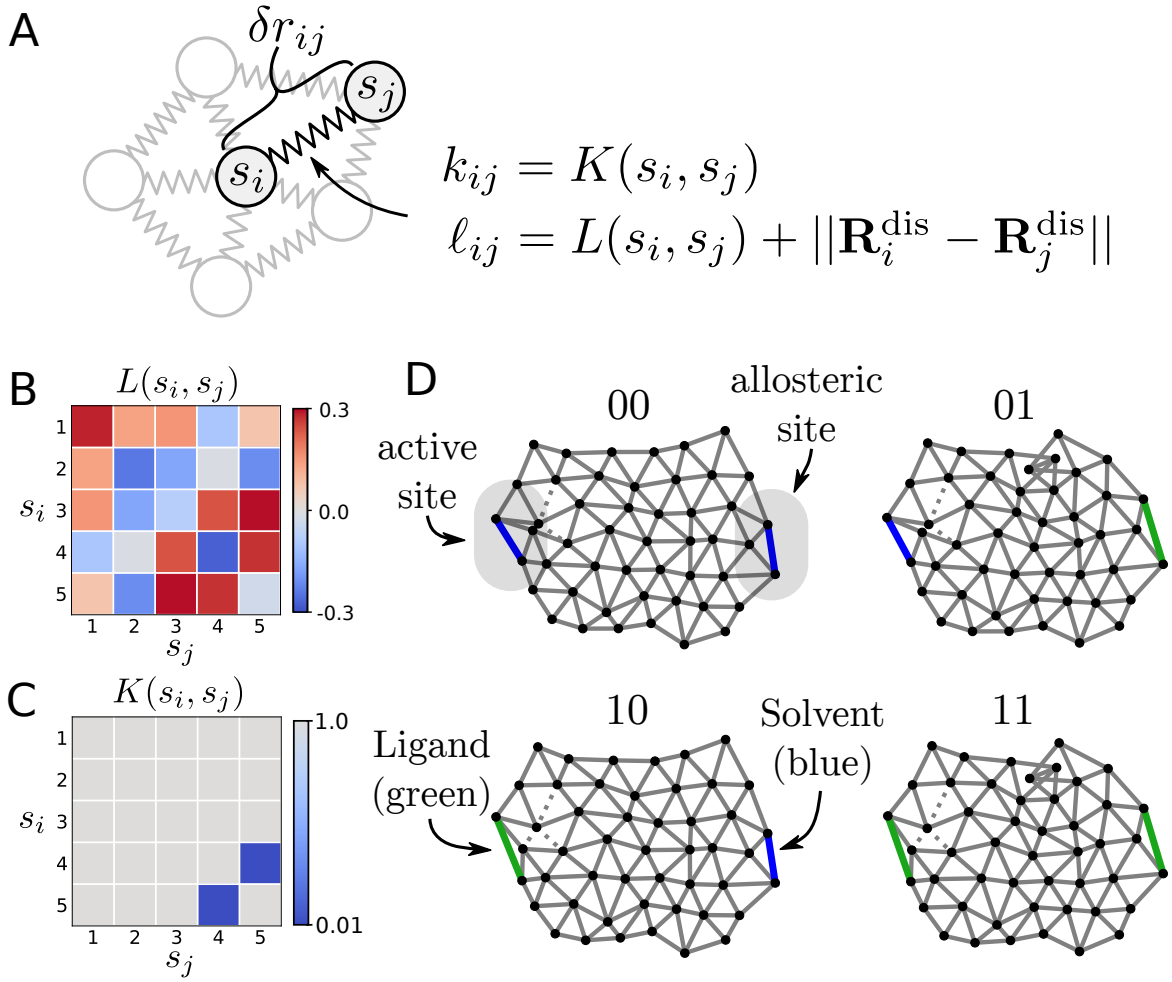

Figure 3.1: The elastic network model – (A) The physical parameters of the networks are determined by a sequence $\mathbf{s} = (s_1, \ldots, s_N)$ that specifies the type $s_i \in \{1, ..., Q\}$ of each node i. Nodes are organized in a two-dimensional triangular lattice. The spring connecting nodes i and j has stiffness $K(s_i, s_j)$ and rest length $L(s_i, s_j) + ||\mathbf{R}_i^{\rm dis} - \mathbf{R}_j^{\rm dis}||$ (Methods). (B) The table $L(s_i, s_j)$ has entries drawn uniformly in $[-\sigma a, \sigma a]$ where σ controls the disorder of the interactions. (C) The table $K(s_i, s_j)$ has all entries with $K(s_i, s_j) = 1$ except for one soft interaction with $K(s_i, s_j) = 0.01$. (D) Ground-state structures of an elastic network for the four possible ligand combinations. Solid lines represent stiff springs ($K(s_i, s_j) = 1$) and dashed lines represent soft springs ($K(s_i, s_j) = 0.01$). Ligand binding is modeled by changing the rest length of springs between two pairs of nodes that define the active or allosteric sites. One value of the rest length defines a ligand (in green) and the other is the solvent (in blue).

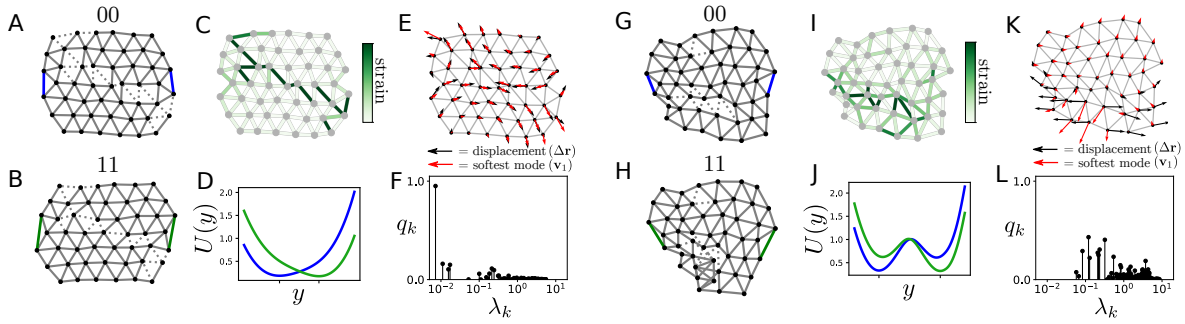

Figure 3.2: Archetypes of networks with two different allosteric mechanisms – (A-F) show a network evolved with homogeneous interactions ($\sigma = 0$), which displays a single-state mechanism. (G-L) show a network evolved with disordered interactions ($\sigma = 0.3$), which displays a two-state mechanism. (A-B) Ground state structures of the fully-solvated (00) and fully-bound (11) networks. (C) Bond strain between the structures in A and B. (D) Energy of the fully-solvated (blue) and fully-bound (green) networks along the conformational coordinate y interpolating between the structures in A and B (Methods). (E) Structural displacements between the structures in A and B (00 $\rightarrow$ 11, in black) and motion of the softest mode of the unbound state (00, in red), showing that the two are aligned. (F) Overlap q_k between the structural displacement upon binding ligand $\Delta\mathbf{r}$ and each normal mode of the network $\mathbf{v}_k$ ($q_k = |\mathbf{v}_k \cdot \Delta\mathbf{r}/\|\Delta\mathbf{r}\|\ |$) as a function of the mode stiffness λ_k, which shows, as in E, a strong overlap along the first mode. (G-L) The same analyses for a network with a two-state mechanism, showing, in contrast, a major conformational change (H versus G), an energy with two minima along the conformational coordinate, and no overlap between the displacement induced by the ligand and the softest normal modes (K-L).

We evolve the sequence $\mathbf{s}$ of a network using a Monte Carlo algorithm with the analog of mutations consisting of randomly changing the type of the node and a fitness defined by $\Delta\Delta E$ (Methods).

3.3 Results

Physical constraints on allostery

Previous elastic networks models used to evolve allostery [53, 40, 9, 54, 12] shared two key design properties. First, they lacked frustration, the condition in which stressed springs occur in the ground state. This design results in energy landscapes with effectively one minimum. Second, mutations only changed the spring stiffness of interactions. Our model implements these design properties when $\sigma = 0$.

In this limit, evolving networks for allostery reproduce the mechanism described in previous works [54, 49, 40] – a soft normal mode connects the active site to the allosteric site, and ligand binding induces a strain that aligns with this soft mode (Fig. 3.2A-F). To explain, a soft normal mode defines a direction of motion along which the system can fluctuate substantially with near isoenergetic changes. We quantify the implication of this motion in allostery by computing the overlap between the network's softest mode $\mathbf{v}_1$ and the allosteric displacement $\Delta\mathbf{r}$ ($q_1 = |\mathbf{v}_1 \cdot \Delta\mathbf{r}/\|\Delta\mathbf{r}\|\ |$) (Methods). The energy along the conformational coordinate, $U(y) = U(\mathbf{R}_{00} + y\Delta\mathbf{r})$, where $\mathbf{R}_{00}$ represents the conformation in the unbound ground state, has a single minimum that shifts upon ligand binding, corresponding to a conformational change (Fig. 3.2D). For $\sigma = 0$, the ground-state structures in the unbound $\mathbf{R}_{00}$ and bound $\mathbf{R}_{11}$ conditions belong to the same basin of attraction (Fig. 3.2D). Thus, we say that ligand binding induces a single-state conformational change (see Methods), in contrast to cases where the basins of attraction differ (e.g., Fig. 3.2J). Together, a large overlap of the conformational change with a single soft mode and the presence of a single energetic basin

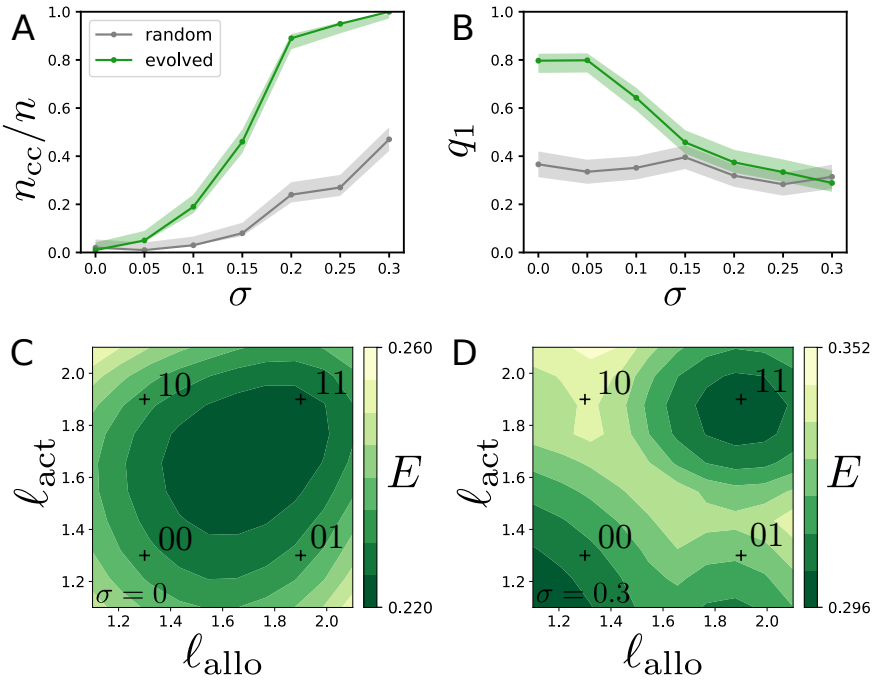

Figure 3.3: Interaction disorder controls the mechanism of allostery – (A-B) Statistics over $n = 100$ networks evolved to maximize $\Delta\Delta E$ over 500 Monte Carlo iterations as a function of the disorder σ of the interaction table $L(s_i, s_j)$. (A) Fraction of networks that undergo a multi-state conformational change n_{cc}/n (error bars are 95% Wilson CI). (B) Mean overlap between the softest mode of the network $\mathbf{v}_1$ and the allosteric displacement upon ligand binding $\Delta\mathbf{r}$ computed as $q_1 = |\mathbf{v}_1 \cdot \Delta\mathbf{r}/\|\Delta\mathbf{r}\|\,|$ (error bars are 95% Wald CI). (C-D) Examples of ground state energy surfaces $E(\ell_{\text{act}}, \ell_{\text{allo}})$ for networks evolved with homogeneous and disordered interactions, respectively. The "+" marks the locations of different binding combinations, $\ell_{\text{act}}, \ell_{\text{allo}} = (\ell_0, \ell_0), (\ell_1, \ell_0), (\ell_0, \ell_1), (\ell_1, \ell_1)$.

define "single-state allostery".

Making the energy landscape more rugged by taking $\sigma > 0$ qualitatively changes this picture (Fig. 3.2G-L). A network evolved for allostery in this context can now switch upon binding to a different stable state that is separated by an energy barrier, a multi-state conformational change (Fig. 3.2J). Additionally, the allosteric displacement no longer necessarily overlaps with the softest mode (Fig. 3.2L). This mechanism defines "multi-state allostery".

Which of these mechanisms emerge over evolution depends critically on the diversity of available interactions imposed by σ: as σ increases, networks become more frustrated, resulting in more rugged energy landscapes. The fraction of evolved networks with a multi-state

conformational change (symbolized by n_{cc}/n) increases while the overlap between the softest mode and the allosteric displacement decreases (Fig. 3.3A-B). This is also the case for random networks (gray curves in Fig. 3.3A-B), but evolved networks show significant enrichment of multi-state mechanisms for large σ and of single-state mechanisms for low σ (green curves). In between these limits exists a continuum of mechanisms that are characterized by intermediate values of n_{cc}/n and q_1. The results of Fig. 3.3A-B are robust to parameter choice (Fig. 3.8) and hold for 3d networks as well (Fig. 3.9).

The difference between mechanisms is also illustrated by representing the ground-state energy of evolved networks as a function of different binding ligands, corresponding to varying the rest lengths ℓ_{act} and ℓ_{allo} of the springs defining the active and allosteric sites (Fig. 3.3C-D). In this representation, the ground state energy landscape associated with a single-state allosteric network typically takes the form of an anisotropic basin elongated in the $\ell_{\text{act}} = \ell_{\text{allo}}$ direction such that $E_{11} + E_{00} < E_{10} + E_{01}$. On the other hand, the energy landscape associated with a multi-state allosteric network can display two minima around $\ell_{\text{act}} = \ell_{\text{allo}} = \ell_0$ and $\ell_{\text{act}} = \ell_{\text{allo}} = \ell_1$, which also achieves $E_{11} + E_{00} < E_{10} + E_{01}$.

Evolutionary constraints on allostery

The previous results show that the diversity of available physical interactions determines the mechanism of allostery. Under conditions where both mechanisms can evolve, which does evolution favor? We address this question by considering a set of interactions that contains both homogeneous ($\sigma = 0$) and disordered ($\sigma = 0.3$) rest length deviation distributions (Fig. 3.4A). Networks evolved with such an interaction table have effectively the choice to populate a part of sequence space with either smooth or rugged local energy landscapes. Simulations show that networks evolved under a selection for cooperativity have a greater number of disordered interactions (those between nodes of type 1-5) than those of random networks (random: 24%, evolved: 34%). Correspondingly, the vast majority of these evolved

networks display multi-state conformational changes (random: 10%, evolved: 90%) and an overlap with the softest mode comparable to those of random networks (random: $q_1 = 0.32$, evolved: $q_1 = 0.36$). These results are represented by the data-point $E_{\text{unfolded}} = \infty$ in Fig. 3.4. They indicate that the multi-state mechanism is more competitive than the single-state mechanism. That is, when the interactions provide sufficient disorder, networks tend to evolve towards multi-state allostery.

In real proteins, the analog of our interaction tables are interactions between the amino acids. The physics of these interactions is largely fixed and σ is therefore not subject to physiological control. But some tunable parameters may play a role similar to σ and effectively control the ruggedness of the energy landscape. One such parameter is thermal stability, which is itself subject to natural selection. As a proxy for thermal stability, we introduce here an arbitrarily defined energy E_{unfolded} to represent the energy of a non-functional unfolded state. To impose a stability constraint, we again select networks based on $\Delta\Delta E$ but now restrict the evolution to sequences satisfying $E_{00} < E_{\text{unfolded}}$.

By evolving networks for varying values of E_{unfolded}, we verify that smaller values of E_{unfolded} result in more stable networks (Fig. 3.4F). The most stable networks are less likely to undergo a multi-state conformational change upon ligand binding (Fig. 3.4C) and, on average, show a greater overlap between the allosteric displacement and the softest mode (Fig. 3.4E). Additionally, the usage of disordered interactions decreases with decreasing E_{unfolded} (Fig. 3.4D). These results show how an additional selective pressure, here stability, can alter the likelihood of evolving a single or multi-state mechanism of allostery. The underlying phenomenon is the same as before – stable networks minimize frustration and thus tend to populate smoother parts of the landscape, effectively corresponding to a smaller σ. Thus, thermal stability is a parameter that can, in principle, control the mechanism of allostery.

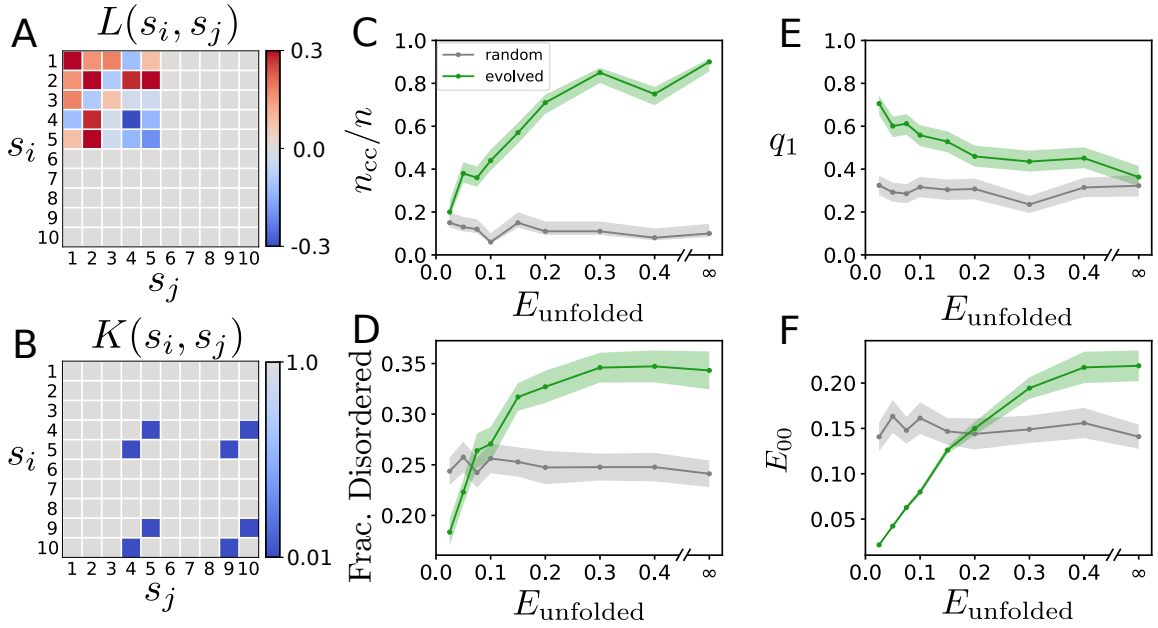

Figure 3.4: Additional selective pressures can modulate the mechanism of allostery – (A) An example of a rest length deviation table $L(s_i, s_j)$ designed to support both homogeneous and disordered interactions. (B) Spring-constant interaction table $K(s_i, s_j)$. (C-F) Properties of networks evolved under a joint pressure for cooperativity (large $\Delta\Delta E$) and stability (small E_{00}) as a function of the intensity E_{unfolded} of the selective pressure for stability (statistics over 100 networks evolved through 500 Monte Carlo iterations). (C) Fraction of networks that undergo a two-state conformational change (error bars are 95% Wilson CI). (D) Fraction of interactions between nodes of type 1-5 ($(s_i, s_j) \in \{1, 2, 3, 4, 5\}^2$; error bars are 95% Wilson CI). (E) Mean overlap of the allosteric displacement upon ligand binding (00→11) and the softest non-zero mode of the network in the unbound state (error bars are 95% Wald CI). (F) Ground-state energy of the unbound state (errors bars are 95% Wald CI). In the absence of constraint for stability ($E_{\text{unfolded}} = \infty$), networks evolve a multi-state mechanism using the disordered interactions. As the constraint for stability is increased (E_{unfolded} decreased), they tend to evolve a single-state mechanism relying on non-disordered interactions.

1d model

The two archetypal mechanisms displayed by our two-dimensional network model can be illustrated in an even simpler one-dimensional model. This model consists of two rigid bars connected by three springs – two harmonic springs represent the active and allosteric sites, and a single elastic spring with the potential to flip mediates the mechanism of allostery (Fig. 3.5A). The energy of this model is

$$U(x) = \frac{1}{2}\Big[k_a(x - \ell_{\text{act}})^2 + k_m(|x| - \ell_m)^2 + k_a(x - \ell_{\text{allo}})^2\Big]. \tag{3.5}$$

The ground-state energy $E(\ell_{\text{act}}, \ell_{\text{allo}}) = \min_x U(x)$ is harmonic with a single minimum when $\ell_m = 0$ and has two minima when $\ell_m > 0$ (Fig. 3.5CD). As in the 2d elastic network, we represent solvent and ligand by the algebraic values ℓ_0 and ℓ_1, respectively. For simplicity, we assume $\ell_0 = -\ell_1$. Under these assumptions, the cooperativity is (see Appendix)

$$\Delta\Delta E = \frac{k_a\,(k_a\delta + 2k_m\ell_m)\,\delta}{2k_a + k_m}, \tag{3.6}$$

with $\delta = |\ell_1 - \ell_0|$. The mechanism is strictly single-state only for $\ell_m = 0$, in which case $\Delta\Delta E$ cannot exceed $k_a\delta^2/2$. On the other hand, when $\ell_m > 0$, $\Delta\Delta E$ can take arbitrarily large values and scales as $\Delta\Delta E \sim k_a\ell_m\delta$ when $k_m \to \infty$. A continuum of mechanisms exists between these two extremes (Fig. 3.5E) but, when viewing ℓ_m as a physical property of the landscape and k_m as an evolutionary parameter, two distinct regimes emerge: when $\ell_m < \delta/4$, a single-state mechanism with a soft mode ($k_m = 0$) is optimal while when $\ell_m > \delta/4$, a two-state mechanism with a large barrier ($k_m = \infty$) is optimal. Finally, if ℓ_m is itself subject to evolution, maximal cooperativity $\Delta\Delta E$ is achieved by the two-state mechanism ($\ell_m = \infty$, $k_m = \infty$).

The analytical prediction of the 1d model (3.6) can be compared with data from the 2d

model by defining 2d analogs, $\tilde{k}_m$ and $\tilde{\ell}_m$, of the 1d model's reduced parameters, k_m/k_a and ℓ_m/δ. We define $\tilde{k}_m = \lambda_1/\tilde{\lambda}$, where λ_1 is the stiffness of the softest non-zero mode and $\tilde{\lambda}$ is the median mode stiffness. This quantity captures the stiffness of the allosteric mode in single-state allostery, which k_m/k_a measures in the 1d model. In the 1d model, ℓ_m is related to the height of the barrier of $U(x)$ when $k_a = 0$: $\Delta U_{\text{barrier,1d}} = k_m \ell_m^2/2$. To define an equivalent quantity for the 2d elastic network model, we consider $\tilde{\ell}_m = \delta^{-1}\sqrt{2\Delta U_{\text{barrier}}/\lambda_1}$ when $k_{\text{act}} = k_{\text{allo}} = 0$ and $\Delta U_{\text{barrier}}$ is the height of the network's barrier (See Methods). We find that non-allosteric random networks have large values of $\tilde{k}_m$ and small values of $\tilde{\ell}_m$ for all values of σ (Fig. 3.6A). At small values of sigma, evolved, allosteric networks localize to the single-state region where $\tilde{k}_m$ and $\tilde{\ell}_m$ are both small as predicted by the 1d model. Increasing σ enables networks to have larger energy barriers and larger values of $\tilde{\ell}_m$ (Fig. 3.10A). Evolved networks at large σ take advantage of this by switching to a multi-state mechanism and localizing to the large $\tilde{k}_m$, large $\tilde{\ell}_m$ region. Comparing Fig. 3.5E and Fig. 3.6A shows the remarkable ability of the 1d theory to qualitatively describe the complex behavior from the 2d network.

Equation (3.6) predicts that cooperativity of the two mechanisms should scale differently with the magnitude of ligand binding perturbation $\delta = |\ell_1 - \ell_0|$ ($\Delta\Delta E \sim \delta^\gamma$, single-state: $\gamma = 2$ and multi-state: $\gamma = 1$). When $\sigma = 0$ and networks use the single-state mechanism, we find $\gamma \approx 1.95$ for evolved networks (Fig. 3.6B). Increasing σ results in decreasing values of γ toward unity. This result suggests a testable hypothesis: If smaller ligands induce more subtle perturbations, then allosteric proteins that bind small molecules should use the multi-state mechanism more often than allosteric proteins whose ligands are other large proteins.

To summarize, the 1d model identifies the key elements necessary for understanding the connection between single-state and multi-state allostery. It suggests that the specific details of the 2d network, which are absent in the 1d model, can vary with little effect (Fig. 3.8).

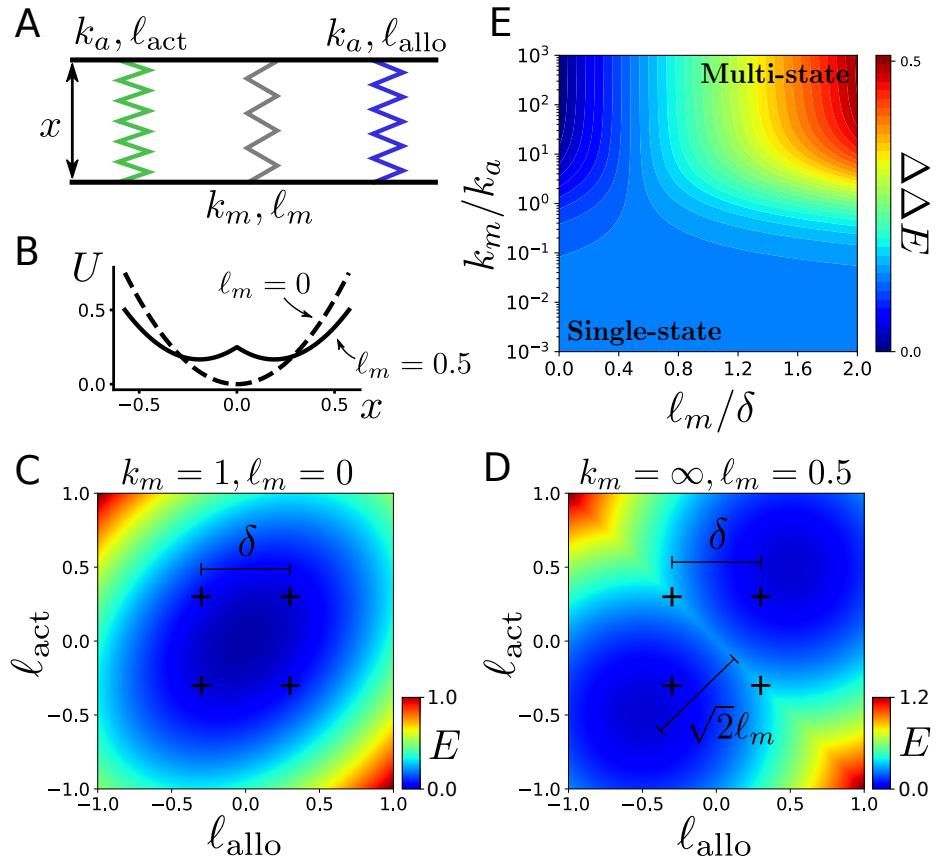

Figure 3.5: A 1d model recapitulates the results obtained with 2d elastic network– (A) The model consists of three springs connecting two rigid bars constrained to move in one dimension. Two springs are analogous to the ligand springs of the elastic network. The third spring, whose contribution to the energy is $k_m(|x| - \ell_m)^2/2$, mediates the mechanism of allostery and can flip. (B) Total energy $U(x)$ as a function of x for two values of ℓ_m: the energy landscape has a single minimum $\ell_m = 0$ and two minima when $\ell_m > 0$. (C) The ground state energy of the 1d model, $E(\ell_{\text{act}}, \ell_{\text{allo}})$. Small values of k_m, ℓ_m correspond to a single-state mechanism. (D) The ground state energy of the 1d model, $E(\ell_{\text{act}}, \ell_{\text{allo}})$. Large values of k_m, ℓ_m correspond to a multi-state mechanism. (E) Cooperativity $\Delta\Delta E$ as a function of the normalized quantities k_m/k_a and ℓ_m/δ, showing a continuum between purely single-state and strongly two-state mechanisms.

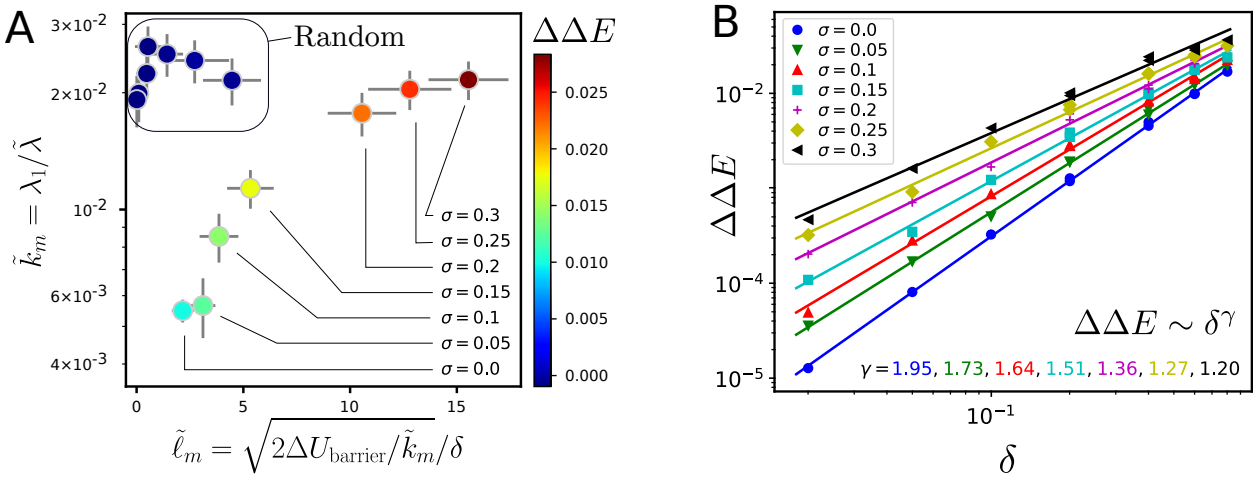

Figure 3.6: 1d model predicts the behavior of the 2d elastic networks. $\tilde{k}_m$ and $\tilde{\ell}_m$ are the 2d elastic network analogs of the 1d model's parameters k_m and ℓ_m. (A) The mean $\tilde{k}_m$ and $\tilde{\ell}_m$, and $\Delta\Delta E$ are plotted for 100 random and 100 evolved networks at different σ. Error bars are 95% CI. Consistent with the 1d model, non-allosteric random networks localize to the large $\tilde{k}_m$ and small $\tilde{\ell}_m$ corner. When σ is small, networks approach the single-state mechanism limit ($\ell_m = 0, k_m = 0$). As σ increases, networks localize towards the multi-state mechanism limit of large k_m, large ℓ_m. (B) Scaling of allosteric cooperativity $\Delta\Delta E$ with the magnitude of ligand binding perturbation $\delta = |\ell_1 - \ell_0|$. Each data point shows the mean $\Delta\Delta E$ averaged over 100 evolved networks with parameters σ and δ. For each σ, data is fit to the power law $\Delta\Delta E \sim \delta^{\gamma}$, and fitted γ values are shown at the bottom. The 1d model predicts that in the single-state limit, $\gamma = 2$, while in the multi-state limit $\gamma = 1$. 2d networks evolved at $\sigma = 0$ use a single-state mechanism and show a scaling of $\gamma \approx 1.95$. As σ increases, networks increasingly use the multi-state mechanism, and values of γ approach one.

3.4 Discussion

In this work, we study the evolutionary origins of single or multiple states in systems selected for allostery using a minimal yet generic physical model of protein allostery. Depending on the ruggedness of the underlying energy landscapes, two archetypal mechanisms emerge: in smooth landscapes, a single-state mechanism evolves, while in rugged landscapes, a multi-state mechanism evolves. In single-state systems, allostery is mediated through the actuation of a soft global mode induced by ligand binding, whereas in multi-state systems, ligand binding stabilizes an alternate pre-existing state. We find that the multi-state mechanism has a greater potential for cooperativity and is therefore evolutionarily favored whenever it has the possibility to evolve. We also find that additional selective pressures can modulate the outcome of evolution; in particular, a strong selection for stability favors the evolution of single-state mechanisms. These results are demonstrated by numerical simulations in a two-dimensional elastic network model and recapitulated by analytical calculations in a simpler one-dimensional model.

Elastic network models have been extensively studied as coarse-grained models for proteins and have been shown to accurately capture thermal fluctuations [2, 1]. Here, we use these models to implement a generic energy landscape in which the allosteric role of soft modes and multiple states can be understood. Multi-state conformational changes take the form of buckling instability in the elastic network model, while in proteins, state transitions may take many different physical forms [50, 42, 27, 52]. Regardless, the essential feature of multi-state conformational switching is a barrier between two energy minima, which is shared in simple models and real proteins. The fact that our results extend to 3d networks (Fig. 3.9) and they are recapitulated by a 1d model of three springs (Figures 3.5 and 3.6) indicate that they are robust to details of the geometry of the network and to the nature of the potential. Indeed, the only feature necessary to control single- or multi-state outcomes

is tunable ruggedness. An implication is that, as seen by simulations (Fig. 3.4F), multi-state proteins varied through directed evolution protocols to optimize stability should lose their multi-state character due to loss of ruggedness, a prediction that can be experimentally tested. These findings illustrate the clarifying value of simple physical models in isolating the essential parameters from the large ensemble of complex properties exhibited by natural proteins.

For computational expedience, the simulations here are at zero temperature, ignoring changes in system entropy. However, the distinction between single-state and multi-state mechanisms extends to finite temperatures straightforwardly by simply considering the free energy instead of the ground-state energy. We carried out this generalization for the one-dimensional model, showing that temperature does not modify the general conclusions reported here (see Appendix, Fig. 3.11). In future work, it will be valuable to extend this work to consider "dynamic allostery" in which long-range interactions are driven purely by propagated changes in entropy [7, 29, 36]. The route to this extension is by enabling ligand binding to stiffen ligand binding sites rather than applying a force or a displacement. Our model also does not explicitly account for partial or global unfolding [30] but allosteric mechanisms where ligand binding differentially stabilizes the folded and unfolded ensembles are also instances of multi-state mechanisms when folding is a cooperative process [22].

The distinction between single and multi-state mechanisms of allostery reflects the two classes of phenomenological models that have been introduced to describe allostery, namely the MWC and KNF models [31, 25]. The KNF model, where state changes only upon ligand binding, assumes a single-state mechanism, while the MWC model, where two states preexist ligand binding, assumes a two-state mechanism. Indeed, the physical model described here can be reformulated from a thermodynamic perspective to be analogous to MWC and KNF models (Appendix). The MWC and KNF models are archetypes at the two ends of a continuum of models for allostery that interpolate between them [20]. Thus, the work presented

here provides a foundation for understanding the assumptions underlying these models, and perhaps more importantly, the evolutionary origin of specific models for allostery.

The central parameter controlling single- or multi-state allostery is the heterogeneity σ of interactions, leading to frustration and ruggedness in the energy landscape of the model networks. Indeed, a significant prior work shows that real proteins are frustrated networks [10, 11] and that this property is important for allostery [14]. Since conformational switching between stable states [13, 50, 23], folding intermediates [3] and misfolding [6] are commonplace in proteins, we conclude that amino acid interactions display the kind of heterogeneity in natural proteins to enable the evolution of multi-state allostery. Indeed, these considerations, together with the work presented here, suggest that a multi-state mechanism is statistically more likely in natural allosteric proteins.

This statement is consistent with the diversity of mechanisms underlying allostery observed in proteins. Previous work using Normal Mode Analysis to estimate the largest overlap between the allosteric displacement and any normal mode ($\max_i\ q_i$) of proteins has found a broad range of values. Several studies converge to find that the largest overlaps in allosteric proteins are of the order of 0.5 with a standard deviation of the order 0.2 [37, 55]. When we measure the largest overlap $\max_i\ q_i$ rather than the overlap with the softest mode q_1 we find overlaps of a similar order ($\gtrsim 0.5$) even for non-allosteric random networks (Fig. 3.12E-F). Additionally, we find that many evolved allosteric networks lie in the continuum between the two archetypal mechanisms, with both an energy barrier separating multiple states and some overlap with the softest mode $q_1 > 0.5$ (Fig. 3.12A-D,K,L). Thus, the empirical finding that the allosteric conformational change overlaps with the softest mode does not signify the absence of a multi-state conformational change. This point has been made by Gur, Zomot, and Bahar based on analysis of elastic networks by molecular dynamics simulations [16].

An interesting perspective is the potential value of simplified models for better understanding computational approaches for inferring allosteric networks from extant sequence

data [39]. Indeed, statistical analyses of homologous protein sequences have demonstrated the existence of sparse, collectively evolving networks of amino acids within proteins that mediate allosteric communication [26, 47, 17]. It will be interesting to use the simplified models presented here as a ground truth to study how sequence-based inference process depends on both the sampling of input data and the parameters that control the emergence of different forms of allostery.

While our work focuses on allostery in the context of proteins, the implications of these results extend more broadly to the emerging field of learning in physical systems [43]. The idea of physical learning is to start with a randomly configured (and non-functional) physical system and to iteratively optimize its performance for a chosen task by varying the many physical parameters [45, 44, 46]. For example, recent studies have taken this approach to train an elastic network to perform an allosteric task [40, 41, 21, 46]. Typically, networks are designed with minimal frustration, resulting in single-state allostery, but multi-state behavior has been empirically shown to emerge when rest lengths are allowed to vary [21, 46]. The work presented here provides a clear rationale for these observations and predicts that by design with frustration, more efficient and varied allosteric functions may be achieved. It will be interesting to test these ideas using now emerging methods to prototype physical materials that embody the simulated networks [40, 35, 34]. Such experiments in macroscopic materials would provide a clear test of the ideas presented in this work, even as we await practical methods for engineering allosteric proteins.

3.5 Methods

To build a network, nodes are first placed on a triangular lattice (with spacing a) with their positions given by $\mathbf{R}_i^{\text{lat}}$. An adjacency matrix defined by nearest neighbors, $A_{ij} = 1$ if $||\mathbf{R}_i^{\text{lat}} - \mathbf{R}_j^{\text{lat}}|| = a$ and $A_{ij} = 0$, otherwise. The nodes are then displaced by a random uniform perturbation $\Delta\mathbf{R}_i \sim ([-a\epsilon, a\epsilon], [-a\epsilon, a\epsilon])$ to achieve a disordered structure $\mathbf{R}_i^{\text{dis}} =$

$\mathbf{R}_i^{\text{lat}} + \Delta\mathbf{R}_i$. The dimensionless parameter ϵ controls the extent of the spatial disorder and is taken to be $\epsilon = 0.1$ unless stated otherwise. Each node is assigned a value $s_i \in \{1, 2, \ldots, Q\}$ giving the network a sequence $\mathbf{s} = (s_1, \ldots, s_N)$. Springs are connected between nodes with stiffness and rest lengths that depend on the sequence $\mathbf{s}$,

$$k_{ij} = A_{ij} K(s_i, s_j) \tag{3.7}$$

$$\ell_{ij} = L(s_i, s_j) + ||\mathbf{R}_i^{\text{dis}} - \mathbf{R}_j^{\text{dis}}|| \tag{3.8}$$

The values of $K(s_i, s_j)$ and $L(s_i, s_j)$ are given by $Q \times Q$ symmetric interaction tables. Specifically, we consider all interactions in $K(s_i, s_j)$ to be stiff ($K = 1$) except for one randomly chosen entry that is soft ($K = 0.01$). The entries of $L(s_i, s_j)$ are drawn uniformly in $[-a\sigma, a\sigma]$ where σ is a dimensionless parameter controlling the disorder in the rest lengths deviations.

The full energy of a network with conformation $\mathbf{r} = (\mathbf{r}_1, \ldots, \mathbf{r}_N)$ sequence s is

$$\begin{aligned} U(\mathbf{r}, \mathbf{s}, \ell_{\text{act}}, \ell_{\text{allo}}) = & \frac{1}{2} \sum_{i>j} k_{ij} (\delta r_{ij} - \ell_{ij})^2 \\ & + \frac{1}{2} k_{\text{rep}} \sum_{i>j} (1 - A_{ij}) \Theta(\ell_{\text{rep}} - \delta r_{ij}) (\delta r_{ij} - \ell_{\text{rep}})^2 \\ & + \frac{1}{2} k_{\text{act}} (\delta r_{\text{act}} - \ell_{\text{act}})^2 \\ & + \frac{1}{2} k_{\text{allo}} (\delta r_{\text{allo}} - \ell_{\text{allo}})^2. \end{aligned} \tag{3.9}$$

where $\mathbf{r}_i = (x_i, y_i)$ is the position of node i and $\delta r_{ij} = ||\mathbf{r}_i - \mathbf{r}_j||$ is the distance between nodes i and j. To prevent non-physical network collapse behaviors, the second term of (3.9) defines a harmonic repulsion term between non-adjacent nodes. Θ is the Heaviside function so that $\Theta(\ell_{\text{rep}} - \delta r_{ij}) = 1$ if $\ell_{\text{rep}} > \delta r_{ij}$ and 0 otherwise. $\ell_{\text{rep}} = 0.7$ and $k_{\text{rep}} = 2$ are the distance cutoff and spring constant for the harmonic repulsion term, respectively. All networks simulated in this work have a size of $N = 49$ nodes.

The third and fourth terms in (3.9) detail the contribution of ligand binding to the active and allosteric sites, respectively. The active site is chosen by picking two nodes on one side of the network that are previously unconnected and connecting them with a spring of rest length ℓ_{act} and stiffness k_{act}. δr_{act} measures the distance between these two nodes. The allosteric site is chosen in the same way, but on the opposite side of the network. For this work $k_{\text{act}} = k_{\text{allo}} = 1$. Importantly ℓ_{act} and ℓ_{allo} are independent of $\mathbf{s}$.

The ground state energy of the network is computed as,

$$E(\mathbf{s}, \ell_{\text{act}}, \ell_{\text{allo}}) = \min_{\mathbf{r}} U(\mathbf{r}, \mathbf{s}, \ell_{\text{act}}, \ell_{\text{allo}}) \tag{3.10}$$

Binding is modeled by changing the rest length of a binding site spring from one value representing the "solvent" ℓ_0 to another value representing the "ligand" ℓ_1 (colored bonds in Fig. 3.1D). The binding cooperativity is computed as,

$$\begin{aligned} \Delta\Delta E(\mathbf{s}) = &(E(\mathbf{s}, \ell_1, \ell_0) - E(\mathbf{s}, \ell_0, \ell_0)) \\ &- (E(\mathbf{s}, \ell_1, \ell_1) - E(\mathbf{s}, \ell_0, \ell_1)) \end{aligned} \tag{3.11}$$

Disorder enters in three forms in our model, once from variability in the stiffnesses of the springs, which is enabled by the heterogeneity of the stiffness table $K(s_i, s_j)$. A second form enters through the spatial disorder in the base conformation $\mathbf{R}_j^{\text{dis}}$. In the case of $\epsilon > 0$ and $\sigma = 0$, the rest lengths reduce to the pairwise distances of the disordered lattice conformation $\ell_{ij} = ||\mathbf{R}_i^{\text{dis}} - \mathbf{R}_j^{\text{dis}}||$, which results in $U(\mathbf{s}, \mathbf{R}^{\text{dis}}) = 0$ (ignoring the effect of ligands). This implies that spatial disorder originating from $\epsilon > 0$ does not contribute to the frustration of the network. Finally, when $\sigma > 0$ the rest lengths can deviate from $||\mathbf{R}_i^{\text{dis}} - \mathbf{R}_j^{\text{dis}}||$ by an amount given by $L(s_i, s_j)$. Only the disorder in $L(s_i, s_j)$ gives rise to frustration in the network. The realizations of $K(s_i, s_j)$, $L(s_i, s_j)$ and $\mathbf{R}_i^{\text{dis}}$ are fixed during the evolution of network.

Estimating ground states. We estimate the ground state of a network with a version of the Basin-Hopping algorithm [51] where a genetic algorithm is used instead of a Monte Carlo algorithm to search conformation space. The algorithm (1) initializes a population of p copies of a network; (2) perturbs ($\mathbf{r} \to \mathbf{r} + \boldsymbol{\eta},\ \boldsymbol{\eta} \sim \mathcal{N}$) and relaxes each structure to a local minimum using the FIRE algorithm [4]; (3) removes the $p/2$ structures with the highest relaxed energy; (4) replicates each remaining structure; (5) repeats steps 2-4 $N_{\text{iterations}}$ times; (6) outputs the structure with the lowest energy. We take $p = 20$ and $N_{\text{iterations}} = 100$, which we find to be sufficient for estimating the ground state (See Fig. 3.7D for an estimate of the error in the algorithm).

Definition of single-state and multi-state mechanisms. Let $\mathbf{R}_{00}$ and $\mathbf{R}_{11}$ denote the unbound ($\ell_{\text{act}} = \ell_{\text{allo}} = \ell_0$) and bound ($\ell_{\text{act}} = \ell_{\text{allo}} = \ell_1$) ground-state conformations, respectively,

$$\mathbf{R}_{ii} = \arg\min_{\mathbf{r}} U(\mathbf{r}, \mathbf{s}, \ell_i, \ell_i), \quad i = 0, 1. \tag{3.12}$$

We define $\mathbf{R}'_{00}$ as the structure relaxed from $\mathbf{R}_{11}$ in absence of ligand ($\ell_{\text{act}} = \ell_{\text{allo}} = \ell_0$) and $\mathbf{R}'_{11}$ as the structure relaxed from $\mathbf{R}_{00}$ in presence of the two ligands ($\ell_{\text{act}} = \ell_{\text{allo}} = \ell_1$). We say that the mechanism is single-state if $\mathbf{R}_{00} = \mathbf{R}'_{00}$ and $\mathbf{R}_{11} = \mathbf{R}'_{11}$, and multi-state otherwise.

Normal modes. Normal modes are computed by eigenvalue decomposition of the Hessian matrix H of the energy in the unbound state $\mathbf{R}_{00}$ when the active and allosteric site springs are removed, $k_{\text{act}} = k_{\text{allo}} = 0$. The components of H are,

$$H_{ij} = \frac{\partial^2}{\partial x_i \partial x_j} \bar{U}\Big|_{\mathbf{r}=\mathbf{R}_{00}}, \tag{3.13}$$

$$\bar{U} = U(\mathbf{r}, \mathbf{s}, \ell_0, \ell_0, k_{\text{act}} = 0, k_{\text{allo}} = 0). \tag{3.14}$$

There are three zero modes ($\lambda_k = 0$) corresponding to global rotation $\mathbf{v}_{\text{rot}}$ and two global

translations $\mathbf{v}_x$ and $\mathbf{v}_y$. The nonzero modes and their stiffnesses are denoted $\mathbf{v}_k$ and λ_k with $\lambda_i \leq \lambda_j$ if $i > j$, with $\mathbf{v}_1$ being the softest nonzero mode.

Allosteric displacement. Given $\mathbf{d} = \mathbf{R}_{11} - \mathbf{R}_{00}$, the allosteric displacement $\Delta\mathbf{r}$ is computed as

$$\Delta\mathbf{r} = \mathbf{d} - (\mathbf{d} \cdot \mathbf{v}_{\text{rot}})\mathbf{v}_{\text{rot}} - (\mathbf{d} \cdot \mathbf{v}_x)\mathbf{v}_x - (\mathbf{d} \cdot \mathbf{v}_y)\mathbf{v}_y. \tag{3.15}$$

Overlaps. The overlap between a nonzero normal mode $\mathbf{v}_k$ and the allosteric displacement $\Delta\mathbf{r}$ is computed as

$$q_k = \left| \frac{\Delta\mathbf{r}}{\|\Delta\mathbf{r}\|} \cdot \mathbf{v}_k \right|. \tag{3.16}$$

Conformational coordinate. The conformational coordinate y is defined by $\mathbf{r}(y) = \mathbf{R}_{00} + y\Delta\mathbf{r}$ and its associated energy by $U(y) = U(\mathbf{r}(y), \mathbf{s})$.

Monte Carlo evolution. Networks are "evolved" using a Metropolis Monte Carlo method with an error-catching step due to the stochastic nature of the ground state finding algorithm. A candidate sequence $\mathbf{s}'$, one mutation away from the current sequence $\mathbf{s}$, is accepted with probability $p = \exp((\Delta\Delta E(\mathbf{s}') - \Delta\Delta E(\mathbf{s}))/T_{\text{evo}})$ where $T_{\text{evo}} = 10^{-5}$. Following the acceptance or rejection step, the ground states of the current sequence, E_{00}, E_{10}, E_{01}, E_{11} are systematically reevaluated. If a lower ground state energy is found, the current sequence is set to the previous sequence, and ground states are recomputed. This step prevents inaccurate ground state estimates from causing fictitiously large values of $\Delta\Delta E$. Importantly, the error in the ground state finding algorithm does not affect the results as demonstrated by Fig. 3.8P – the same results are found with more exhaustive sampling and thus lower rates of error.

Elastic network analogs of 1d model parameters. In the 1d model, k_m can be interpreted as the stiffness of the allosteric mode. To define an equivalent quantity for the 2d elastic network model, we consider $\tilde{k}_m = \lambda_1/\tilde{\lambda}$, where λ_1 is the stiffness of the softest non-zero mode and $\tilde{\lambda}$ is the median stiffness. In the 1d model, ℓ_m is related to the height of

the barrier of $U(x)$ when $k_a = 0$: $\Delta U_{\text{barrier}} = k_m \ell_m^2/2$. To define an equivalent quantity for the 2d elastic network model, we consider $\tilde{\ell}_m = \delta^{-1}\sqrt{2\Delta U_{\text{barrier}}/\lambda_1}$ when $k_{\text{act}} = k_{\text{allo}} = 0$. We define $\Delta U_{\text{barrier}} = 0$ if $U(y)$ has one minimum ($U'(y) = 0, U''(y) > 0$). If $U(y)$ has two minima, we take y_1 and y_2 to be their locations and y_3 to be the location of the maximum in between. We define, $\Delta U_{\text{barrier}} = U(y_3) - \max(U(y_1), U(y_2))$. Scenarios with more than two minima are not observed.

References

[1] Ali Rana Atilgan, SR Durell, Robert L Jernigan, Melik C Demirel, O Keskin, and Ivet Bahar. Anisotropy of fluctuation dynamics of proteins with an elastic network model. *Biophysical journal*, 80(1):505–515, 2001.

[2] Ivet Bahar, Ali Rana Atilgan, and Burak Erman. Direct evaluation of thermal fluctuations in proteins using a single-parameter harmonic potential. *Folding and Design*, 2 (3):173–181, 1997.

[3] Yawen Bai, Tobin R Sosnick, Leland Mayne, and S Walter Englander. Protein folding intermediates: native-state hydrogen exchange. *Science*, 269(5221):192–197, 1995.

[4] Erik Bitzek, Pekka Koskinen, Franz Gähler, Michael Moseler, and Peter Gumbsch. Structural relaxation made simple. *Physical review letters*, 97(17):170201, 2006.

[5] Jean-Pierre Changeux and Stuart J Edelstein. Allosteric mechanisms of signal transduction. *Science*, 308(5727):1424–1428, 2005.

[6] Fabrizio Chiti and Christopher M Dobson. Protein misfolding, functional amyloid, and human disease. *Annu. Rev. Biochem.*, 75:333–366, 2006.

[7] A Cooper and DTF Dryden. Allostery without conformational change. *European Biophysics Journal*, 11(2):103–109, 1984.

[8] Qiang Cui and Martin Karplus. Allostery and cooperativity revisited. *Protein science*, 17(8):1295–1307, 2008.

[9] Sandipan Dutta, Jean-Pierre Eckmann, Albert Libchaber, and Tsvi Tlusty. Green function of correlated genes in a minimal mechanical model of protein evolution. *Proceedings of the National Academy of Sciences*, 115(20):E4559–E4568, 2018.

[10] Diego U Ferreiro, Joseph A Hegler, Elizabeth A Komives, and Peter G Wolynes. Localizing frustration in native proteins and protein assemblies. *Proceedings of the National Academy of Sciences*, 104(50):19819–19824, 2007.

[11] Diego U Ferreiro, Joseph A Hegler, Elizabeth A Komives, and Peter G Wolynes. On the role of frustration in the energy landscapes of allosteric proteins. *Proceedings of the National Academy of Sciences*, 108(9):3499–3503, 2011.

[12] Holger Flechsig. Design of elastic networks with evolutionary optimized long-range communication as mechanical models of allosteric proteins. *Biophysical journal*, 113(3): 558–571, 2017.

[13] Hans Frauenfelder, Fritz Parak, and Robert D Young. Conformational substates in proteins. *Annual review of biophysics and biophysical chemistry*, 17(1):451–479, 1988.

[14] Stefano Gianni and Per Jemth. Allostery frustrates the experimentalist. *Journal of Molecular Biology*, page 167934, 2022.

[15] K Gunasekaran, Buyong Ma, and Ruth Nussinov. Is allostery an intrinsic property of all dynamic proteins? *Proteins: Structure, Function, and Bioinformatics*, 57(3):433–443, 2004.

[16] M Gur, E Zomot, and I Bahar. Global motions exhibited by proteins in micro-to milliseconds simulations concur with anisotropic network model predictions. *The Journal of chemical physics*, 139(12):09B612_1, 2013.

[17] Najeeb Halabi, Olivier Rivoire, Stanislas Leibler, and Rama Ranganathan. Protein sectors: evolutionary units of three-dimensional structure. *Cell*, 138(4):774–786, 2009.

[18] Kerstin Helmstaedt, Sven Krappmann, and Gerhard H Braus. Allosteric regulation of catalytic activity: Escherichia coli aspartate transcarbamoylase versus yeast chorismate mutase. *Microbiology and molecular biology reviews*, 65(3):404–421, 2001.

[19] Mathieu Hemery and Olivier Rivoire. Evolution of sparsity and modularity in a model of protein allostery. *Physical review E*, 91(4):042704, 2015.

[20] Judith Herzfeld and H Eugene Stanley. A general approach to co-operativity and its application to the oxygen equilibrium of hemoglobin and its effectors. *Journal of molecular biology*, 82(2):231–265, 1974.

[21] Daniel Hexner, Andrea J Liu, and Sidney R Nagel. Periodic training of creeping solids. *Proceedings of the National Academy of Sciences*, 117(50):31690–31695, 2020.

[22] Vincent J Hilser and E Brad Thompson. Intrinsic disorder as a mechanism to optimize allosteric coupling in proteins. *Proceedings of the National Academy of Sciences*, 104 (20):8311–8315, 2007.

[23] Leo C James, Pietro Roversi, and Dan S Tawfik. Antibody multispecificity mediated by conformational diversity. *Science*, 299(5611):1362–1367, 2003.

[24] Kenji Kamata, Morihiro Mitsuya, Teruyuki Nishimura, Jun-ichi Eiki, and Yasufumi Nagata. Structural basis for allosteric regulation of the monomeric allosteric enzyme human glucokinase. *Structure*, 12(3):429–438, 2004.

[25] DE Koshland Jr, G Nemethy, and D Filmer. Comparison of experimental binding data and theoretical models in proteins containing subunits. *Biochemistry*, 5(1):365–385, 1966.

[26] Steve W Lockless and Rama Ranganathan. Evolutionarily conserved pathways of energetic connectivity in protein families. *Science*, 286(5438):295–299, 1999.

[27] Liang Ma and Qiang Cui. Activation mechanism of a signaling protein at atomic resolution from advanced computations. *Journal of the American Chemical Society*, 129 (33):10261–10268, 2007.

[28] Lauren T May, Katie Leach, Patrick M Sexton, and Arthur Christopoulos. Allosteric modulation of G protein–coupled receptors. *Annu. Rev. Pharmacol. Toxicol.*, 47:1–51, 2007.

[29] Thomas CB McLeish, TL Rodgers, and Mark R Wilson. Allostery without conformation change: modelling protein dynamics at multiple scales. *Physical biology*, 10(5):056004, 2013.

[30] Diana M Mitrea and Richard W Kriwacki. Regulated unfolding of proteins in signaling. *FEBS letters*, 587(8):1081–1088, 2013.

[31] Jacque Monod, Jeffries Wyman, and Jean-Pierre Changeux. On the nature of allosteric transitions: a plausible model. *J Mol Biol*, 12(1):88–118, 1965.

[32] Jacques Monod, Jean-Pierre Changeux, and François Jacob. Allosteric proteins and cellular control systems. *Journal of molecular biology*, 6(4):306–329, 1963.

[33] José Nelson Onuchic and Peter G Wolynes. Theory of protein folding. *Current opinion in structural biology*, 14(1):70–75, 2004.

[34] Nidhi Pashine. Local rules for fabricating allosteric networks. *Physical Review Materials*, 5(6):065607, 2021.

[35] Nidhi Pashine, Daniel Hexner, Andrea J Liu, and Sidney R Nagel. Directed aging, memory, and nature's greed. *Science advances*, 5(12):eaax4215, 2019.

[36] Nataliya Popovych, Shangjin Sun, Richard H Ebright, and Charalampos G Kalodimos. Dynamically driven protein allostery. *Nature structural & molecular biology*, 13(9):831–838, 2006.

[37] Riccardo Ravasio, Solange Marie Flatt, Le Yan, Stefano Zamuner, Carolina Brito, and Matthieu Wyart. Mechanics of allostery: contrasting the induced fit and population shift scenarios. *Biophysical journal*, 117(10):1954–1962, 2019.

[38] Olivier Rivoire. Parsimonious evolutionary scenario for the origin of allostery and co-evolution patterns in proteins. *Physical Review E*, 100(3):032411, 2019.

[39] Olivier Rivoire, Kimberly A Reynolds, and Rama Ranganathan. Evolution-based functional decomposition of proteins. *PLoS computational biology*, 12(6):e1004817, 2016.

[40] Jason W Rocks, Nidhi Pashine, Irmgard Bischofberger, Carl P Goodrich, Andrea J Liu, and Sidney R Nagel. Designing allostery-inspired response in mechanical networks. *Proceedings of the National Academy of Sciences*, 114(10):2520–2525, 2017.

[41] Jason W Rocks, Henrik Ronellenfitsch, Andrea J Liu, Sidney R Nagel, and Eleni Katifori. Limits of multifunctionality in tunable networks. *Proceedings of the National Academy of Sciences*, 116(7):2506–2511, 2019.

[42] Benjamin Schuler, Everett A Lipman, and William A Eaton. Probing the free-energy surface for protein folding with single-molecule fluorescence spectroscopy. *Nature*, 419 (6908):743–747, 2002.

[43] Menachem Stern and Arvind Murugan. Learning without neurons in physical systems. *Annual Review of Condensed Matter Physics*, 14(1):417–441, 2023.

[44] Menachem Stern, Chukwunonso Arinze, Leron Perez, Stephanie E Palmer, and Arvind Murugan. Supervised learning through physical changes in a mechanical system. *Proceedings of the National Academy of Sciences*, 117(26):14843–14850, 2020.

[45] Menachem Stern, Matthew B Pinson, and Arvind Murugan. Continual learning of multiple memories in mechanical networks. *Physical Review X*, 10(3):031044, 2020.

[46] Menachem Stern, Daniel Hexner, Jason W Rocks, and Andrea J Liu. Supervised learning in physical networks: From machine learning to learning machines. *Physical Review X*, 11(2):021045, 2021.

[47] Gürol M Süel, Steve W Lockless, Mark A Wall, and Rama Ranganathan. Evolutionarily conserved networks of residues mediate allosteric communication in proteins. *Nature structural biology*, 10(1):59–69, 2003.

[48] Attila Szabo and Martin Karplus. A mathematical model for structure-function relations in hemoglobin. *Journal of molecular biology*, 72(1):163–197, 1972.

[49] Tsvi Tlusty, Albert Libchaber, and Jean-Pierre Eckmann. Physical model of the genotype-to-phenotype map of proteins. *Physical Review X*, 7(2):021037, 2017.

[50] Brian F Volkman, Doron Lipson, David E Wemmer, and Dorothee Kern. Two-state allosteric behavior in a single-domain signaling protein. *Science*, 291(5512):2429–2433, 2001.

[51] David J Wales and Jonathan PK Doye. Global optimization by basin-hopping and the lowest energy structures of lennard-jones clusters containing up to 110 atoms. *The Journal of Physical Chemistry A*, 101(28):5111–5116, 1997.

[52] Yechun Xu, Jacques Ph Colletier, Hualiang Jiang, Israel Silman, Joel L Sussman, and Martin Weik. Induced-fit or preexisting equilibrium dynamics? lessons from protein crystallography and md simulations on acetylcholinesterase and implications for structure-based drug design. *Protein Science*, 17(4):601–605, 2008.

[53] Le Yan, Riccardo Ravasio, Carolina Brito, and Matthieu Wyart. Architecture and

coevolution of allosteric materials. *Proceedings of the National Academy of Sciences*, 114(10):2526–2531, 2017.

[54] Le Yan, Riccardo Ravasio, Carolina Brito, and Matthieu Wyart. Principles for optimal cooperativity in allosteric materials. *Biophysical journal*, 114(12):2787–2798, 2018.

[55] Wenjun Zheng, Bernard R Brooks, and D Thirumalai. Low-frequency normal modes that describe allosteric transitions in biological nanomachines are robust to sequence variations. *Proceedings of the National Academy of Sciences*, 103(20):7664–7669, 2006.

Appendix for Chapter 3

3.6 Supplemental Information

Method for adding disorder in network connectivity.

In the main text, the method to build networks resulted in a connectivity (adjacency matrix A_{ij}) of that of a triangular lattice. To introduce disorder in the connectivity, we place nodes on a triangular lattice with their positions given by $\mathbf{R}_i^{\text{lat}}$. The nodes are then displaced by a random uniform perturbation $\Delta\mathbf{R}_i \sim ([-\epsilon, \epsilon], [-\epsilon, \epsilon])$ to achieve a disordered structure $\mathbf{R}_i^{\text{dis}}$ $= \mathbf{R}_i^{\text{lat}} + \Delta\mathbf{R}_i$. An adjacency matrix is defined as follows,

$$A_{ij} = \begin{cases} 1, & i \neq j \text{ and } ||\mathbf{R}_{\text{i}}^{\text{dis}} - \mathbf{R}_{\text{j}}^{\text{dis}}|| < \text{c} \\ 0, & \text{otherwise} \end{cases}$$

The value of c is chosen such that the mean coordination $z = \sum_{ij} A_{ij}/N$ takes a desired value.

3d Networks

Three dimensional networks share the same definition as 2d networks (Eq. (3.7), (3.8), (3.9)) except for the following differences: $\mathbf{r}_i = (x_i, y_i, z_i)$, nodes are initially placed on a 3d hexagonal closed packed lattice rather than 2d triangular lattice, and $\Delta\mathbf{R}_i \sim ([-a\epsilon, a\epsilon], [-a\epsilon, a\epsilon], [-a\epsilon, a\epsilon])$. The values of the distance cutoff and spring constant for the harmonic repulsion term remain the same in 3d, $\ell_{\text{rep}} = 0.7$ and $k_{\text{rep}} = 2$.

1d model at zero temperature

For a system of harmonic springs, the energy takes the form,

$$V(x) = \frac{1}{2}\sum_i k_i(x-\ell_i)^2 = \frac{1}{2}\left(\sum_i k_i\right)\left(x - \frac{\sum_i k_i\ell_i}{\sum_i k_i}\right)^2 + V_{\min} \tag{3.17}$$

where

$$V_{\min} = \min_x V(x) = \frac{1}{2}\left(\sum_i k_i\ell_i^2 - \frac{(\sum_i k_i\ell_i)^2}{\sum_i k_i}\right). \tag{3.18}$$

The 1d model of allostery is given by

$$U(x) = \frac{1}{2}k_a(x-\ell_{\text{act}})^2 + \frac{1}{2}k_a(x-\ell_{\text{allo}})^2 + \frac{1}{2}k_m(|x|-\ell_m)^2. \tag{3.19}$$

Putting (3.19) in the form of (3.17) gives

$$V(x,\ell_m) = \frac{1}{2}(2k_a+k_m)\left(x - \frac{k_a(\ell_{\text{act}}+\ell_{\text{allo}})+k_m\ell_m}{2k_a+k_m}\right)^2 + V_{\min}(\ell_m) \tag{3.20}$$

where

$$V_{\min}(\ell_m) = \frac{1}{2}\left[k_a(\ell_{\text{act}}^2+\ell_{\text{allo}}^2) + k_m\ell_m^2 - \frac{(k_a(\ell_{\text{act}}+\ell_{\text{allo}})+k_m\ell_m)^2}{2k_a+k_m}\right]. \tag{3.21}$$

$U(x)$ can be written as a piecewise function,

$$U(x) = \begin{cases} V(x,-\ell_m), & x \le 0 \\ V(x,\ell_m), & x > 0. \end{cases} \tag{3.22}$$

The ground state of U is defined by $E = \min_x U(x) = \min_\pm V_{\min}(\pm\ell_m)$. Taking the physical conditions $k_a > 0$, $k_m > m$ and $\ell_m > 0$, this gives

$$E(\ell_{\text{act}}, \ell_{\text{allo}}) = \frac{k_a}{2(2k_a + k_m)} \left(k_a(\ell_{\text{act}} - \ell_{\text{allo}})^2 + k_m(\ell_{\text{act}}^2 + \ell_{\text{allo}}^2 + 2\ell_m^2) - 2k_m|(\ell_{\text{act}} + \ell_{\text{allo}})\ell_m| \right) \tag{3.23}$$

Cooperative allostery is computed as

$$\Delta\Delta E = E(\ell_1, \ell_0) + E(\ell_0, \ell_1) - E(\ell_1, \ell_1) - E(\ell_0, \ell_0), \tag{3.24}$$

where ℓ_0 and ℓ_1 represent the solvent and the ligand, respectively. In the 1d model $\Delta\Delta E$ reduces to,

$$\Delta\Delta E = \frac{k_a}{2k_a + k_m} \left(k_a|\ell_1 - \ell_0|^2 + 2k_m|\ell_m|(|\ell_1| + |\ell_0| - |\ell_1 + \ell_0|) \right). \tag{3.25}$$

If $\ell_1 = -\ell_0$ and $\delta = |\ell_1 - \ell_0|$,

$$\Delta\Delta E = \frac{k_a(k_a\delta + 2k_m\ell_m)\delta}{2k_a + k_m}. \tag{3.26}$$

The mechanism changes from single-state to multi-state at the transition rest length $\ell_m^* = \delta/4$. When $\ell_m < \delta/4$, $\Delta\Delta E$ is optimized at $k_m = 0$ and can not exceed $k_a\delta^2/2$. When $\ell_m > \delta/4$, $\Delta\Delta E$ is optimized at $k_m = \infty$ and can take arbitrarily large values ($\Delta\Delta E = 2k_a\ell_m\delta$). The first term in (3.26) is the contribution from being able to actuate the (potentially) soft allosteric mode and the second term is the contribution from the two-state switch.

1d model at finite temperature

In the canonical ensemble, the partition function Z of a system with energy $U(x) = kx^2/2$ at temperature T (the Boltzmann constant is folded in T such that T has units of energy)

is given by

$$Z = \int e^{-E(x)/T} dx = \int_{-\infty}^{\infty} e^{-kx^2/2T} dx = \sqrt{\frac{2\pi T}{k}}, \tag{3.27}$$

and its free energy is

$$F = -T \ln Z = \frac{T}{2} \ln \frac{k}{2\pi T}. \tag{3.28}$$

The energy of the 1d model (3.19) takes the form of two parabolas that abut at $x = 0$. The partition function is

$$Z = \int_{-\infty}^{0} e^{-V(x,-\ell_m)/T} dx + \int_{0}^{\infty} e^{-V(x,\ell_m)/T} dx \tag{3.29}$$

Setting $\kappa = 2k_a + k_m$ and $\lambda(\ell_m) = (k_a(\ell_{\text{act}} + \ell_{\text{allo}}) + k_m \ell_m)/(2k_a + k_m)$ gives

$$Z = e^{-V_{\min}(-\ell_m)/T} \int_{-\infty}^{0} e^{-\kappa(x-\lambda(-\ell_m))^2/2T} dx + e^{-V_{\min}(\ell_m)/T} \int_{0}^{\infty} e^{-\kappa(x-\lambda(\ell_m))^2/2T} dx \tag{3.30}$$

$$= \frac{1}{2}\sqrt{\frac{\pi T}{\kappa}} \left[e^{-V_{\min}(-\ell_m)/T} \left(1 + \text{erf}\left(-\sqrt{\frac{\kappa}{2\text{T}}} \lambda(-\ell_{\text{m}}) \right) \right) + e^{-V_{\min}(\ell_m)/T} \left(1 + \text{erf}\left(\sqrt{\frac{\kappa}{2\text{T}}} \lambda(\ell_{\text{m}}) \right) \right) \right] \tag{3.31}$$

where erf is the error function.

In the limit where $k_m/k_a \to \infty$ the energy simplifies to

$$U(x) = \begin{cases} \frac{k_a}{2}\left((x - \ell_{\text{act}})^2 + (\ell_m - \ell_{\text{allo}})^2\right) & x = -\ell_m \\ \frac{k_a}{2}\left((x - \ell_{\text{act}})^2 + (\ell_m - \ell_{\text{allo}})^2\right) & x = \ell_m \\ \infty & \text{otherwise} \end{cases} \tag{3.32}$$

and the free energy becomes

$$F(\ell_{\rm act},\ell_{\rm allo}) = -T\ln\left[e^{-\frac{k_a}{2T}((\ell_m+\ell_{\rm act})^2+(\ell_m+\ell_{\rm allo})^2)} + e^{-\frac{k_a}{2T}((\ell_m-\ell_{\rm act})^2+(\ell_m-\ell_{\rm allo})^2)}\right] \quad (3.33)$$

Taking $\ell_0 = -\delta/2$ and $\ell_1 = \delta/2$ the cooperativity is

$$\Delta\Delta F = F(\delta/2,-\delta/2) + F(-\delta/2,\delta/2) - F(\delta/2,\delta/2) - F(-\delta/2,-\delta/2), \quad (3.34)$$

and after some algebra,

$$\Delta\Delta F = 2T\ln\cosh\left(k_a\ell_m\delta/T\right). \quad (3.35)$$

In the opposite limit where $k_m/k_a \to 0$,

$$U(x) = \frac{k_a}{2}(x-\ell_{\rm act})^2 + \frac{k_a}{2}(x-\ell_{\rm allo})^2 \quad (3.36)$$

$$= k_a\left(x - \frac{\ell_{\rm act}+\ell_{\rm allo}}{2}\right)^2 + \frac{k_a}{4}\left(\ell_{\rm act}-\ell_{\rm allo}\right)^2 \quad (3.37)$$

$$(3.38)$$

and the free energy is

$$F(\ell_{\rm act},\ell_{\rm allo}) = \frac{k_a}{4}(\ell_{\rm act}-\ell_{\rm allo})^2 - \frac{T}{2}\ln\frac{\pi T}{k_a} \quad (3.39)$$

Taking $\ell_0 = -\delta/2$ and $\ell_0 = \delta/2$ the cooperativity is

$$\Delta\Delta F = F(\delta/2,-\delta/2) + F(-\delta/2,\delta/2) - F(\delta/2,\delta/2) - F(-\delta/2,-\delta/2) \quad (3.40)$$

and after some algebra

$$\Delta\Delta F = \frac{1}{2}k_a\delta^2. \quad (3.41)$$

When $T > 0$, the transition point between mechanisms occurs for

$$\ell_m^*(T) = \frac{T}{k_a\delta} \ln\left[e^{k_a\delta^2/4T} + \sqrt{e^{k_a\delta^2/2T} - 1}\right] \tag{3.42}$$

Thermodynamical models

Our models can be coarse-grained to obtain a thermodynamic description comparable to the formulation of the MWC and KNF models. This is achieved by defining "states" with given free energies, from which equilibrium probabilities are computed from Boltzmann's law. A state corresponds in our models to a distinct local minimum of the energy or free energy landscape. At finite temperatures, a further requirement is that the free energy barriers are large relative to the temperature so that a local equilibrium occurs within the states. If two states have free energies F_1 and F_2 with a maximum $F^\dagger$ along the conformational coordinate that connects them, this assumption amounts to $F^\dagger - \max(F_1, F_2) \ll T$ in units where the Boltzmann constant is $k_B = 1$. A description can also be given in terms of kinetic rates $k_{1\to2}$ and $k_{2\to1}$ for the transition between the states, which may, for instance, be of the form $k_{1\to2} = k_0 e^{-(F^\dagger - F_1)/T}$ and $k_{2\to1} = k_0 e^{-(F^\dagger - F_2)/T}$.

One possible coarse-graining of the 1d model could assert that two conformational states exist: state T corresponding to $x < 0$ and state R corresponding to $x > 0$. This coarse-graining separates the two states by the barrier at $x = 0$. With two binding sites, there would be a total of eight states: T00, T10, T01, T11, R00, R10, R01, R11 (the last two digits represent the state of ligand binding as in Figure 3.1). Taking ℓ_0 and ℓ_1 to be the rest lengths of the springs representing the unbound and bound states, the free energies of the eight states are,

$$F_{Tij} = -T \ln\left(\int_{-\infty}^{0} e^{-\frac{1}{2}\left(k_a(x-\ell_i)^2 + k_a(x-\ell_j)^2 + k_m(x+\ell_m)^2\right)/T} dx\right) \tag{3.43}$$

$$F_{Rij} = -T \ln \left(\int_0^\infty e^{-\frac{1}{2}(k_a(x-\ell_i)^2 + k_a(x-\ell_j)^2 + k_m(x-\ell_m)^2)/T} dx \right) \tag{3.44}$$

A quantity of particular interest is the fraction of occupied binding sites Y at a ligand concentration c,

$$Y(c) = 0 * P_{00}(c) + \frac{1}{2} * P_{01}(c) + \frac{1}{2} * P_{10}(c) + 1 * P_{11}(c) \tag{3.45}$$

$$Y(c) = \frac{ce^{-F_{T10}/T} + ce^{-F_{R10}/T} + c^2 e^{-F_{T11}/T} + c^2 e^{-F_{R11}/T}}{e^{-F_{T00}/T} + e^{-F_{R00}/T} + 2ce^{-F_{T10}/T} + 2ce^{-F_{R10}/T} + c^2 e^{-F_{T11}/T} + c^2 e^{-F_{R11}/T}} \tag{3.46}$$

3.7 Supplemental Figures

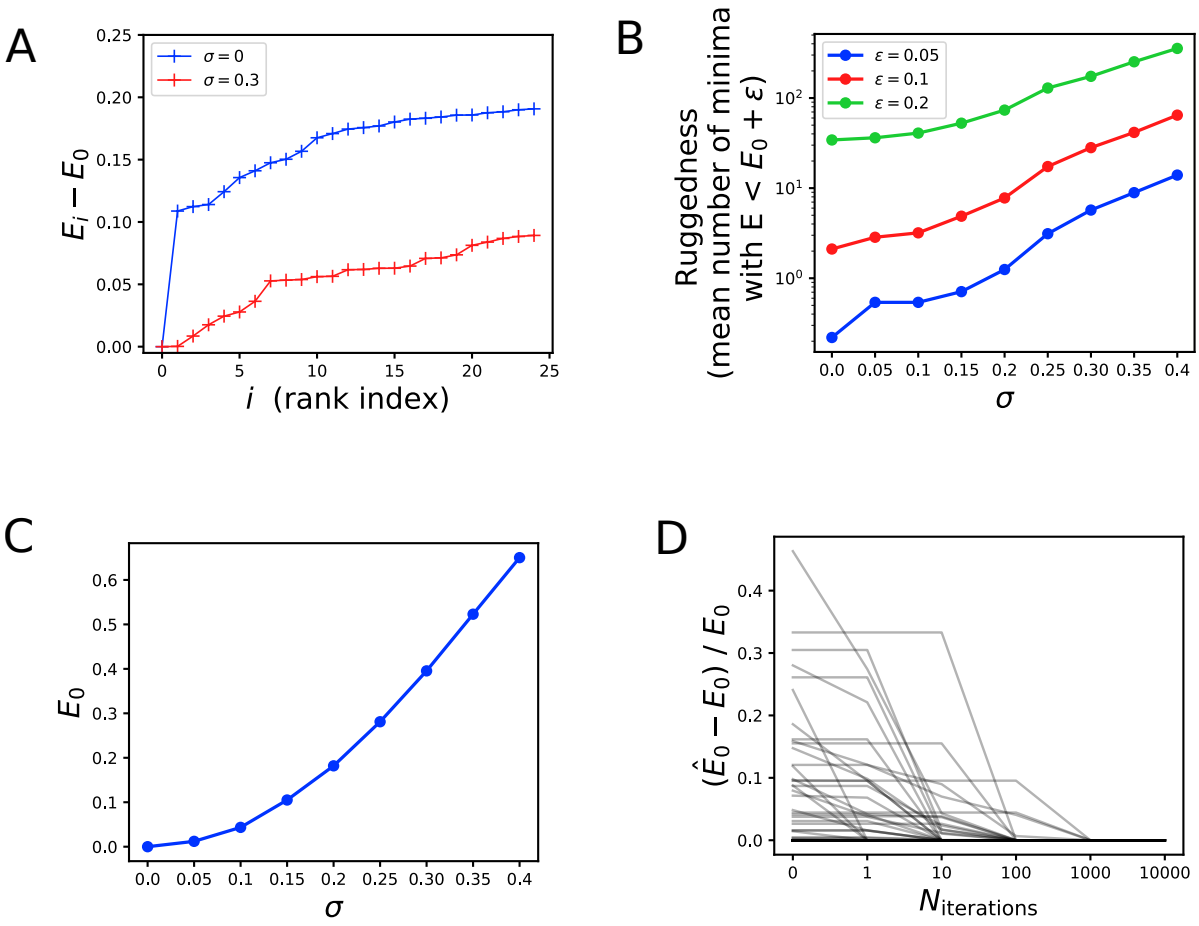

Figure 3.7: Ruggedness and frustration increase with σ. (A) The energies of the 25 lowest minima relative to the ground state energy (E_0) for a network with $\sigma = 0$ (blue) and $\sigma = 0.3$ (red). The networks with ordered interactions ($\sigma = 0$) have a ground state far more stable than any other minima, whereas networks with disordered interactions $\sigma = 0.3$ have many near-degenerate low energy states. (B) We measure the ruggedness of an energy landscape as the number of minima within ϵ of the ground state energy (E_0). For each σ, we plot the ruggedness averaged over 100 random networks. Higher σ implies more low-energy minima relative to the ground state. Minima are found with the ground-state finding algorithm (Methods). (C) Frustration, the extent to which bonds are stressed, is measured by the ground state energy E_0. A ground state where all springs are relaxed has $E_0 = 0$. For each σ, 100 random networks are generated and their ground states are estimated with the ground-state finding algorithm (Methods). (D) The error in the estimated ground state energy $\hat{E}_0$ for an increasing number of iterations of the ground state finding algorithm for 100 random networks. ($\sigma = 0.3$ and population size $p = 20$). At 100 iterations, 96% of ground state estimates are correct. The energies after 10000 iterations are taken to be the true ground state energies, E_0. These data show that the ground state can be estimated with sufficient accuracy even when the energy landscapes are rugged with many minima.

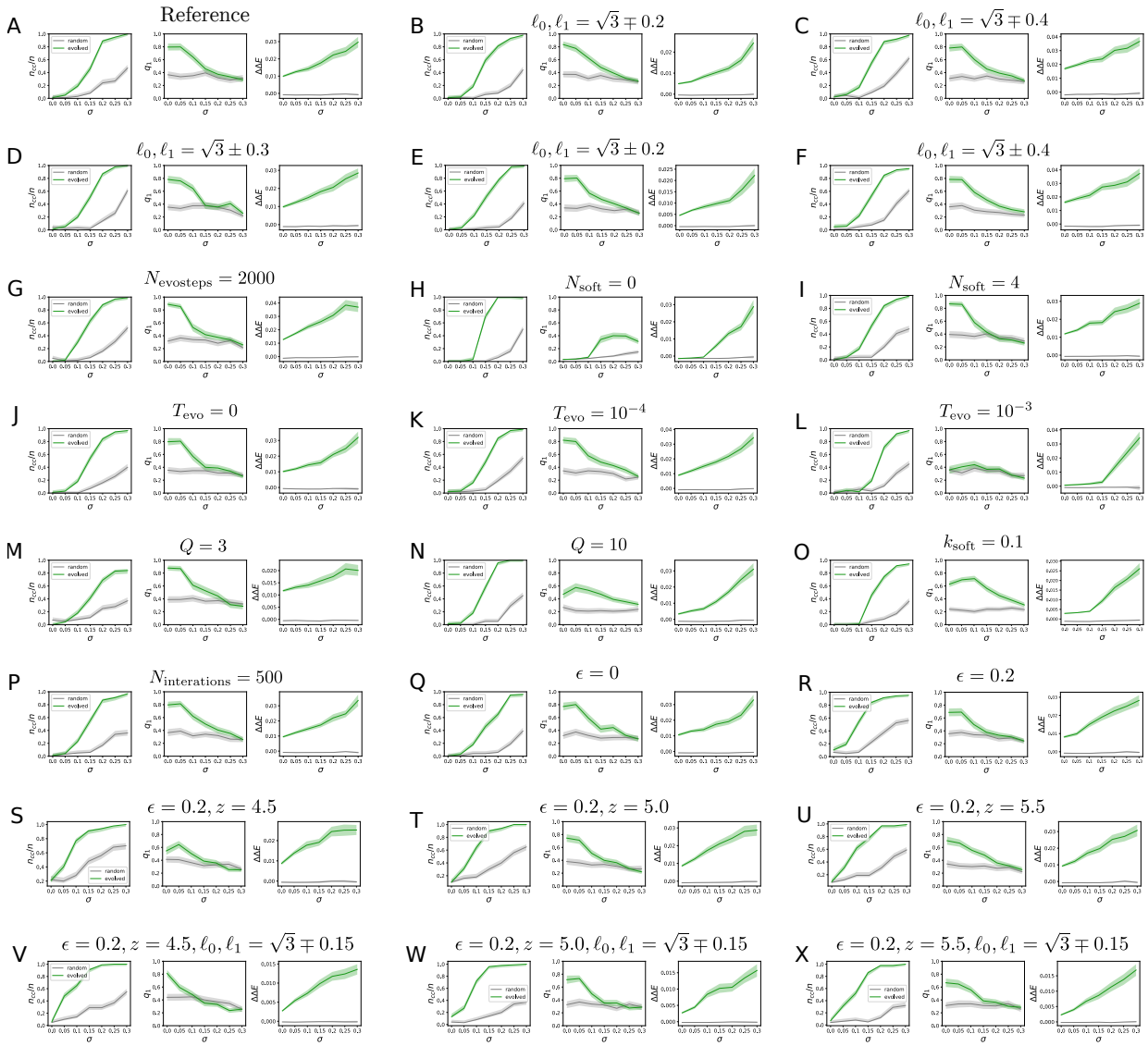
A
Reference
B
$\ell_0, \ell_1 = \sqrt{3} \mp 0.2$
C
$\ell_0, \ell_1 = \sqrt{3} \mp 0.4$
D
$\ell_0, \ell_1 = \sqrt{3} \pm 0.3$
E
$\ell_0, \ell_1 = \sqrt{3} \pm 0.2$
F
$\ell_0, \ell_1 = \sqrt{3} \pm 0.4$
G
$N_{\text{evosteps}} = 2000$
H
$N_{\text{soft}} = 0$
I
$N_{\text{soft}} = 4$
J
$T_{\text{evo}} = 0$
K
$T_{\text{evo}} = 10^{-4}$
L
$T_{\text{evo}} = 10^{-3}$
M
$Q = 3$
N
$Q = 10$
O
$k_{\text{soft}} = 0.1$
P
$N_{\text{interations}} = 500$
Q
$\epsilon = 0$
R
$\epsilon = 0.2$
S
$\epsilon = 0.2, z = 4.5$
T
$\epsilon = 0.2, z = 5.0$
U
$\epsilon = 0.2, z = 5.5$
V
$\epsilon = 0.2, z = 4.5, \ell_0, \ell_1 = \sqrt{3} \mp 0.15$
W
$\epsilon = 0.2, z = 5.0, \ell_0, \ell_1 = \sqrt{3} \mp 0.15$
X
$\epsilon = 0.2, z = 5.5, \ell_0, \ell_1 = \sqrt{3} \mp 0.15$

Figure 3.8: Robustness of Figure 3.3AB with respect to various parameters. Each panel shows the fraction of networks that undergo a multi-state conformational change upon binding ligand n_{cc}/n, the mean overlap of the allosteric mode with the softest mode q_1, and the mean cooperativity $\Delta\Delta E$ for 100 random (gray) and evolved (green) networks. In panels B-Q only one parameter is changed from the reference in panel A. (A) Same data as in Figure 3.3AB where the parameters of the simulation are: $\ell_0 = \sqrt{3} - 0.3$, $\ell_1 = \sqrt{3} + 0.3$, $k_0 = k_1 = 1$, $N_{\text{evosteps}} = 500$, $N_{\text{soft}} = 2$, $T_{\text{evo}} = 10^{-5}$, $Q = 5$, $k_{\text{soft}} = 0.01$, $N_{\text{iterations}} = 100$, and spatial disorder $\epsilon = 0.1$. (B-F) Results do not significantly change with different choices of ligands, except that cooperativity decreases when the difference between ℓ_0 and ℓ_1 decreases, as predicted by the 1d model. (G) Results do not change when the number of interactions of the Monte Carlo evolution is increased from $N_{\text{evosteps}} = 500$ to $N_{\text{evosteps}} = 2000$. (H) When there are no soft interactions permitted between nodes, $N_{\text{soft}} = 0$, (i.e. if $K(s_i, s_j) = 1$ for all entries) no cooperativity evolves at low σ. (I) Doubling the number of soft interactions from $N_{\text{soft}} = 2$ to $N_{\text{soft}} = 4$ does not significantly change the results. (JKL) Changing the temperature of the evolutionary Monte Carlo T_{evo} does not change the results as long as it is sufficiently small, $T_{\text{evo}} < 10^{-3}$. At $T_{\text{evo}} \geq 10^{-3}$ nearly no cooperativity evolves at small σ. (MN) The results are unchanged with a different number of node types Q. (O) The results are unchanged when the softness of the soft interactions is increased to $k_{\text{soft}} = 0.1$. (P) The results are unchanged if the number of iterations of the basin hopping algorithm is increased from $N_{\text{iterations}} = 100$ to $N_{\text{iterations}} = 500$. (QR) The results are unchanged when the spatial disorder is removed $\epsilon = 0$ (corresponding to $D_{ij} = 0$) or increased $\epsilon = 0.2$. (S-X) The results are unchanged if networks are built with an alternate method where disorder is allowed in the connectivity (A_{ij}). z is the mean coordination (see SI).

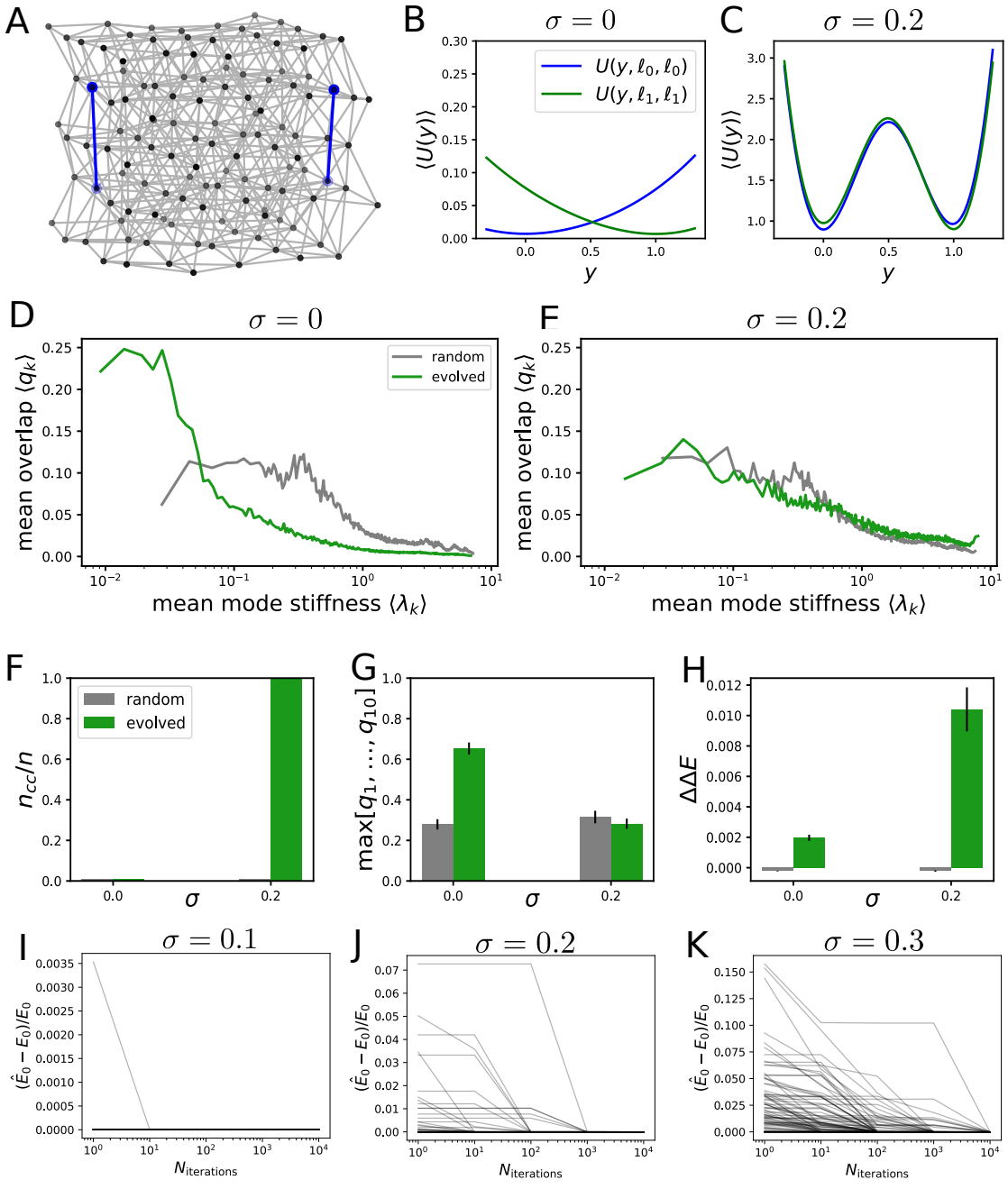
A
B
$\sigma = 0$
$U(y, \ell_0, \ell_0)$
$U(y, \ell_1, \ell_1)$
$\langle U(y) \rangle$
y
C
$\sigma = 0.2$
$\langle U(y) \rangle$
y
D
$\sigma = 0$
random
evolved
mean overlap $\langle q_k \rangle$
mean mode stiffness $\langle \lambda_k \rangle$
F
$\sigma = 0.2$
mean overlap $\langle q_k \rangle$
mean mode stiffness $\langle \lambda_k \rangle$
F
random
evolved
n_{cc}/n
σ
G
$\max[q_1, \ldots, q_{10}]$
σ
H
$\Delta\Delta E$
σ
I
$\sigma = 0.1$
$(\hat{E}_0 - E_0)/E_0$
$N_{\text{iterations}}$
J
$\sigma = 0.2$
$(\hat{E}_0 - E_0)/E_0$
$N_{\text{iterations}}$
K
$\sigma = 0.3$
$(\hat{E}_0 - E_0)/E_0$
$N_{\text{iterations}}$

Figure 3.9: 3d networks show same behaviors as 2d networks. (a) A visualization of a $5 \times 5 \times 5$ 3d network. Blue springs on opposite sides of the network are the active and allosteric sites. The data in the following subplots are from simulations with the following parameters: $\ell_0, \ell_1 = 2\sqrt{3}/3 \mp 0.15$, $k_0 = k_1 = 1$, $N_{\text{evosteps}} = 10^3$, $N_{\text{soft}} = 2$, $T_{\text{evo}} = 10^{-5}$, $Q = 5$, $k_{\text{soft}} = 0.01$, $N_{\text{iterations}} = 100$, and spatial disorder $\epsilon = 0.1$. (BC) Mean energy of the fully-solvated (blue) and fully-bound (green) networks along the conformational coordinate y interpolating between the two ground state structures $\mathbf{R}_{00}$ and $\mathbf{R}_{11}$ of evolved networks, averaged over 100 replicates. When $\sigma = 0$ (subplot B), the energy has a single minimum, and when $\sigma = 0.2$ (subplot C), energies are bistable. (DE) The mean overlap (averaged over 100 replicates) $\langle q_k \rangle$ between the structural displacement upon binding ligand $\Delta\mathbf{r}$ and each normal mode of the evolved network $\mathbf{v}_k$ ($q_k = |\mathbf{v}_k \cdot \Delta\mathbf{r}/\|\Delta\mathbf{r}\|\ |$) plotted against the mean mode stiffness $\langle \lambda_k \rangle$. When $\sigma = 0$ (subplot D), the softest modes overlap with the allosteric displacement indicative of a single-state mechanism. (F) The fraction of networks that undergo a multi-state conformational change upon binding ligand n_{cc}/n, for 100 random (gray) and evolved (green) networks. (G) The mean of the maximum overlap of the allosteric mode with any of the 10 softest modes q_k, $k = 1, \ldots, 10$, for 100 random (gray) and evolved (green) networks. (H) The mean cooperativity $\Delta\Delta E$ for 100 random (gray) and evolved (green) networks. (IJK) The error in the estimated ground state energy $\hat{E}_0$ for an increasing number of iterations of the ground state finding algorithm for 100 random networks (population size $p = 20$). For $\sigma = 0.2$ and 100 iterations, 95% of ground state estimates are correct. The energies after 10^4 iterations are taken to be the true ground state energies, E_0.

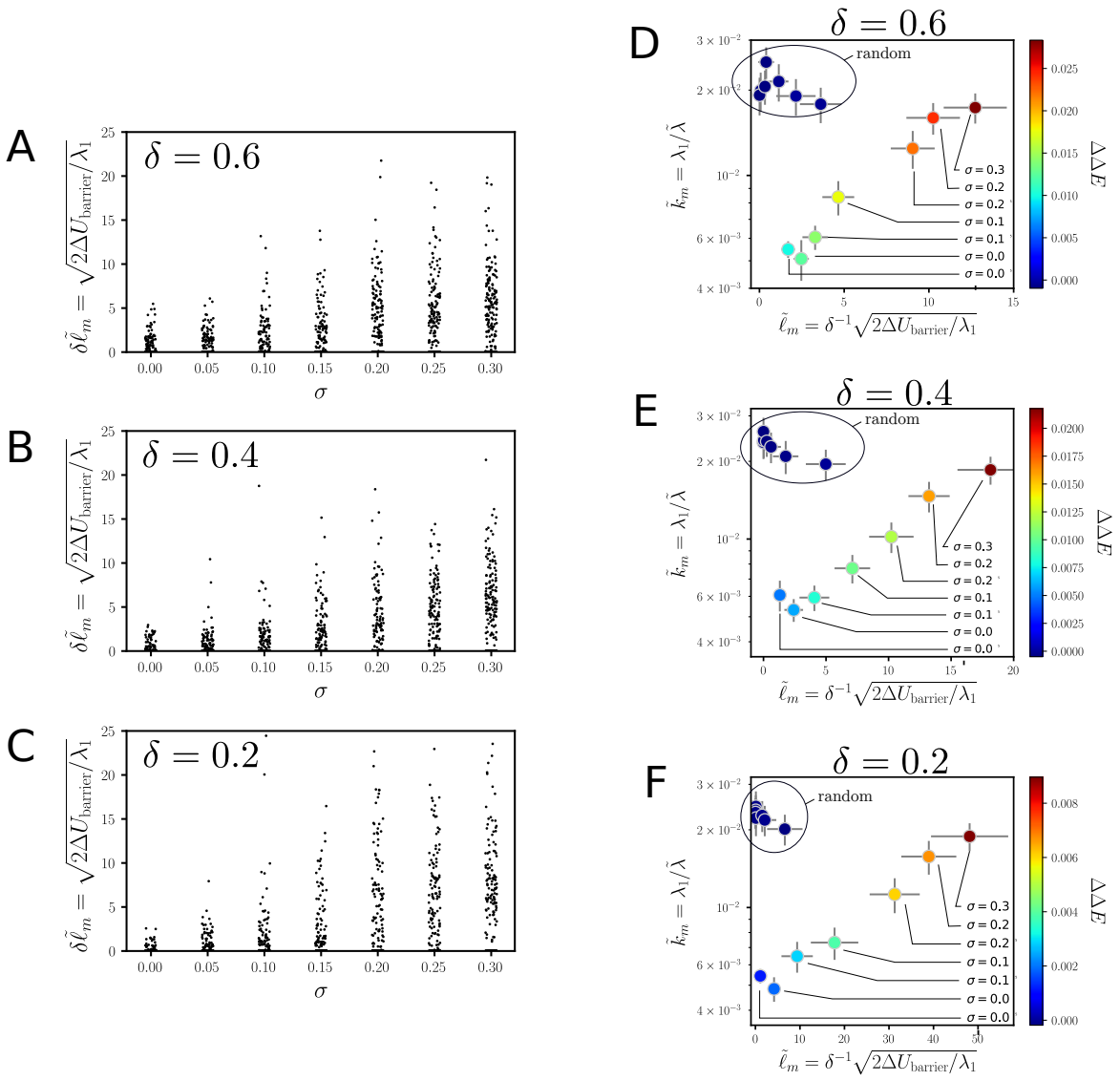

Figure 3.10: The properties of the 1d model recapitulate the properties of the 2d elastic network. $\tilde{k}_m$ and $\tilde{\ell}_m$ are the 2d elastic network analogs of the 1d model's reduced parameters k_m/k_a and ℓ_m/δ. See methods for their definitions and motivations. (ABC) For each σ, $\tilde{\ell}_m\delta$ of each of the 100 random and 100 evolved networks is plotted, showing an estimate of the range of possible values of $\tilde{\ell}_m\delta$ given σ. (DEF) The mean $\tilde{k}_m$ and $\tilde{\ell}_m$, and $\Delta\Delta E$ are plotted for 100 random and 100 evolved networks at different σ. Consistent with the 1d model, non-allosteric random networks have a large $\tilde{k}_m$ and small $\tilde{\ell}_m$. When σ is small, networks approach the single-state mechanism limit ($\ell_m = 0, k_m = 0$). As σ increases, networks localize towards the multi-state mechanism limit of large k_m, large ℓ_m. Error bars are 95% CI.

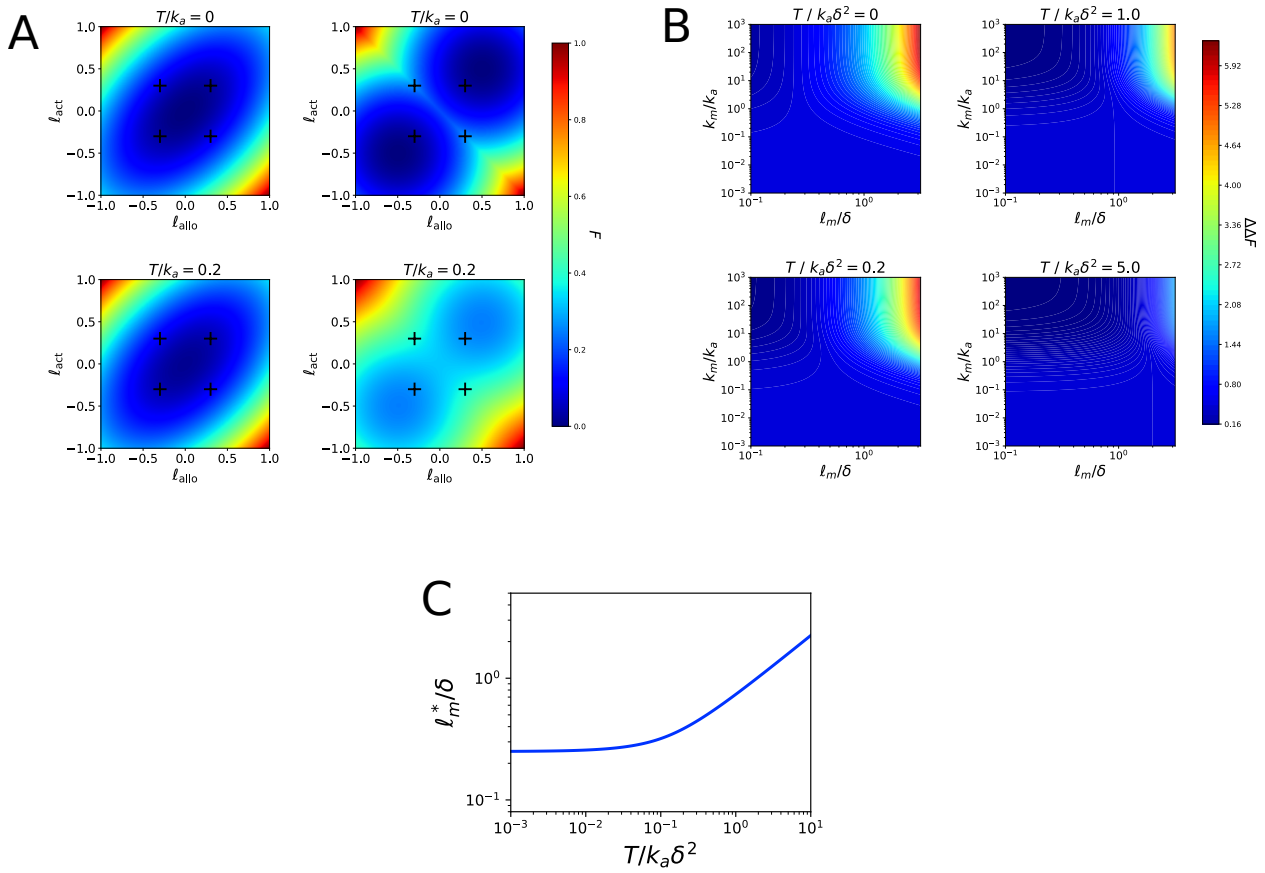

Figure 3.11: 1d model at finite temperature. (A) Free energy surfaces as a function of different binding ligands, corresponding to varying the rest lengths ℓ_{act} and ℓ_{allo} of the springs defining the active and allosteric sites. The two panels on the left show the free energy surfaces of a single-state mechanism ($k_m = 1$ and $\ell_m = 0$) at $T/k_a = 0$ and $T/k_a = 0.2$. The two panels on the right show the free energy surfaces of a multi-state mechanism ($k_m = \infty$ and $\ell_m = 0.5$) at $T/k_a = 0$ and $T/k_a = 0.2$. (B) The cooperativity $\Delta\Delta F$ as a function of the normalized quantities k_m/k_a and ℓ_m/δ for different temperatures. (C) A plot of $\ell_m^*(T)$, the value of ℓ_m where the single and multi-state mechanisms provide equal cooperativity at temperature T.

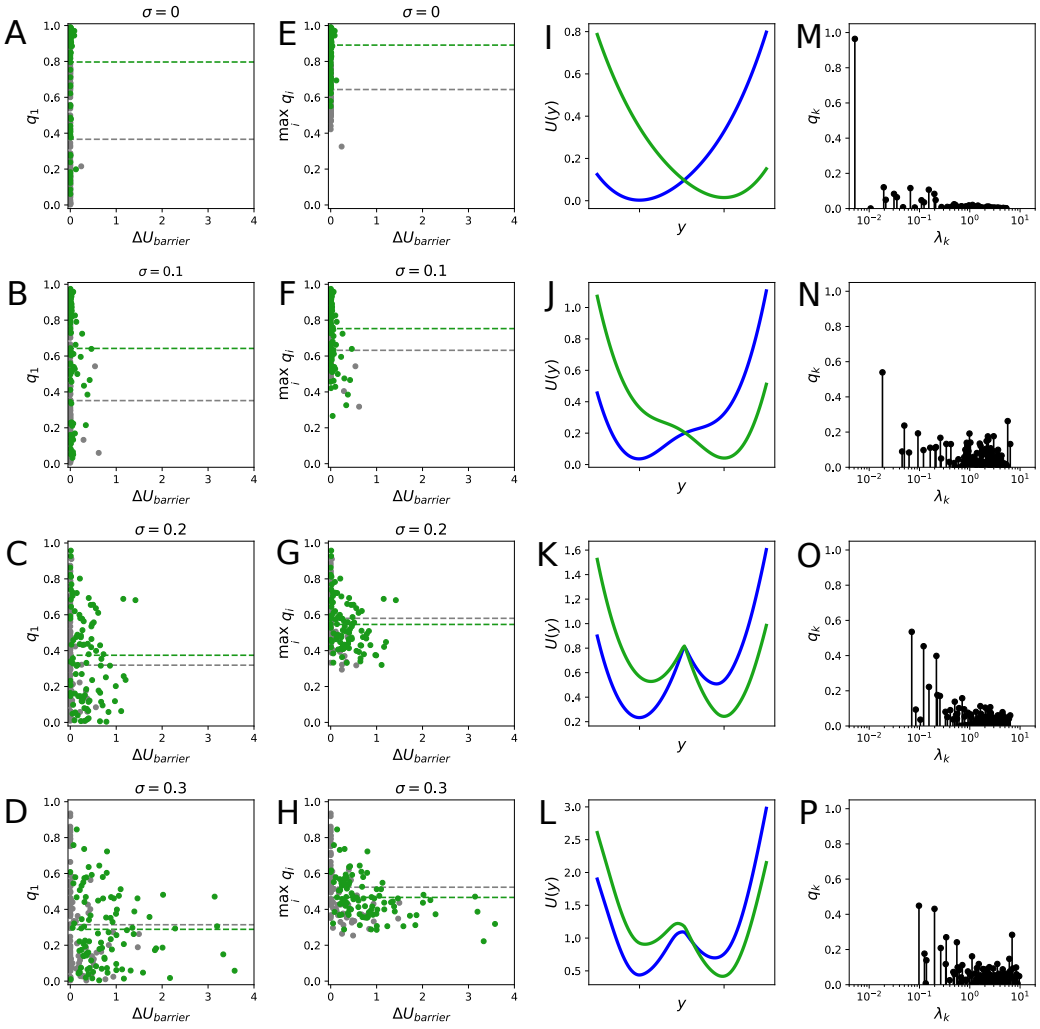
A
B
C
D
E
F
G
H
I
J
K
L
M
N
O
P
$\sigma = 0$
$\sigma = 0.1$
$\sigma = 0.2$
$\sigma = 0.3$
q_1
$\max_i q_i$
$\Delta U_{barrier}$
$U(y)$
y
q_k
λ_k

Figure 3.12: A continuum of mechanisms exists in the 2d elastic network. (A-D) The barrier height $\Delta U_{\text{barrier}}$ (see SI text for definition) and overlap with the softest mode q_1 are plotted for both random (grey points) and evolved (green points) networks at different values of rest length interaction disorder σ. Grey and green horizontal lines indicate the mean of q_1 for the random and evolved networks, respectively. (E-H) The barrier height $\Delta U_{\text{barrier}}$ and the maximal overlap of the allosteric displacement with any mode, $\max_i\ q_i$ is plotted for both random (grey points) and evolved (green points) networks at different values of rest length interaction disorder σ. Grey and green horizontal lines indicate the mean of $\max_i\ q_i$ for the random and evolved networks, respectively. (I,M) The energy along the allosteric displacement $U(y)$ and the overlaps of each mode q_k vs. the mode stiffness λ_k of an example evolved sequence from the population shown in A and E. (J,N) $U(y)$ and q_k vs. λ_k of an example evolved sequence from the population shown in B and F. (K,O) $U(y)$ and q_k vs. λ_k of an example evolved sequence from the population shown in C and G. (L,P) $U(y)$ and q_k vs. λ_k of an example evolved sequence from the population shown in D and H. The networks in I-P were chosen as examples of when $q_1 \gtrapprox 0.5$ even when energy barriers start to emerge. Networks with multi-state conformational change have $\Delta U_{\text{barrier}} > 0$.

CHAPTER 4

AN EVOLUTIONARY SCENARIO FOR THE ORIGIN OF ALLOSTERY

ABSTRACT

Although allosteric properties are ubiquitous in proteins, their evolutionary origins remain unclear. While functional traits like allostery can be attributed to positive selection from fitness advantages, experimental findings suggest that direct selection alone does not fully explain their initial emergence. Studies reveal that proteins harbor unused allosteric architectures, a phenomenon referred to as latent allostery. What can explain this? Computational and experimental work suggest that such architectures can enable evolvability by wiring many distant sites to active sites. Intuitively, the connection between these two properties is that when many sites are 'wired' to the active site, there are more positions where mutations can alter binding site function, enabling more rapid adaptation. We hypothesize that fluctuating selective pressures select for evolvable designs and, as a consequence, select for allosteric architectures. Using a minimal physical model, we show that periodically switching selective pressures promote the emergence of evolvable, allosteric sequences. However, the outcome depends critically on the mutation rate and switching timescale. We develop a method to decompose evolutionary forces and identify two regimes: one where selection for generalist binding drives latent allostery, and another where the fluctuating selective pressures drives evolvability. Our results demonstrate that a protein's design reflects not only its current function but also the statistical features of its evolutionary history.

The project described in this chapter was conceived by Rama Ranganathan, Olivier Rivoire, and me. All simulations and analyses were performed by me. This work is in preparation for submission.

4.1 Introduction

Previous chapters focused on the physics of allostery—the principles that enable allostery and their implementation in different physical models. A fundamental remaining question is how allosteric properties can arise through evolution. Often, the evolutionary origin of

a trait—such as allosteric regulation in a protein—is attributed to it conferring a fitness benefit, thereby putting it under positive selection. While this effect certainly plays a role in building and maintaining allosteric machinery, findings from experiments suggest it may not fully account for the initial emergence of allostery in proteins.

Experiments have shown that allosteric properties can exist in proteins even when these properties do not contribute to the protein's native function. For example, Reynolds and Ranganathan demonstrated that the metabolic enzyme dihydrofolate reductase (DHFR) contains numerous allosteric hotspots across its surface that, when perturbed, can modulate active site function [9]. These hotspots were identified by systematically inserting a light-sensitive domain (LOV2) at all surface-exposed regions and measuring the resulting light-dependent activity of DHFR. Upon exposure to blue light, an alpha helix of the LOV2 domain unfolds and locally perturbs the insertion region of the enzyme. None of the identified hotspots are known allosteric effector binding sites or sites of post-translational modification such as phosphorylation. This type of allostery, which is not part of the protein's native function, is referred to as *latent allostery* because its existence becomes apparent only when specifically probed.

In a different example, the yeast kinase Fus3 is naturally allosterically regulated by the scaffolding protein Ste5. Coyle, Flores, and Lim investigated homologs of Fus3 from a fungal strain that evolved without a Ste5 homolog; these Fus3 orthologs are not allosterically regulated in their native context [1]. Through in vitro studies, they found that many of these non-natively allosteric homologs could nonetheless be allosterically regulated by Ste5. This shows that these proteins possess a latent allosteric capacity that predates the emergence of their allosteric binding partner.

It is important to emphasize how latent allostery relates to the common picture of allosteric regulation. In Chapter 2, we showed that for allosteric coupling between two ligand binding events (e.g., substrate binding at the active site and effector binding at the allosteric

site), two conditions must be satisfied: (1) The protein, in the absence of ligand, must have an allosteric design that couples binding sites, either through the soft mode principle or the multi-state principle. (2) Ligand binding must interact with the protein in a way that engages this allosteric design. For example, in a protein with an allosteric soft mode, a ligand that pushes the protein in a conformational direction orthogonal to the soft mode will fail to engage it, yielding no allosteric communication. Allosteric regulation has both of these features. A *latently* allosteric protein, on the other hand, satisfies only the first condition—the allosteric design—but lacks binding of the allosteric effector. This could occur because the effector is missing (as in Fus3 homologs mentioned above) or because the allosteric binding site lacks sufficient affinity for the effector, so it never binds. The key idea of latent allostery is that an underlying allosteric potential exists but goes unused during the protein's native function.

The two examples in DHFR and Fus3 homologs make it clear that direct selection for regulation does not explain the origin of latent allostery in proteins and offers the possibility that functional allosteric regulation may originate from co-opted preexisting latent allosteric features. What could be the origin of latent allostery in proteins? One hypothesis, proposed by Rivoire is that latent allostery arises from the need for specific binding—the ability to bind a target ligand while avoiding similar non-target molecules [10]. Simulations of minimal models support this hypothesis: selection for specific binding yields models with allosteric architectures, where distant perturbations regulate ligand binding [10]. Interestingly, sequences that acquired allostery in this way were more evolvable than non-allosteric ones—that is, they more readily produced mutations enabling adaptation to new selective pressures. The underlying link is that allosteric sequences had more positions 'wired' to the binding site, so many mutations at these sites could alter binding specificity, enabling adaptation.

In an experimental line of work, Ranganathan and co-workers showed that evolvability

physically depends on allostery. For both the third PDZ domain of PSD-95 [8] and the TEM-1 β-lactamase [11], the adaptive mutations—those that enabled new functions—were measured. In the PDZ domain, the new function was the ability to bind a non-native peptide ligand and in the TEM-1 β-lactamase, the new function was the ability to hydrolyze cefotaxime, a β-lactam antibiotic that the wild-type enzyme poorly hydrolyzes. Some adaptive mutations, termed direction-switching mutations, abolished the wild-type function while conferring new function. Others, termed conditionally neutral mutations, preserved wild-type function but also enabled new activity. These conditionally neutral mutations facilitate evolvability as their neutrality allows them to persist in the population and are poised to sweep when selection favors the new function. The authors found that direction-switching mutations clustered at the binding site (in PDZ) or the active site (in TEM-1), while conditionally neutral mutations were more often located farther away—sometimes on distant surfaces. These mutations work allosterically, modifying active site function from a distance. Thus, the data from both proteins demonstrate that their evolvability relies on allostery.

Thus, in both minimal physical models and proteins, evolvability has been linked to allostery. If evolvability need be physically encoded through allosteric architectures, could allostery itself arise as a byproduct of selection for evolvability? We hypothesize that evolution in fluctuating environments will select for evolvable sequences and, as a consequence, will select for allosteric sequences.

The first part of our hypothesis supposes that evolvability can emerge under fluctuating selective pressures. This assumes that evolvability itself can evolve—a question that has attracted significant attention. Computational studies across various evolving systems have demonstrated that evolvability can, indeed, arise under changing selective conditions [5, 3, 7, 2, 4, 6]. The underlying principle is that fluctuating selection pressures, over the long term, favor genotypes capable of rapidly adapting to new environments. Importantly, these studies show that fluctuating selective pressures leave a signature in the physical architecture

of evolved systems. For example, the evolved gene regulatory networks in [2] develop hub-like designs, where some genes are highly copied and control others, such that single mutations can have widespread effects on gene expression. Similarly, evolving Boolean logic circuits and RNA secondary structures under systematically changing environments lead to modular physical architectures that allow small mutations to produce large phenotypic changes [5, 7]. Analogously, we hypothesize that protein designs will reflect their evolutionary history of selective pressures, with allostery emerging as a mechanistic implementation of evolvability.

In the rest of the chapter, we test this hypothesis using the model proposed by Rivoire [10]. We evolved populations of these models under periodically switching selective pressures, where selection alternated between favoring binding to one ligand and favoring binding to a different ligand. We find that the data support the hypothesis: fluctuating environments indirectly select for evolvable allosteric sequences. However, this result strongly depends on the timescale of selection fluctuations (denoted τ) and the mutation rate (denoted μ). Under some conditions, the opposite emerges—sequences that are highly mutationally robust, less evolvable with no long-range effects.

We propose a method to decompose the evolutionary forces that drive the emergence of traits like evolvability and latent allostery. Specifically, we separate the contribution to a trait that arises as a byproduct of a protein's current function from contributions driven by the history of selective pressures during evolution. Applying this method reveals two distinct regions in μ-τ space where evolvability and latent allostery emerge, each arising from a different evolutionary reason. Under low mutation rates and fast switching, latent allostery emerges as a byproduct of generalist binding, while when the external switching timescale matches the internal adaptive timescale, latent allostery arises from the need to adapt to fluctuating environments.

The data show that, in principle, the design of a protein is shaped by the statistical features of its evolutionary history in addition to its current selection.

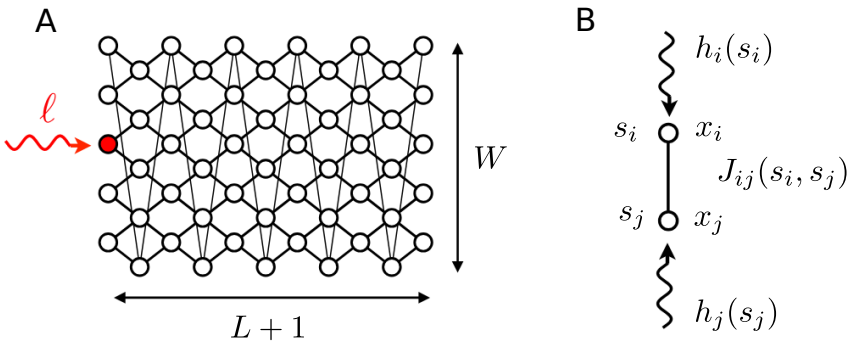

Figure 4.1: (a) The evolvable spin glass model of a protein adapted from [10]. The model is defined on a 2d square lattice with periodic boundaries connecting the top to the bottom (thin vertical lines). The lattice has size $L+1$ (length) by W (width), where we use $L = 10, W = 5$ for this work. The red site is the binding site, where a field ℓ is applied to model ligand binding. (b) Each site carries a spin variable $x_i \in \{-1, +1\}$ and an amino acid type $s_i \in \{1, \ldots, q\}$. The fields on site i, $h_i(s_i)$, and the couplings between sites i and j, $J_{ij}(s_i, s_j)$, are determined by the sequence of amino acid types $\mathbf{s} = (s_1, \ldots, s_N)$.

In the following section, I define the physical model of a protein (Section 4.2) and describe the evolutionary dynamics used to evolve populations of sequences (Section 4.3). Then, in Sections 4.4 and 4.5, I define and measure the evolvability and latent allostery of evolved sequences, respectively.

4.2 The Model

We use a minimal physical model that aims to capture two essential features of proteins: (1) amino acids interact via short-range potentials, so long-range effects arise from collective interactions among many coupled residues; (2) the energy landscape is rugged and sequence-dependent, allowing for the evolution of physical features of the model. Mathematically, the model takes the form of a spin glass where spin variables $x_i = \pm 1$ represent the physical degrees of freedom of a protein (i.e. the atomic coordinates). The model is defined on a 2d square lattice of size $L+1$ by W with semi-periodic boundary conditions to give a geometry of a cylinder, Fig. 4.1A. Spins interact only with their nearest neighbors in a way that depends on the model's sequence $\mathbf{s} = (s_1, s_2, \ldots, s_N)$. Each element of the sequence,

$s_i \in \{1, \ldots, q\}$, takes the place of an amino acid type in a protein sequence and it is these s_i that evolve over time. For this work, we consider $q = 5$. The energy of the model is defined,

$$U(\mathbf{x}, \mathbf{s}, \ell) = \sum_{\langle ij \rangle} J_{ij}(s_i, s_j) x_i x_j + \sum_i h_i(s_i) x_i + \ell x_b, \tag{4.1}$$

where $\langle ij \rangle$ run over the nearest-neighbor bonds of the lattice shown in Fig.4.1A. For every bond $\langle ij \rangle$, the q^2 values of $J_{ij}(s_i s_j)$ are selected at random from the normal distribution $\mathcal{N}(0, \sigma)$ with $\sigma = 3$ and are fixed during evolution. The q values for the $h_i(s_i)$ of every site i are selected similarly. The couplings $J_{ij}(s_i, s_j)$ and the fields $h_i(s_i)$ relate sequence $\mathbf{s}$ to energy U. The last term in (4.1) implements ligand binding: a single site b is chosen as the binding site and a force (field) ℓ is applied on the site. The site b is included in the sums in (4.1). We use three field values: λ_0 for solvent interaction, and λ_1, λ_2 for ligands 1 and 2, respectively. In this work, we use $\ell_0 = 0$, $\ell_1 = 1$, and $\ell_2 = -1$. The molecular phenotype under selection is the binding free energy which is

$$\Delta F_k(\mathbf{s}) = F(\mathbf{s}, \ell_k) - F(\mathbf{s}, \ell_0) \tag{4.2}$$

where

$$F(\mathbf{s}, \ell) = -\beta^{-1} \log \sum_{x_i = \pm 1} e^{-\beta U(\mathbf{x}, \mathbf{s}, \ell)}. \tag{4.3}$$

is the free energy of the system that depends on the identity of the bound ligand $k = 0, 1, 2$. $\beta = (k_B T)^{-1}$ is the inverse temperature. We set $\beta = 1$, fixing the energy scale. With $\beta\sigma = 3$, typical interactions exceed $k_B T$, as in proteins where hydrogen bonds are ~ 1–$3\, k_B T$. The free energy can be solved exactly using transfer matrices (see SI).

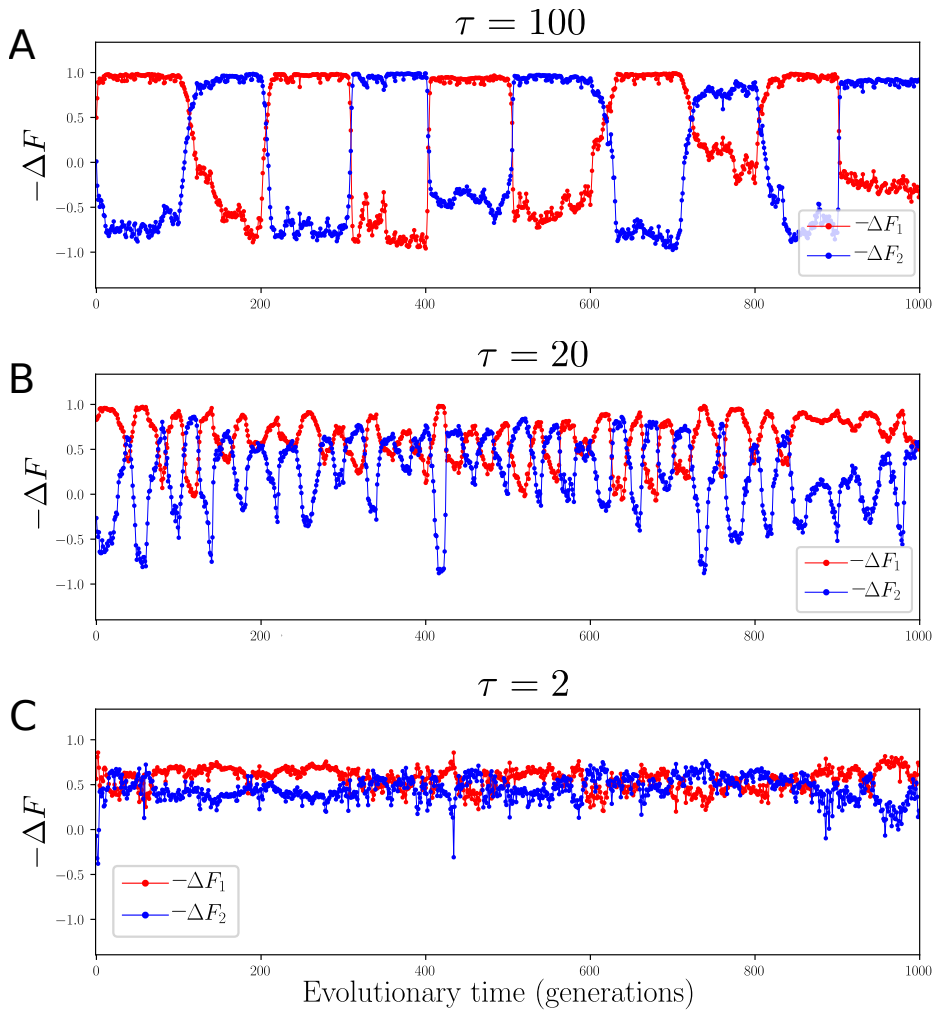

Figure 4.2: The population averaged binding energies for ligand 1 (red) and ligand 2 (blue) over evolutionary time with population size $P = 200$ and mutation rate $\mu = 0.01$. (A) With a long selective period $\tau = 100$, the population fully adapts to an optimal binding energy. (B) As the switching period decreases to $\tau = 20$, the populations do not have time to fully adapt. (C) At very short switching periods, $\tau = 2$, no periodicity is seen in the population dynamics, instead, the population settles to a generalist solution that can bind both ligands.

4.3 Evolutionary simulations

The binding energies $\Delta F_1, \Delta F_2$ depend only on the sequence, yielding two sequence-to-function maps that can be used to evolve a population. We perform evolutionary simulations of a population with a fixed size of P individuals with selection switching periodically between acting on ΔF_1 and ΔF_2. To be precise, we denote the binding energy to ligand $k \in \{1, 2\}$ of the jth sequence in the population as ΔF_k^j. The population at generation $t+1$ is sampled from the population at generation t from the distribution,

$$p_t^j = \frac{e^{-a\Delta F_{k(t)}^j}}{\sum_i e^{-a\Delta F_{k(t)}^i}}, \quad \text{with} \quad k(t) = 1 + \left\lfloor \frac{t-1}{\tau} \right\rfloor \bmod 2. \tag{4.4}$$

When the selective pressure $a > 0$, this update rule rewards tighter binding (greater $-\Delta F$) with increased probability of survival and reproduction. The switching selective pressure is implemented by $k(t)$, which alternates between $k = 1$ and $k = 2$ every τ generations. Each generation, every site in every sequence mutates with probability μ (mutation rate). Mutation of site i amounts to changing its current s_i to a random value selected from the set $\{1, 2, \ldots, q\} \setminus \{s_i\}$.

In Fig. 4.2, we show how populations adapt to changing selective pressures. For instance, in panel A, during the first 100 periods, the population is under selection for binding ligand 1, and the population quickly adapts to strongly binding ligand 1. At generation $t = 101$, the selective pressure switches to act on ligand 2, and the population consequently adapts over the subsequent generations to successfully bind ligand 2. For analysis, one hundred sequences are randomly sampled from the second half of each trajectory. This random sampling ensures that any effects that depend on the time since a selective pressure change are averaged out. We simulate 200 replicate trajectories for each choice of μ, τ pair and consider a range of μ and τ.

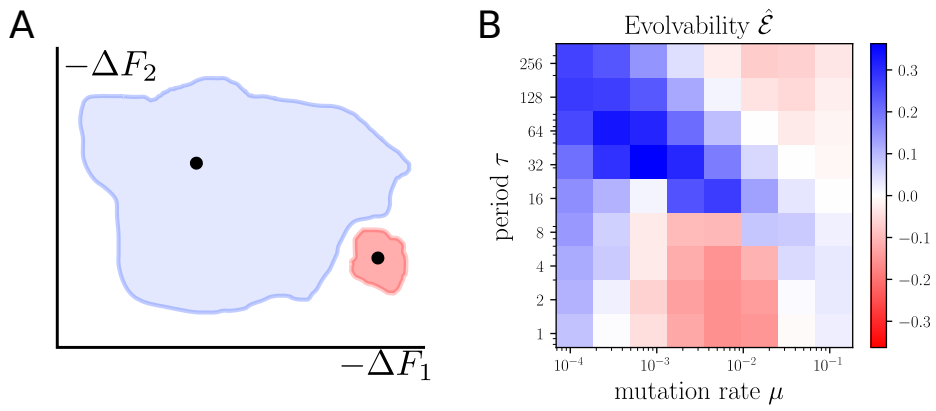

Figure 4.3: (A) A cartoon illustrates how a difference in the breadth of mutational effects of two sequences can be a proxy for evolvability. The black dots indicate two sequences, and clouds around them represent the range spanned by the collection of all their single mutants. The blue cloud is larger, meaning that within one mutation, the sequence can adapt to more regions of binding space. We use the broadness of the distribution of mutational effects to quantify evolvability (4.5). (B) The mean evolvability relative to random sequences $\hat{\mathcal{E}}$ (4.6) of sequences sampled from evolutionary simulations with selection switching period τ, mutation rate μ and population size $P = 200$.

4.4 Measuring Evolvability

We first test if sequences evolved under fluctuating selection are more evolvable than randomly generated sequences. To quantify evolvability, we define a simple metric based on the breadth of single-mutation effects in binding space (4.6). The idea, illustrated in Fig. 4.3A, is that a sequence is more evolvable if single mutations can access a wide range of binding space, compared to a sequence whose mutations are mostly neutral and require multiple steps to reach new binding phenotypes. To quantify this idea, we measure the binding free energies of a sequence (referred to as wild type (wt)), $\Delta\mathbf{F}^{\mathrm{wt}} = (\Delta F_1^{\mathrm{wt}}, \Delta F_2^{\mathrm{wt}})$. Then, for all of the $N \times (q-1)$ single mutants (indexed by α) we compute their binding energies $\Delta\mathbf{F}^{\alpha} = (\Delta F_1^{\alpha}, \Delta F_2^{\alpha})$ and define the evolvability as the root mean square mutational deviations:

$$\mathcal{E} = \sqrt{\frac{1}{(q-1)N} \sum_{\alpha=1}^{(q-1)N} \|\Delta\mathbf{F}^{\alpha} - \Delta\mathbf{F}^{\mathrm{wt}}\|^2}. \tag{4.5}$$

To make this metric more interpretable, we report the evolvability relative to the mean evolvability of uniformly distributed random sequences $\langle \mathcal{E} \rangle_0$, averaged over all sampled sequences (indexed by j):

$$\hat{\mathcal{E}} = \frac{1}{N_{\text{seqs}}} \sum_{j=1}^{N_{\text{seqs}}} \frac{\mathcal{E}_j - \langle \mathcal{E} \rangle_0}{\langle \mathcal{E} \rangle_0}. \tag{4.6}$$

We use this metric to evaluate the evolvability of sequences evolved under switching selection of period τ, mutation rate μ, and population size $P = 200$. (100 sequences per trajectory and 200 trajectories give $N_{\text{seqs}} = 20000$). This is shown in Fig. 4.3B, where the evolvability of evolved sequences significantly deviates from that of random sequences. In addition to regions of increased evolvability, we find regions of reduced evolvability at fast switching speeds and intermediate mutation rates. These sequences are more robust to mutation.

4.4.1 Decomposing phenotypes

What causes evolvability to increase or decrease under different evolutionary conditions? Evolvability is an indirect trait—it is never directly selected, but can change over time as a consequence of selection on other traits. One possible explanation is that evolvability arises due to genetic correlations with directly selected traits (e.g. binding energies), even without fluctuating selection. For example, in [10], the model defined in this chapter was used to show that static selection for binding specificity resulted in sequences that were both specific as well as allosteric. For the data in Fig. 4.3B, the evolvability may correlate with an underlying binding function and arise as a consequence. Alternatively, it may not have any correlation with function at all, but rather emerge as a byproduct of the sequence's changing evolutionary history.

We propose a new method to separate these two contributions. First, we describe this method using a generic trait ψ to establish notation, then apply it to evolvability and later, to other traits associated with allostery. The essential idea is to compare the trait ψ of

evolved sequences with the expected value of the trait of random sequences that share the same binding phenotype $(\Delta F_1, \Delta F_2)$. To do this, we take advantage of a feature of the model that all sequences lie on a bounded 1d curve in the 2d binding space (Fig. 4.4A). We uniformly sample random sequences, measure their binding energies, and bin them into 50 evenly sized bins along the 1d curve, shown in Fig. 4.4B. We parameterize binding space with the bin number ϕ, which takes value $\phi = -1$ for extreme ligand 2 specialists (top left, Fig. 4.4B), value $\phi = 1$ for extreme ligand 1 specialists (bottom right, Fig. 4.4B), and $\phi \approx 0$ identifies generalists—sequences that bind both ligand 1 and 2 (see Methods for details).

The mean of the trait ψ of sequences for a specific bin ϕ, denoted as $\langle \psi | \phi \rangle_0$, reflects the association of a trait with a particular function. (Note that this notation is not related to Dirac notation of Quantum Mechanics; it is simply a way of denoting conditional expectation). Fig. 4.4C shows this quantity when the trait is evolvability. We can use $\langle \psi | \phi \rangle_0$ as a null expectation with which to compare the evolved sequences. As with evolvability (4.6), we are interested in the trait, relative to the random sequence mean $\langle \psi \rangle_0$, averaged over evolved sequences. We introduce the following decomposition:

$$\begin{aligned}
\hat{\psi} &= \frac{1}{N_{\text{seqs}}} \sum_{j=1}^{N_{\text{seqs}}} \frac{\psi_j - \langle \psi \rangle_0}{\langle \psi \rangle_0} \\
&= \underbrace{\frac{1}{N_{\text{seqs}}} \sum_{j=1}^{N_{\text{seqs}}} \frac{\psi_j - \langle \psi | \phi_j \rangle_0}{\langle \psi \rangle_0}}_{\hat{\psi}_{\text{h}}} + \underbrace{\frac{1}{N_{\text{seqs}}} \sum_{j=1}^{N_{\text{seqs}}} \frac{\langle \psi | \phi_j \rangle_0 - \langle \psi \rangle_0}{\langle \psi \rangle_0}}_{\hat{\psi}_{\text{f}}} \\
&= \hat{\psi}_{\text{h}} + \hat{\psi}_{\text{f}}
\end{aligned} \tag{4.7}$$

Here, ψ_j and ϕ_j are the raw trait and bin number of the jth sequence sampled from the evolutionary trajectories, respectively. In $\hat{\psi}_{\text{h}}$, the term $\psi_j - \langle \psi | \phi_j \rangle_0$ removes any contributions from the current function; it purely reflects the contributions from the evolutionary history. In contrast, the term $\langle \psi | \phi_j \rangle_0 - \langle \psi \rangle_0$ in $\hat{\psi}_{\text{f}}$, reports only the trait associated with

the specific function ϕ_j.

ψ represents a generic trait on which to define the decomposition (4.7). For a specific trait, such as evolvability $\mathcal{E}$, the substitution $\psi \to \mathcal{E}$ defines $\hat{\mathcal{E}}, \hat{\mathcal{E}}_{\mathrm{h}}$, and $\hat{\mathcal{E}}_{\mathrm{f}}$. We plot $\hat{\mathcal{E}}_{\mathrm{h}}$ in Fig. 4.4D and find that it isolates the ridge of enhanced evolvability observed in Fig. 4.3B. Since these heat maps are on a log-log plot, the diagonal ridge seems, at least by eye, to be well described by $\mu\tau N = \text{const}$. In this case, it appears that $\mu\tau N \approx 3.5$, and represents the mean number of mutations a sequence will incur during an evolutionary epoch. Further analysis is needed to determine whether this relationship holds quantitatively.

The other feature in Fig. 4.4D is the region of reduced evolvability under fast switching. When $\tau = 1$, the selective pressure switches every generation and effectively acts as static selection for generalists. We verify this by measuring a score, $G = \min(-\Delta F_1, -\Delta F_2)$, which quantifies how strongly a sequence binds both ligands (Fig. 4.4F). Starting from the $\tau = 1$, $\mu = 10^{-4}$ corner of Fig. 4.4D and increasing the mutation rate, the evolvability due to history decreases. At higher mutation rates, excess evolvability in an already well-adapted generalist increases the mutational load, reducing fitness. Instead, the opposite phenotype—reduced evolvability—is advantageous, as it will experience a smaller effective mutational load. This concept of localizing to regions of sequence space where mutations are neutral at high mutation rates has been described as 'survival of the flattest' [12].

$\hat{\mathcal{E}}_{\mathrm{f}}$, is shown in Fig. 4.4E. This contribution is strongest in the low-mutation-rate, fast-switching regime—precisely where generalists emerge. Since $\hat{\mathcal{E}} = \hat{\mathcal{E}}_{\mathrm{f}} + \hat{\mathcal{E}}_{\mathrm{h}}$, the total evolvability reflects two components: one from the generalist function and one from the need to adapt in a fluctuating environment.

4.5 Latent Allostery

What physical designs enable some sequences to be more evolvable than others? Some clues come from the spatial pattern of mutational sensitivity. Fig. 4.5A shows an example of an

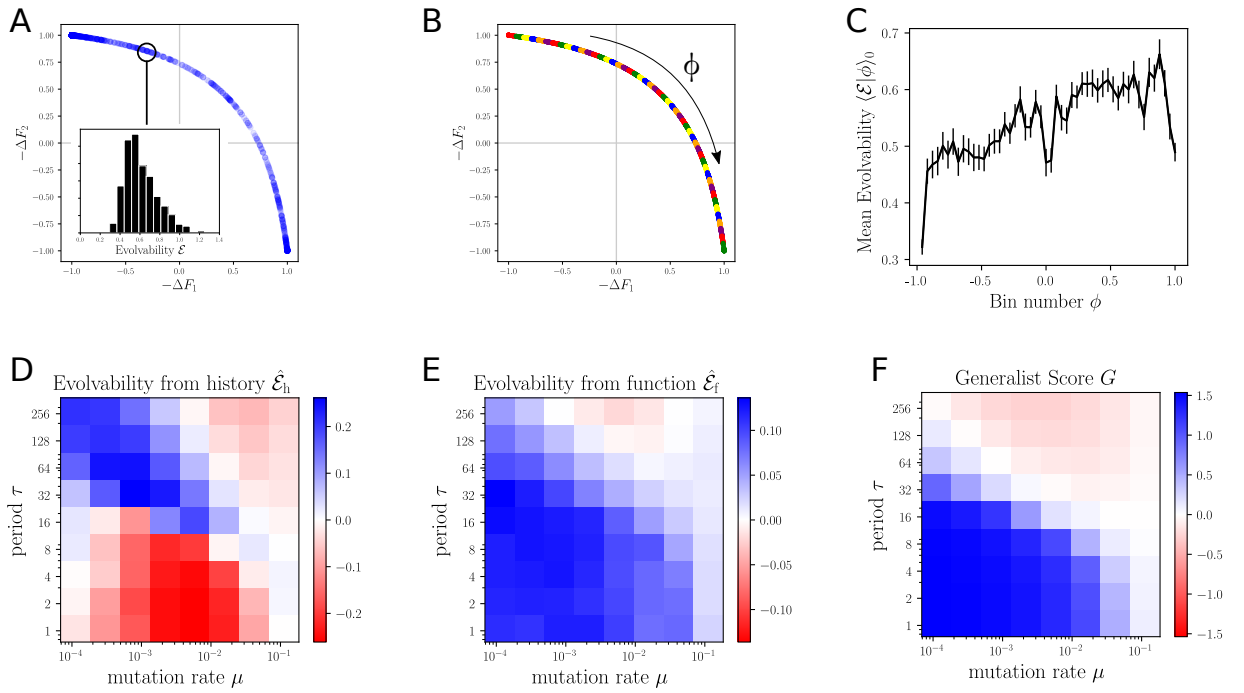

Figure 4.4: The evolvability $\mathcal{E}$ of a sequence has two contributions. (A) All sequences live on a 1d curve in the binding space $-\Delta F_1, -\Delta F_2$. 1000 random sequences are plotted by blue dots. Random sequences sampled from a narrow segment of this curve (small circle) share similar function but vary in evolvability (inset). (B) 50 bins are used to bin binding space. Each color segment represents a bin. $\phi \in [-1, 1]$ parameterizes the 1d curve where sequences live. (C) The mean evolvability of 250 random sequences for each bin ϕ. Error bars are 95% CI. (D) The evolvability contribution from evolutionary history $\hat{\mathcal{E}}_h$. (E) The evolvability contribution from underlying function $\hat{\mathcal{E}}_f$. (F) The mean generalist score, $G = \min(-\Delta F_1, -\Delta F_2)$, averaged over evolved sequences. Larger values indicate stronger generalists.

evolvable sequence. The size of each green dot reflects the mutational sensitivity at that position. This sequence has a large fraction of sensitive sites, including many on the far side of the lattice from the binding site, and so these sites are allosterically coupled as they control function at a distance. By contrast, a low-evolvability sequence, shown in Fig. 4.5C, has only a few sensitive positions. These two examples support a hypothesis that links evolvability and allostery. To be evolvable, a sequence must have many function-altering mutations. As a result, many positions are mutationally sensitive. But not all of these sites can be at the active site—some must lie farther away and work allosterically to modulate binding. Thus, evolvability requires allostery.

Does this connection between evolvability and allostery extend beyond the two examples considered? We can use the distance d to the furthest sensitive mutation (up to a threshold) as a reporter of latent allosteric capacity. We use the decomposition (4.7) to define relative and decomposed quantities $\hat{d}, \hat{d}_{\mathrm{h}}, \hat{d}_{\mathrm{f}}$, and show how they vary across a range of μ and τ in Fig. 4.4EFG. We find strong similarity between it and the evolvability $\hat{\mathcal{E}}$ of Fig. 4.3B. Just as with evolvability, the contribution from history shows a diagonal element.

To go beyond mutation-based measures of allostery, we consider two other quantities: participation ratio and an experimentally inspired allosteric scan.

Physically, ligand binding is modeled by applying a field to the binding site spin. This can shift the magnetization at other sites if they are coupled through the interactions J_{ij}. In a protein, the analog would be a binding-induced conformational change. Fig. 4.5B and D show ω_i, the change in magnetization of spin i between the ligand 1 and ligand 2 bound conditions (Methods), for the same two sequences of Fig. 4.5A and C, respectively. The sequence with extended mutational effects also has a large number of sites that experience a conformational change. The extent of spin flips is measured by the participation ratio, $\bar{\omega} = \frac{1}{N}\sum_{i=1}^{N}\omega_i$. When all the spins flip upon changing ligand, $\bar{\omega} = 1$, and when no spins flip, $\bar{\omega} = 0$.

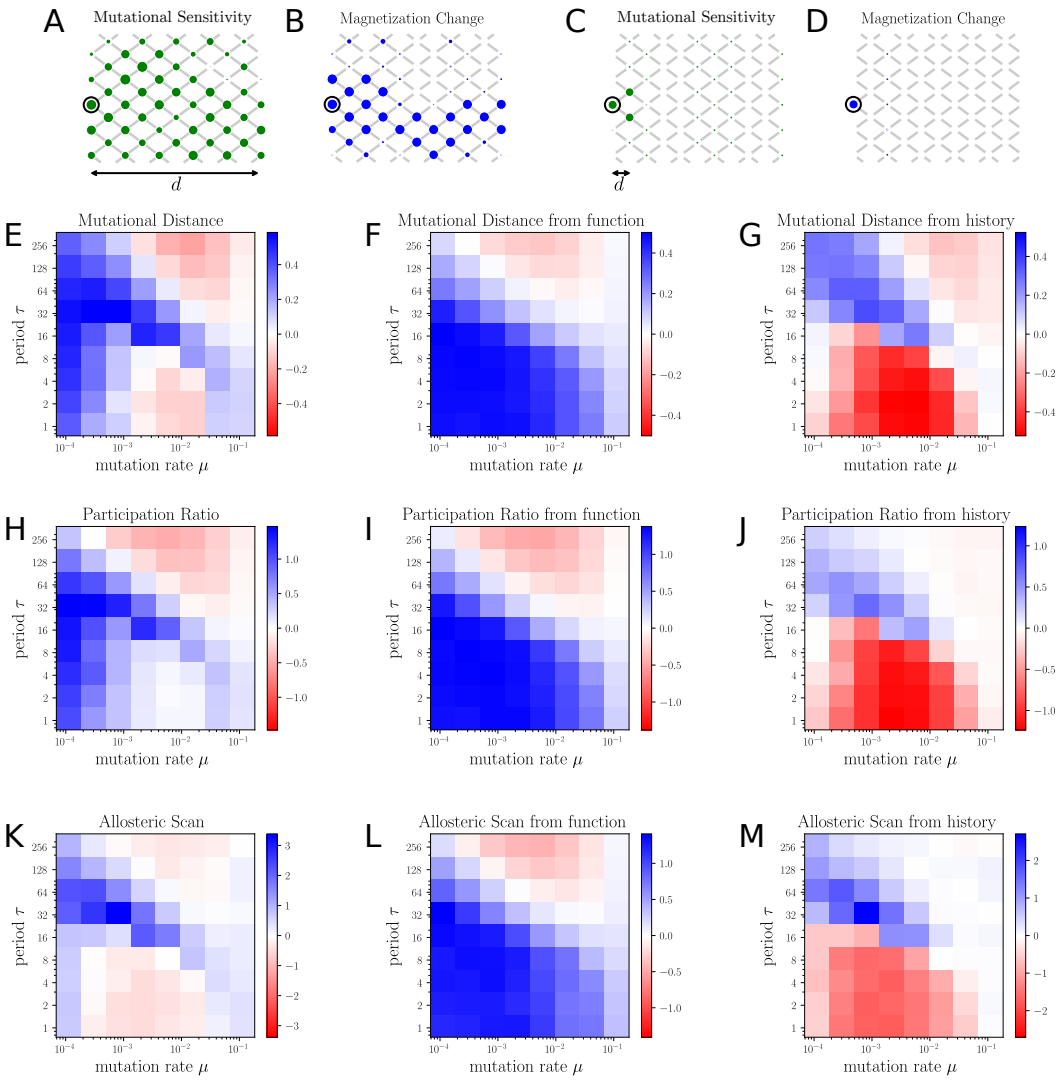

Figure 4.5: Allostery evolves under certain fluctuating selective pressures. (A) A map of the mutational sensitivity (size of green dot) on the structure of the model for an evolvable sequence. (B) A map of the magnitude of the change in magnetization (size of blue dot) upon binding different ligands for the same evolvable sequence as A. (C) A map of the mutational sensitivity (size of green dot) on the structure of the model for a non-evolvable sequence. (D) A map of the magnitude of the change in magnetization (size of blue dot) upon binding different ligands for the same non-evolvable sequence as C. (E) The mean mutational distance $\hat{d}$, (F) the mean mutational distance from function $\hat{d}_{\mathrm{f}}$, (G) the mean mutational distance from history $\hat{d}_{\mathrm{h}}$ of sequences evolved over a range of selection switching timescales τ and mutation rates μ. (H) The mean participation ratio $\hat{\omega}$, (I) the mean participation ratio from function $\hat{\omega}_{\mathrm{f}}$, (J) the mean participation ratio from history $\hat{\omega}_{\mathrm{h}}$ of sequences evolved over a range of selection switching timescales τ and mutation rates μ. (K) The mean allosteric scan $\widehat{\Delta\Delta F}$, (L) the mean allosteric scan from function $\widehat{\Delta\Delta F}_{\mathrm{f}}$, (M) the mean allosteric scan from history $\widehat{\Delta\Delta F}_{\mathrm{h}}$ of sequences evolved over a range of selection switching timescales τ and mutation rates μ.

To see how the participation ratio of evolved sequences depends on the mutation rate and switching period, we use the decomposition (4.7) to define the relative and decomposed quantities $\hat{\bar{\omega}}, \hat{\bar{\omega}}_{\mathrm{h}}, \hat{\bar{\omega}}_{\mathrm{f}}$, and plot them in Figs. 4.5H,I,J. We find that evolutionary conditions (μ, τ) that promote long-range mutational effects also promote large participation ratios.

In proteins, latent allosteric effects can become functional if they couple the active site to distant surfaces that serve as novel allosteric effector binding sites or phosphorylation sites. To quantify this in our model, we introduce a measure inspired by the experimental method of Reynolds et al.[9]. In this assay, we simulate ligand binding by applying fields λ_1, λ_2 to each site on the side of the lattice opposite the original binding site, one at a time, and measure the resulting change in binding energy. Some positions are more strongly coupled than others. To report on the most coupled allosteric hotspot, we record the largest change in binding energy across all perturbations, denoted $\Delta\Delta F$ (Methods). We show the averaged and normalized allosteric scan $\widehat{\Delta\Delta F}$, as well as the contributions from function $\widehat{\Delta\Delta F}\mathrm{f}$ and history $\widehat{\Delta\Delta F}\mathrm{h}$, in Fig.4.5K,L,M. This allosteric scan quantity shows similar dependence on mutation rate and switching period as other metrics of allostery, such as $\hat{\omega}$ and $\widehat{\Delta\Delta F}$.

4.6 Discussion

All three measures of long-range allosteric coupling—$\hat{d}, \hat{\omega}, \widehat{\Delta\Delta F}$—and the evolvability metric $\hat{\mathcal{E}}$ exhibit remarkably similar patterns across mutation rates and switching periods. Each decomposes similarly into contributions from function and history. These results support the hypothesis that allostery underpins evolvability by 'wiring' more sites to the binding site, such that mutations at these sites can alter its function. A greater number of such sites increases the number of mutational paths to new functions. Thus, variable environments can promote the emergence of latent allostery.

Interestingly, evolvability and allostery also emerge under static selection for generalist binding (bottom left corner of Fig. 4.4E and Fig. 4.5F,I,J). This parallels the results of

Rivoire [10], where selection for binding specificity yields evolvable, allosteric sequences. Indeed, specificity and generalist binding take on similar definitions in the model, as both share the constraint that the binding site must perform two functions. For generalist binding, the model must bind two ligands; for specificity, it must bind one ligand while excluding a similar one.

The results presented in this chapter provide strong support for the hypothesis that latent allostery can emerge as a byproduct of fluctuating selective pressures. However, the generality of these findings remains unclear. Specifically, what essential features must a system possess to exhibit behavior similar to the model considered? One way to address this question is to propose a simpler model that includes only those essential features and test whether the same results emerge. In the case of the spin glass model, an essential feature is that in some sequences (those that are allosteric), mutations at many positions can alter fitness (Fig. 4.5A), whereas in others (non-allosteric), only a few positions do so (Fig. 4.5C). This property depends only on a defined fitness landscape and does not require explicit physical interactions between sites. By constructing a model at the level of the fitness landscape, it may be possible to define a simpler system in which the evolutionary dynamics can be predicted analytically.

In proteins and other macromolecules, allostery plays a critical role in regulating biological functions. While much work has focused on understanding how allostery works (including Chapters 2 and 3), much less is known about how allosteric properties emerge through evolution. In this chapter, I propose that allostery need not arise for any functionally beneficial reason but may instead emerge as a byproduct of something more fundamental: fluctuating environments. Since allosteric proteins serve as building blocks in higher-level systems—such as signaling networks and protein complexes—this work offers a key step toward understanding how complex biological systems readily evolve.

4.7 Methods

4.7.1 Parameterize Function Space.

A feature of the model is that all sequences lie on a bounded 1d curve in the 2d binding space (Fig. 4.4A). We divide this space into $N_{\text{bins}} = 50$ bins, shown in Fig. 4.4B. All of the sequences in a single bin have approximately the same ligand binding energies. The bins are indexed by the bin number n, with $n = 0$ containing extreme ligand 2 specialists (top left, Fig. 4.4B) and bin $n = N_{\text{bins}} - 1$ containing extreme ligand 1 specialists (bottom right, Fig. 4.4B). We introduce the normalized bin number $\phi = \frac{2n}{N_{\text{bins}}-1} - 1$ that locates specialists at $\phi = \pm 1$. Thus, ϕ parameterizes the region of binding space accessible to sequences.

4.7.2 Measures of Allostery

Mutational Distance: For a reference sequence, each single mutant α will have an associated effect on the binding energies, $\delta_\alpha = \|\Delta\mathbf{F}^\alpha - \Delta\mathbf{F}^{\text{wt}}\|$ and associated distance from the binding site, r_α (shortest number of steps on lattice from binding site to mutated site). We define the 'mutational distance' as the distance of the furthest sensitive ($\delta_\alpha \geq \theta$) mutant from the binding site,

$$d = \max_{\alpha:\delta_\alpha > \theta} r_\alpha. \tag{4.8}$$

In this work, we take θ to be the root-mean-square (RMS) distance from the centroid of uniformly distributed random sequences in binding space. This sets the scale of binding energies.

Participation ratio: We also measure the conformational change upon binding ligands. In the spin glass, this is measured by the extent of the change of the magnetization of the spins. The magnetization of spin i when field ℓ is applied to the binding site $\langle x_i \rangle_\ell$. We measure

the change in magnetization between ligand 1-bound and ligand 2-bound states,

$$\omega_i = \frac{1}{2}\left|\langle x_i\rangle_{\ell_2} - \langle x_i\rangle_{\ell_1}\right| \ , \quad \bar{\omega} = \frac{1}{N}\sum_{i=1}^{N}\omega_i. \tag{4.9}$$

Allosteric Scan This measure is designed to quantify latent allostery in a way that may be more realistic for a protein. Essentially, it measures how strongly allosteric hotspots on the distant side of the lattice are coupled to the binding site. To implement it, first, we perturb each spin i on the distant surface by applying fields ℓ_1 and ℓ_2. This mimics ligands interacting with the protein at sites other than the binding site. Using a notation similar to that used for mutations, we will represent the binding energy of a sequence without any allosteric perturbation to be ΔF_k^{wt}, where $k = 1, 2$ determines the ligand. When an allosteric ligand binds to site i of the allosteric surface and applies field $\ell_l, l = 1, 2$ to that site, the binding energy is denoted $\Delta F_k^{j,l}$. The effect of binding an allosteric ligand on the active site binding energy is denoted $\Delta\Delta F_k^{i,l} = \Delta F_k^{i,l} - \Delta F_k^{\mathrm{wt}}$. As a measure of the latent allosteric potential of the sequence, we define the latent allosteric coupling as:

$$\Delta\Delta F = \max_{i,k,l}\left|\Delta\Delta F_k^{i,l}\right|. \tag{4.10}$$

References

[1] Scott M Coyle, Jonathan Flores, and Wendell A Lim. Exploitation of latent allostery enables the evolution of new modes of map kinase regulation. *Cell*, 154(4):875–887, 2013.

[2] Anton Crombach and Paulien Hogeweg. Evolution of evolvability in gene regulatory networks. *PLoS computational biology*, 4(7):e1000112, 2008.

[3] Jeremy Draghi and Günter P Wagner. Evolution of evolvability in a developmental

model. *Evolution*, 62(2):301–315, 2008.

[4] Martin J Falk, Jiayi Wu, Ayanna Matthews, Vedant Sachdeva, Nidhi Pashine, Margaret L Gardel, Sidney R Nagel, and Arvind Murugan. Learning to learn by using nonequilibrium training protocols for adaptable materials. *Proceedings of the National Academy of Sciences*, 120(27):e2219558120, 2023.

[5] Nadav Kashtan and Uri Alon. Spontaneous evolution of modularity and network motifs. *Proceedings of the National Academy of Sciences*, 102(39):13773–13778, 2005.

[6] Bhaskar Kumawat, Alexander Lalejini, Monica M Acosta, and Luis Zaman. Evolution takes multiple paths to evolvability when facing environmental change. *Proceedings of the National Academy of Sciences*, 122(1):e2413930121, 2025.

[7] Merav Parter, Nadav Kashtan, and Uri Alon. Facilitated variation: how evolution learns from past environments to generalize to new environments. *PLoS computational biology*, 4(11):e1000206, 2008.

[8] Arjun S Raman, K Ian White, and Rama Ranganathan. Origins of allostery and evolvability in proteins: a case study. *Cell*, 166(2):468–480, 2016.

[9] Kimberly A Reynolds, Richard N McLaughlin, and Rama Ranganathan. Hot spots for allosteric regulation on protein surfaces. *Cell*, 147(7):1564–1575, 2011.

[10] Olivier Rivoire. Parsimonious evolutionary scenario for the origin of allostery and coevolution patterns in proteins. *Physical Review E*, 100(3):032411, 2019.

[11] Michael A Stiffler, Doeke R Hekstra, and Rama Ranganathan. Evolvability as a function of purifying selection in tem-1 β-lactamase. *Cell*, 160(5):882–892, 2015.

[12] Claus O Wilke, Jia Lan Wang, Charles Ofria, Richard E Lenski, and Christoph Adami.

Evolution of digital organisms at high mutation rates leads to survival of the flattest. *Nature*, 412(6844):331–333, 2001.

Appendix for Chapter 4

4.8 The Transfer Matrix Method

The spin glass model defined in this chapter is amenable to exact calculation through transfer matrices. Here, I outline how to compute the partition function, mean magnetization, and spin correlations using this method. I first illustrate the method in the simpler case of a 1D spin glass, and then extend it to the 2D case.

4.8.1 1d spin glass model

Consider the Hamiltonian H for a 1D spin glass with nearest-neighbor interactions and no periodic boundary conditions (i.e., no interaction between spin 1 and N):

$$H(\boldsymbol{\sigma}) = -\sum_{i=1}^{N-1} J_i \sigma_i \sigma_{i+1} - \sum_{i=1}^{N} h_i \sigma_i \tag{4.11}$$

where σ_i are the spin variables, J_i are the interaction strengths between neighboring spins, and h_i are the external fields acting on the spins. This can be rewritten as

$$H = \left(\sum_{i=1}^{N-1} E^{(i)}(\sigma_i, \sigma_{i+1}) \right) - h_N \sigma_N, \quad \text{with} \quad E^{(i)}(\sigma_i, \sigma_{i+1}) = -J_i \sigma_i \sigma_{i+1} - \frac{1}{2}(h_i \sigma_i + h_{i+1} \sigma_{i+1}) \tag{4.12}$$

The superscript on $E^{(i)}$ indicates the coupling and field dependence on i. The partition function Z is given by:

$$Z = \sum_{\sigma_1} \cdots \sum_{\sigma_N} \exp(-\beta H(\sigma)) \tag{4.13}$$

$$= \sum_{\sigma_1} \cdots \sum_{\sigma_N} \exp\left(-\beta \sum_{i=1}^{N} E^{(i)}(\sigma_i, \sigma_{i+1})\right) \exp(-\beta(-h_N \sigma_N)) \tag{4.14}$$

$$= \sum_{\sigma_1} \cdots \sum_{\sigma_N} \exp(-\beta E^{(1)}(\sigma_1, \sigma_2)) \exp(-\beta E^{(2)}(\sigma_2, \sigma_3)) \ldots \exp(-\beta E^{(N-1)}(\sigma_{N-1}, \sigma_N)) \exp(\beta h_N \sigma_N) \tag{4.15}$$

Define the matrix $T^{(i)}_{\sigma_i \sigma_{i+1}} = \exp(-\beta E^{(i)}(\sigma_i, \sigma_{i+1}))$. Now we can think of the spin variables σ_i, σ_{i+1} as indices of a matrix.

$$Z = \sum_{\sigma_1} \cdots \sum_{\sigma_N} T^{(1)}_{\sigma_1 \sigma_2} T^{(2)}_{\sigma_2 \sigma_3} \ldots T^{(N-1)}_{\sigma_{N-1} \sigma_N} \exp(\beta h_N \sigma_N) \tag{4.16}$$

Recall that matrix multiplication takes the form $C_{ij} = \sum_k A_{ik} B_{kj}$ and the contraction properties $\sum_j A_{ij} v_j = \sum_{j,k} A_{ij} \delta_{jk} v_k$ and $\sum_j A_{ij} v_j B_{jk} = \sum_{j,l} A_{ij} \delta_{jl} v_l B_{lk}$. The partition function can be written as a matrix product,

$$Z = \sum_{\sigma_1} \sum_{\sigma_N} \sum_{\sigma'} \mathcal{T}_{\sigma_i \sigma'} X_{\sigma' \sigma_N} = \mathbf{1}^\top \mathcal{T} X \mathbf{1} \tag{4.17}$$

with $\mathcal{T} = \prod_{i=1}^{N-1} T^{(i)}$, where X is a matrix with entries $X_{\sigma' \sigma_N} = \delta_{\sigma' \sigma_N} \exp(\beta h_N \sigma')$ and $\mathbf{1}$ is the ones vector.

The magnetization can be expressed in similar terms.

$$\langle \sigma_i \rangle = Z^{-1} \sum_{\sigma_1} \cdots \sum_{\sigma_N} \sigma_i \exp(-\beta H(\boldsymbol{\sigma})) \tag{4.18}$$

$$= Z^{-1} \sum_{\sigma_1} \cdots \sum_{\sigma_N} T^{(1)}_{\sigma_1 \sigma_2} \ldots T^{(i-1)}_{\sigma_{i-1}\sigma_i} \sigma_i T^{(i)}_{\sigma_i \sigma_{i+1}} \ldots T^{(N-1)}_{\sigma_{N-1}\sigma_N} \exp(\beta h_N \sigma_N) \tag{4.19}$$

$$= Z^{-1} \sum_{\sigma_1} \sum_{\sigma_N} \left(T^{(1)} T^{(2)} \ldots T^{(i-1)} \tau T^{(i)} \ldots T^{(N-1)} X \right)_{\sigma_1 \sigma_N} \tag{4.20}$$

$$= Z^{-1} \mathbf{1}^\top T^{(1)} T^{(2)} \ldots T^{(i-1)} \tau T^{(i)} \ldots T^{(N-1)} X \mathbf{1} \tag{4.21}$$

where $\tau = \mathrm{diag}([+1, -1])$. A similar calculation leads to the formula for the correlation.

$$\langle \sigma_i \sigma_j \rangle = Z^{-1} \mathbf{1}^\top T^{(1)} \ldots T^{(i-1)} \tau T^{(i)} \ldots T^{(j-1)} \tau T^{(j)} \ldots T^{(N-1)} X \mathbf{1} \tag{4.22}$$

4.8.2 2d spin glass model

For a 2d model, we consider a square lattice with periodic boundary conditions in one direction. The lattice can be divided into L layers of W spins (columns of spins in the

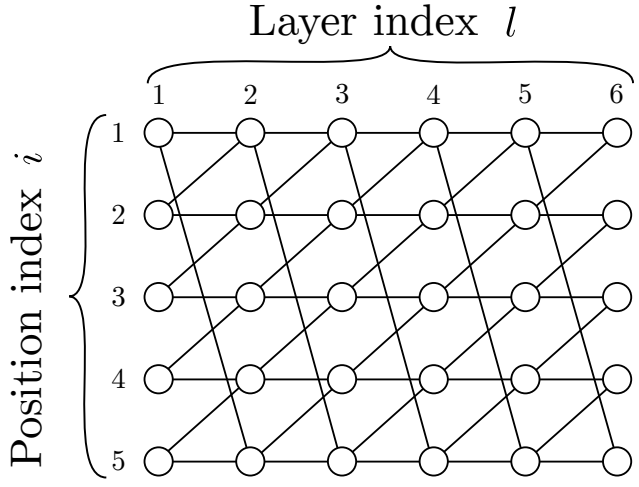

Figure 4.6: Schematic of the connectivity of the spin glass model.

figure). The spin $\sigma_{i,l}$ is located at position i in layer l. Between layers l and $l+1$, the spin

$\sigma_{i,l}$ is coupled to $\sigma_{i,l+1}$ and $\sigma_{i-1,l+1}$ when $i > 1$ and $\sigma_{W,l+1}$ when $i = 1$. The trick for using the transfer matrix method for 2d models is to think of each layer as a coarse-grained 'site' that can take 2^W states, and each layer only interacts with the layer on the left and the layer on the right. Because of this structure, we can write the Hamiltonian as the sum of interaction energies between layers (similar to (4.12)).

$$H(\boldsymbol{\sigma}) = \sum_{l=1}^{L-1} E^{(l)}(\boldsymbol{\sigma}_l, \boldsymbol{\sigma}_{l+1}) - \sum_{i=1}^{W} h_{i,L}\sigma_{i,l} \tag{4.23}$$

with

$$E^{(l)}(\boldsymbol{\sigma}_l, \boldsymbol{\sigma}_{l+1}) = \left(-\sum_{i=1}^{W} J^{-}_{i,l}\sigma_{i,l}\sigma_{i,l+1} + J^{+}_{i,l}\sigma_{i,l}\sigma_{i-1,l+1} + h_{i,l}\sigma_{i,l} \right). \tag{4.24}$$

Here $\boldsymbol{\sigma}_l = (\sigma_{i,l}, \sigma_{i+1,l}, \ldots, \sigma_{W,l})$, and for periodic boundary conditions $\sigma_{0,l} = \sigma_{W,l}$. The partition function can be written as,

$$Z = \sum_{\boldsymbol{\sigma}_1} \cdots \sum_{\boldsymbol{\sigma}_L} \exp(-\beta H(\boldsymbol{\sigma})) \tag{4.25}$$

$$= \sum_{\boldsymbol{\sigma}_1} \cdots \sum_{\boldsymbol{\sigma}_L} \exp\left(-\beta \sum_{l=1}^{L-1} E^{(l)}(\boldsymbol{\sigma}_l, \boldsymbol{\sigma}_{l+1}) \right) \exp(\beta \sum_{i=1}^{W} h_{i,L}\sigma_{i,L}) \tag{4.26}$$

$$= \sum_{\boldsymbol{\sigma}_1} \cdots \sum_{\boldsymbol{\sigma}_L} \exp\left(-\beta E^{(1)}(\boldsymbol{\sigma}_1, \boldsymbol{\sigma}_2) \right) \ldots \exp\left(-\beta E^{(L-1)}(\boldsymbol{\sigma}_{L-1}, \boldsymbol{\sigma}_L) \right) \exp(\beta \sum_{i=1}^{W} h_{i,L}\sigma_{i,L}) \tag{4.27}$$

$$\tag{4.28}$$

Define the transfer matrix $T^{(l)}_{\boldsymbol{\sigma}_l,\boldsymbol{\sigma}_{l+1}} = \exp\left(-\beta E^{(l)}(\boldsymbol{\sigma}_l, \boldsymbol{\sigma}_{l+1})\right)$, which requires interpreting $\boldsymbol{\sigma}_l$ as an index that can take 2^W values.

$$Z = \sum_{\boldsymbol{\sigma}_1} \cdots \sum_{\boldsymbol{\sigma}_L} T^{(1)}_{\boldsymbol{\sigma}_1\boldsymbol{\sigma}_2} T^{(2)}_{\boldsymbol{\sigma}_2\boldsymbol{\sigma}_3} \ldots T^{(L-1)}_{\boldsymbol{\sigma}_{L-1}\boldsymbol{\sigma}_L} \quad \exp(\beta \sum_{i=1}^{W} h_{i,L}\sigma_{i,L}) \tag{4.29}$$

$$= \mathbf{1}^\top \left(\prod_{l=1}^{L-1} T^{(l)} \right) X\mathbf{1}. \tag{4.30}$$

where X is a diagonal matrix: $X_{\boldsymbol{\sigma_L},\boldsymbol{\sigma_L}} = \exp(\beta \sum_{i=1}^{W} h_{i,L}.\sigma_{i,L})$.

To implement the transfer matrix method computationally, one needs to choose the ordering of values $\boldsymbol{\sigma}_l \in \{(\sigma_{1,l}, \ldots, \sigma_{W,l}) \mid \sigma_{1,l}, \ldots, \sigma_{W,l} \in \{1, -1\}\}$. For my implementation, I chose the following ordering for an example where $W = 3$.

Table 4.1: All possible spin configurations $\boldsymbol{\sigma}_l$

$\sigma_{1,l}$	$\sigma_{2,l}$	$\sigma_{3,l}$
1	1	1
-1	1	1
1	-1	1
-1	-1	1
1	1	-1
-1	1	-1
1	-1	-1
-1	-1	-1

Magnetization:

$$\langle \sigma_{i,l} \rangle = Z^{-1} \sum_{\boldsymbol{\sigma}_1} \cdots \sum_{\boldsymbol{\sigma}_L} T^{(1)}_{\boldsymbol{\sigma}_1\boldsymbol{\sigma}_2} \ldots T^{(l-1)}_{\boldsymbol{\sigma}_{l-1}\boldsymbol{\sigma}_l} \sigma_{i,l} T^{(l)}_{\boldsymbol{\sigma}_l\boldsymbol{\sigma}_l+1} \ldots T^{(L-1)}_{\boldsymbol{\sigma}_{L-1}\boldsymbol{\sigma}_L} \quad \exp(\beta \sum_{i=1}^{W} h_{i,L}\sigma_{i,L}) \tag{4.31}$$

What to do with $\sigma_{i,l}$ sandwiched between the transfer matrices? Note that a particular value of $\boldsymbol{\sigma}_l$, a particular row of the table 4.1, the value of $\sigma_{i,l}$ is the ith element of the row in the

table. Thus $\sigma_{i,l}$ is indexed by $\boldsymbol{\sigma}_l$ and thus acts like a vector, and vectors can be de-contracted to a diagonal matrix. The magnetization can be written,

$$\langle \sigma_{i,l} \rangle = \mathbf{1}^\top T^{(1)} \dots T^{(l-1)} \tau_i T^{(l)} \dots T^{(L)} X \mathbf{1}. \tag{4.32}$$

where τ_i is a diagonal matrix with the i-th column of the table placed on the diagonal.

The correlation is computed the same way

$$\langle \sigma_{i,l} \sigma_{j,k} \rangle = \mathbf{1}^\top T^{(1)} \dots T^{(l-1)} \tau_i T^{(l)} \dots T^{(k-1)} \tau_j T^{(k)} \dots T^{(L)} X \mathbf{1}. \tag{4.33}$$